2007

# Dissipative Solitons In The Cubic-quintic Complex Ginzburg-landau Equation:bifurcations And Spatiotemporal Structure

Ciprian Mancas
*University of Central Florida*

# DISSIPATIVE SOLITONS IN THE CUBIC–QUINTIC COMPLEX GINZBURG–LANDAU EQUATION: BIFURCATIONS AND SPATIOTEMPORAL STRUCTURE

by

CIPRIAN STEFAN MANCAS
B.S. University of Central Florida, 2002
M.S. University of Central Florida, 2003

A dissertation submitted in partial fulfillment of the requirements
for the degree of Doctor of Philosophy
in the Department of Mathematics
in the College of Sciences
at the University of Central Florida
Orlando, Florida

Spring Term
2007

Major Professor: Roy S. Choudhury

# ABSTRACT

Comprehensive numerical simulations (reviewed in Dissipative Solitons, Akhmediev and Ankiewicz (Eds.), Springer, Berlin, 2005) of pulse solutions of the cubic–quintic Ginzburg–Landau equation (CGLE), a canonical equation governing the weakly nonlinear behavior of dissipative systems in a wide variety of disciplines, reveal various intriguing and entirely novel classes of solutions. In particular, there are five new classes of pulse or solitary waves solutions, viz. pulsating, creeping, snake, erupting, and chaotic solitons. In contrast to the regular solitary waves investigated in numerous integrable and non–integrable systems over the last three decades, these dissipative solitons are not stationary in time. Rather, they are spatially confined pulse–type structures whose envelopes exhibit complicated temporal dynamics. The numerical simulations also reveal very interesting bifurcations sequences of these pulses as the parameters of the CGLE are varied.

In this dissertation, we develop a theoretical framework for these novel classes of solutions. In the first part, we use a traveling wave reduction or a so–called spatial approximation to comprehensively investigate the bifurcations of plane wave and periodic solutions of the CGLE. The primary tools used here are Singularity Theory and Hopf bifurcation theory respectively. Generalized and degenerate Hopf bifurcations have also been considered to track the emergence of global structure such as homoclinic orbits. However, these results appear difficult to correlate to the numerical bifurcation sequences of the dissipative solitons.

In the second part of this dissertation, we shift gears to focus on the issues of central interest in the area, i.e., the conditions for the occurrence of the five categories of dissipative solitons, as well the dependence of both their shape and their stability on the various parameters of the CGLE, viz. the nonlinearity, dispersion, linear and nonlinear gain, loss and spectral filtering parameters. Our predictions on the variation of the soliton amplitudes, widths and periods with the CGLE parameters agree with simulation results.

For this part, we develop and discuss a variational formalism within which to explore the various classes of dissipative solitons. Given the complex dynamics of the various dissipative solutions, this formulation is, of necessity, significantly generalized over all earlier approaches in several crucial ways. Firstly, the two alternative starting formulations for the Lagrangian are recent and not well explored. Also, after extensive discussions with David Kaup, the trial functions have been generalized considerably over conventional ones to keep the shape relatively simple (and the trial function integrable!) while allowing arbitrary temporal variation of the amplitude, width, position, speed and phase of the pulses.

In addition, the resulting Euler–Lagrange equations are treated in a completely novel way. Rather than consider the stable fixed points which correspond to the well–known stationary solitons or plain pulses, we use dynamical systems theory to focus on more complex attractors viz. periodic, quasiperiodic, and chaotic ones. Periodic evolution of the trial function parameters on stable periodic attractors constructed via the method of multiple scales yield solitons whose amplitudes are non–stationary or time dependent. In particular, pulsating, snake (and, less easily, creeping) dissipative solitons may be treated in this manner. Detailed

results are presented here for the pulsating solitary waves — their regimes of occurrence, bifurcations, and the parameter dependences of the amplitudes, widths, and periods agree with simulation results.

Finally, we elucidate the Hopf bifurcation mechanism responsible for the various pulsating solitary waves, as well as its absence in Hamiltonian and integrable systems where such structures are absent.

Results will be presented for the pulsating and snake soliton cases. Chaotic evolution of the trial function parameters in chaotic regimes identified using dynamical systems analysis would yield chaotic solitary waves. The method also holds promise for detailed modeling of chaotic solitons as well. This overall approach fails only to address the fifth class of dissipative solitons, viz. the exploding or erupting solitons.

*To Teodora, Petruta and Lorinda*

# ACKNOWLEDGMENTS

I would like to acknowledge my advisor, and my friend, Roy Choudhury who inspired all this work, and the comments made by David Kaup on the variational formulation, as well as on soliton perturbation theory. Helpful inputs were also provided by Jianke Yang (Vermont) and Roberto Camassa (Chapel Hill).

# TABLE OF CONTENTS

# LIST OF FIGURES

# CHAPTER ONE: INTRODUCTION

The cubic complex Ginzburg–Landau equation (CGLE) is the canonical equation governing the weakly nonlinear behavior of dissipative systems in a wide variety of disciplines [1]. In fluid mechanics, it is also often referred to as the Newell–Whitehead equation after the authors who derived it in the context of Bénard convection [1, 2].

As such, it is also one of the most widely studied nonlinear equations. Many basic properties of the equation and its solutions are reviewed in [3, 4], together with applications to a vast variety of phenomena including nonlinear waves, second–order phase transitions, superconductivity, superfluidity, Bose–Einstein condensation, liquid crystals and string theory. The numerical studies by Brusch et al. [5, 6] which primarily consider periodic traveling wave solutions of the cubic CGLE, together with secondary pitchfork bifurcations and period doubling cascades into disordered turbulent regimes, also give comprehensive summaries of other work on this system. Early numerical studies [7, 8] and theoretical investigations [9, 10] of periodic solutions and secondary bifurcations are also of general interest for our work here.

Certain situations or phenomena, such as where the cubic nonlinear term is close to zero, may require the inclusion of higher–order nonlinearities leading to the so-called cubic–quintic CGLE. This has proved to be a rich system with very diverse solution behaviors. In particular, a relatively early and influential review by van Saarloos and Hohenberg [11], also recently extended to two coupled cubic CGL equations [12, 13], considered phase–plane counting arguments for traveling wave coherent structures, some analytic and perturbative

solutions, limited comparisons to numerics, and so-called "linear marginal stability analysis" to select the phase speed of the traveling waves.

Among the multitude of other papers, we shall only refer to two sets of studies which will directly pertain to the work in this dissertation. The first class of papers [14, 15, 16] and [17, 18] used dynamical systems techniques to prove that the cubic–quintic CGLE admits periodic and quasi–periodic traveling wave solutions.

The second class of papers [19, 20], primarily involving numerical simulations of the full cubic–quintic CGL PDE in the context of Nonlinear Optics, revealed various branches of plane wave solutions which are referred to as continuous wave (CW) solutions in the Optics literature. More importantly, these latter studies also found various spatially confined coherent structures of the PDE, with envelopes which exhibit complicated temporal dynamics. In [20], these various structures are categorized as plain pulses (or regular stationary solutions), pulsating solitary waves, creeping solitons, slugs or snakes, erupting solitons, and chaotic solitons depending on the temporal behavior of the envelopes. Plain pulses are the regular stationary solitary wave solutions investigated for numerous integrable and non-integrable nonlinear PDEs over the last three decades. However the other five classes of solutions shown in Figs. 1.1–1.5, are novel for this system and they will be one of the primary features we will concentrate on this dissertation. In addition, note that the speed of the new classes of solutions may be zero, constant, or periodic (since it is determined by the boundary conditions it is an eigenvalue, the speed may be in principle also quasiperiodic or chaotic, although no such cases appear to have been reported). All indications are that these

classes of solutions, all of which have amplitudes which vary in time, do not exist as stable structures in Hamiltonian systems. Even if excited initially, amplitude modulated solitary waves restructure into regular stationary solutions [21]. Exceptions to this rule are the integrable models where the pulsating structures are nonlinear superpositions or fundamental solutions [22]. Hence, these classes of solutions are novel and they exist only in the presence of dissipation in the simulations of [20]. Also, secondary complete period doubling cascades of the pulsating solitons leading as usual to regimes of chaos are also found. This last feature for numerical solutions of the full cubic–quintic PDE is strongly reminiscent of the period doubling cascades found in [5, 6] for period solutions of the traveling wave reduced ODEs of the cubic CGLE.

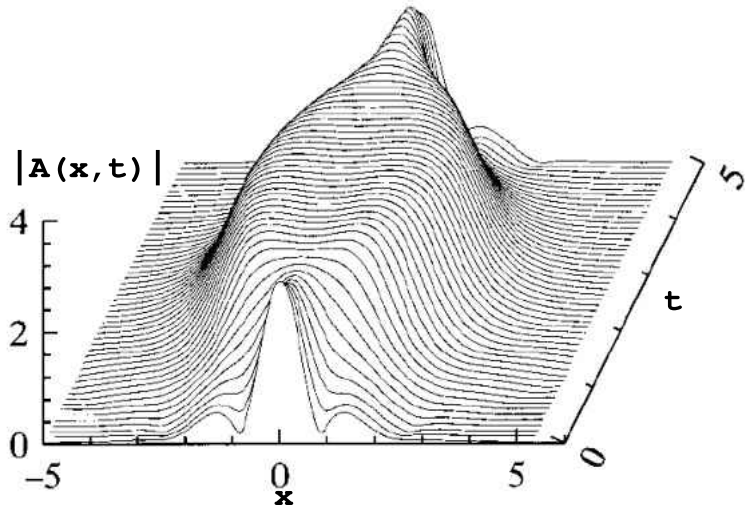


Figure 1.1: Plain pulsating soliton that shows periodic behavior with $\epsilon = -0.1$, $b_1 = 0.08$, $c_1 = 0.5$, $b_3 = -0.66$, $c_3 = 1$, $b_5 = 0.1$, $c_5 = -0.1$

In this context, we note that numerous attempts have been made to extend the well–developed concept of soliton interactions in integrable, conservative systems [23] to more

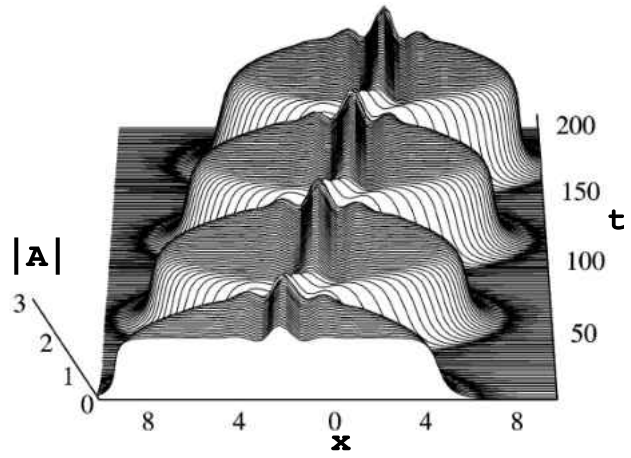


Figure 1.2: Creeping soliton with $\epsilon = -0.1$, $b_1 = 0.101$, $c_1 = 0.5$, $b_3 = -1.3$, $c_3 = 1$, $b_5 = 0.3$, $c_5 = -0.101$

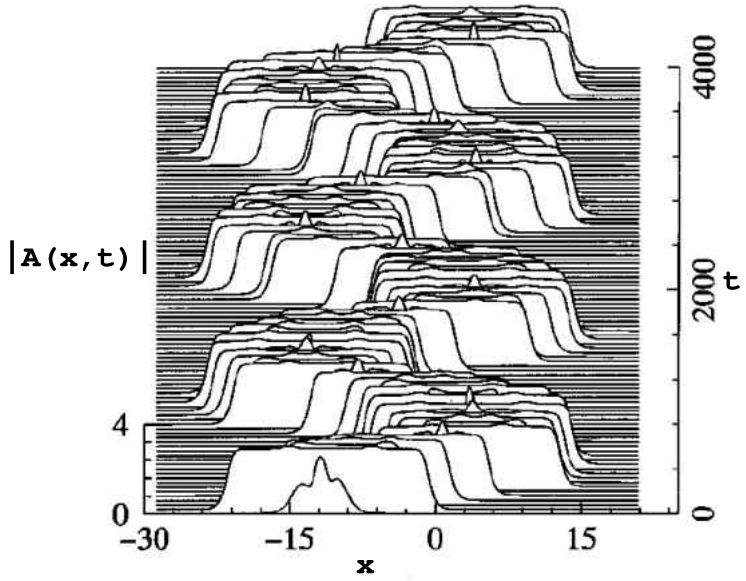


Figure 1.3: Snake or slug solitons with $\epsilon = -0.1$, $b_1 = 0.08$, $c_1 = 0.5$, $b_3 = -0.835$, $c_3 = 1$, $b_5 = 0.11$, $c_5 = -0.08$

realistic active or dissipative media which are governed by non-integrable model equations. The reason is that the complicated spatio–temporal dynamics of such coherent structure solutions are governed by simple systems of ordinary differential equations, or low–dimensional

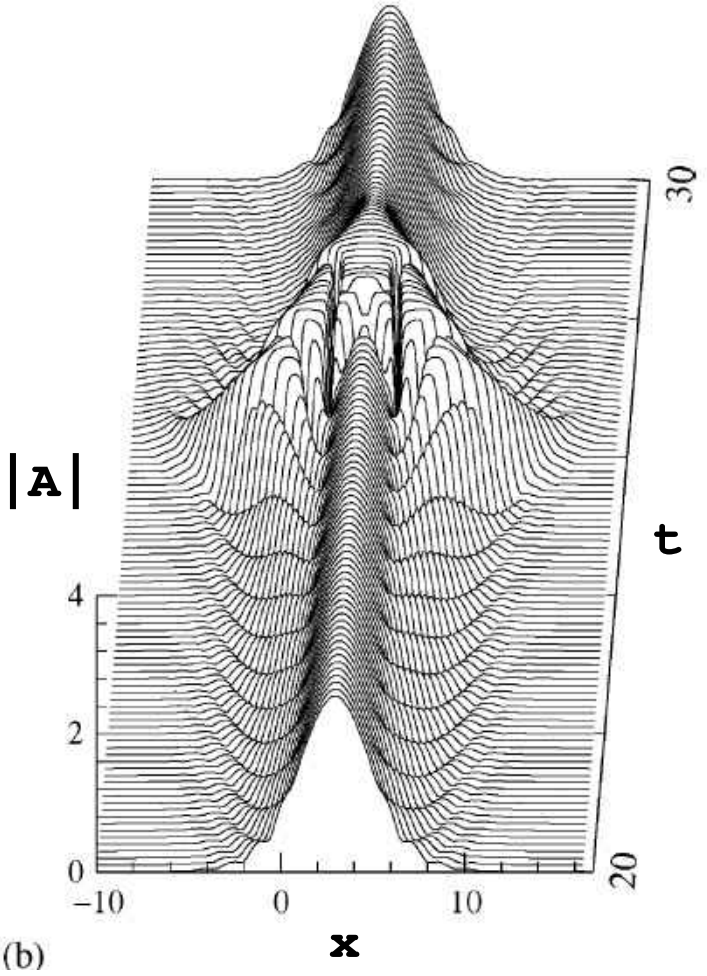


Figure 1.4: Exploding soliton with $\epsilon = -0.1$, $b_1 = 0.125$, $c_1 = 0.5$, $b_3 = -1$, $c_3 = 1$, $b_5 = 0.1$, $c_5 = -0.6$

dynamical systems, rather by the original complex nonlinear partial differential equation model. Hence, various theoretical approaches may be brought to bear on these ODEs.

There are situations [11, 23] and [24, 25] where this approach is appropriate, particularly where the dynamics of various active or dissipative systems is primarily governed by localized coherent structures such as pulses (solitary waves) and kinks (fronts or shocks). Such coherent structures could also be information carriers, such as in Optics. Since such struc-

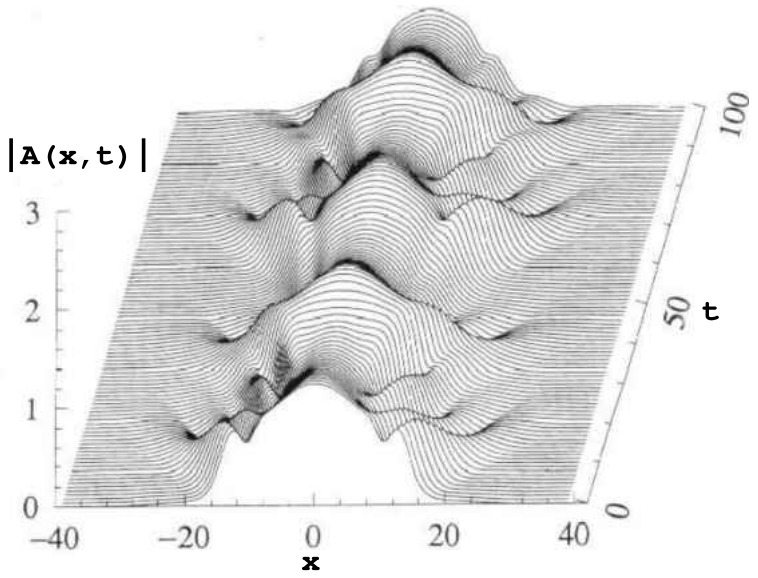


Figure 1.5: Chaotic but spatially localized soliton with $\epsilon = -0.1$, $b_1 = 0.125$, $c_1 = 0.5$, $b_3 = -0.3$, $c_3 = 1$, $b_5 = 0.1$, $c_5 = -1$

tures correspond to spatial modulations, they are also often referred to spatially–localized "patterns". The speeds and locations of the coherent structures may vary in a complex manner as they interact, but their spatial coherence is preserved in such situations. It is tempting to apply this approach to any system which admits pulse and/or kink solutions, but caution is necessary. Coherent structures may be transitory when they are unstable to small disturbances in their neighborhood. Also, only some of them may be actually selected, due to such stability considerations.

Another relevant feature of dissipative systems is that they include energy exchange with external sources. Such systems are no longer Hamiltonian, and the solitons in these systems are also qualitatively different from those in Hamiltonian systems. In Hamiltonian systems, soliton solutions appear as a result of balance between diffraction (dispersion) and

nonlinearity. Diffraction spreads a beam while nonlinearity will focus it and make it narrower. The balance between the two results in stationary solitary wave solutions, which usually form a one parameter family. In dissipative systems with gain and loss, in order to have stationary solutions, the gain and loss must be also balanced. This additional balance results in solutions which are fixed. Then the shape, amplitude and the width are all completely fixed by the parameters of the dissipative equation. This situation is shown schematically in Fig. 1.6. However, the solitons, when they exist, can again be considered as "modes" of dissipative systems just as for nondissipative ones.

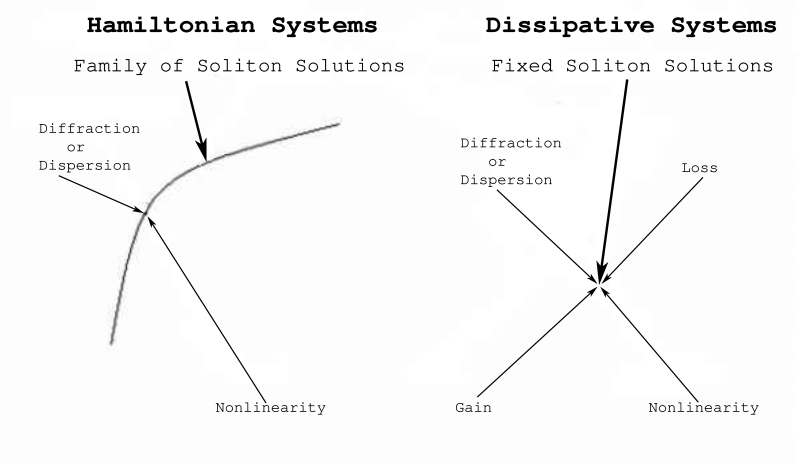


Figure 1.6: Qualitative difference between the soliton solutions in Hamiltonian and dissipative systems

To briefly recapitulate, the numerical results on dissipative solitons [20, 26] indicate:

(a) five new classes of stable amplitude modulated solutions unique to dissipative systems, and

(b) interesting bifurcation sequences of these solutions as parameters are varied.

In addition, a question of great interest [26] is the effect of the system parameters viz. dispersion/nonlinearity/linear and nonlinear gain and loss/spectral filtering on both the structure and the stability of these new classes of dissipative solitons. This last feature was repeatedly mentioned by many speakers in the multi–day session on Dissipative Solitons at the $4^{\text{th}}$ IMACS Conference on Nonlinear Waves held in Athens, Georgia in April 2005.

The above then defines the main themes to be explored in this dissertation. In the first part, comprising Chapters 2 and 3, we use a traveling wave reduction or a so–called spatial approximation to investigate the bifurcations of plane wave and periodic solutions of the CGLE. The primary tools used here are Singularity Theory and Hopf bifurcation theory respectively. We also comment briefly in Chapter 4 on possible extensions of this bifurcation analysis using the theory of generalized Hopf bifurcations to track the emergence of global structure. We have explored this in preliminary fashion, in a manner analogous to the so–called continuous stirred tank reactor system [27, 28]. However, we are not convinced that it is a particularly worthwhile avenue to pursue here since its actual relevance to the simulations in [20] seems questionable.

In the second part of this dissertation, we shift gears to focus on the issues of central interest in the area, i.e., the conditions for the occurrence of the five categories of dissipative solitons (Figs. 1.1–1.5), as well the dependence of both their shape and their stability on the nonlinearity, dispersion, linear and nonlinear gain, loss and spectral filtering parameters.

In the language of the Los Alamos school, the fully spatiotemporal approach followed here may be said to be the "collective coordinates" formulation. In other words, we consider

a pulse or solitary wave at any time as a coherent collective entity (or coordinate). This solitary wave is then temporally modulated. The approaches proposed, and already partially explored, in this second part of the dissertation are the two main theoretical tools usually applied to nonintegrable nonlinear PDEs, viz.

(a) the variational method, and

(b) perturbation theory.

However, each method is very significantly and non–trivially generalized from all earlier applications to deal with our novel classes of dissipative solitary waves. We are very grateful to David Kaup, Jianke Yang and Roberto Camassa for discussions on these formulations. The variational method seems by far the more general of these two approaches, especially as most numerical results in [20] and [26] are far from the near–NLS or near–cubic–quintic–NLS regimes where perturbation theory applies.

An approach based on soliton perturbation theory has recently been employed [29] to explain why non–stationary or amplitude modulated solitary waves should occur in dissipative systems, as well as their non–occurrence in the absence of dissipation. In particular, the occurrence of two of the five classes of dissipative solitons mentioned above, viz. the pulsating solitons and snakes (slugs) may be proved within this formulation in the near–NLS or near–cubic–quintic–NLS regimes. However, the other three classes, viz. the creeping, erupting (exploding), and chaotic solitons cannot be thus explained. In addition, as mentioned above, this approach is severely limited in that most numerical results are not in the

perturbative regime. David Kaup has been insistent that we be very attentive to this. And Nail Akhmediev has mentioned this too in his papers and his personal communications.

We would also like to particularly cite David Kaup's recent work, talks and conversations stressing the power, versatility and accuracy of the variational technique in constructing regular and embedded solitons of various complicated $\chi^2 - \chi^3$ systems. These were instrumental in focusing our attention on this method, and attempting to extend its use to new classes of dissipative solitons. Given this setting, in Chapters 5 and 6 we develop and discuss a variational formalism within which to explore the various classes of dissipative solitons. We will use two different trial functions that will represent two different shapes of the pulsating soliton. As mentioned, this is significantly generalized over earlier formulations in several crucial ways. Firstly, the starting formulations for the Lagrangian are recent [30] and not well explored. Also, after extensive discussions with David Kaup, the trial functions have been generalized considerably over conventional ones to keep the shape relatively simple (and the trial function integrable!) while allowing arbitrary temporal variation of the amplitude, width, position, speed and phase of the pulse. In addition, the resulting Euler–Lagrange equations are treated in a completely novel way. Rather than consider on the stable fixed points which correspond to the well–known stationary solitons or plain pulses, we use dynamical systems theory to focus on more complex attractors viz. periodic, quasiperiodic, and chaotic ones. Periodic evolution of the trial function parameters on a stable periodic attractor would yield solitons whose amplitudes are non–stationary or time dependent. In particular, pulsating, snake (and less easily, creeping) dissipative solitons may be treated

using stable periodic attractors of various trial function parameters. Chaotic evolution of the trial function parameters would yield chaotic solitary waves. This approach explored in Chapter 5, fails only to address the fifth class of dissipative solitons, viz. exploding or erupting solitons. We propose to explore the other two classes extensively within this formulation, including comparisons with numerical solutions and explorations of, and predictions about, the dependence of the soliton structure and stability on the various system parameters. In addition, the numerically documented period doubling seen in earlier simulations of the pulsating solitons is investigated in detail via the use of numerical diagnostics to explore period doublings of the periodic attractors for the trial function parameters. Chapter 7 summarizes the results and conclusions for the plane pulsating and snaking soliton and addresses the future work regarding the chaotic and creeping solitary waves.

# CHAPTER TWO: BIFURCATIONS AND COMPETING COHERENT STRUCTURES IN CGLE: PLANE WAVE (CW) SOLUTIONS

In this chapter, we begin by using Singularity Theory [22] to comprehensively categorize the plane wave (CW) solutions which were partially considered numerically in [19]. In addition, we shall be able to identify co–existing CW solutions in all parameter regimes together with their stability. The resulting dynamic behaviors will include hysteresis among co–existing branches, as well as the existence of isolated solution branches (isolas) separated from the main solution branch.

The remainder of this chapter is organized as follows. Section 2.1 considers two formulations for the traveling-wave reduced ODEs for the cubic-quintic CGLE, as well as CW solutions. Section 2.2 quickly recapitulates the standard stability analysis for individual CW solutions. In Section 2.3, which is the heart of the chapter, Singularity Theory is employed to comprehensively categorize all possible co–existing and competing plane wave solutions in general parameter regimes, as well as special cases corresponding to all possible quartic and cubic normal forms for singularities of codimension up to three. Note that we are computing stability of the traveling waves solutions. In particular, we shall concentrate on plane waves or continuous wave solutions of the full PDE. Section 2.4 considers the corresponding bifurcation diagrams as well as the resulting dynamical behaviors.

## 2.1 Traveling Wave Reduced ODEs

### 2.1.1 Reductions

We shall consider the cubic-quintic CGLE in the form [11]

$$\partial_t A = \epsilon A + (b_1 + ic_1)\partial_x^2 A - (b_3 - ic_3)|A|^2 A - (b_5 - ic_5)|A|^4 A \tag{2.1}$$

noting that any three of the coefficients (no two of which are in the same term) may be set to unity by appropriate scalings of time, space and $A$.

For the most part, we shall employ the polar form used in earlier treatments [5, 11] of the traveling wave solutions of (2.1). This takes the form of the ansatz

$$A(x,t) = e^{-i\omega t}\hat{A}(x - vt) = e^{-i\omega t}a(z)e^{i\phi(z)} \tag{2.2}$$

where

$$z \equiv x - vt \tag{2.3}$$

is the traveling wave variable and $\omega$ and $v$ are the frequency and translation speed (and are determined by the boundary conditions, and are thus eigenvalues of the uniformly translated solutions). Substitution of (2.2),(2.3) in (2.1) leads, after some simplification, to the three mode dynamical system

$$a_z = b \tag{2.4a}$$

$$b_z = a\psi^2 - \frac{(b_1\epsilon + c_1\omega)a + v(b_1 b + c_1\psi a) - (b_1 b_3 - c_1 c_3)a^3 - (b_1 b_5 - c_1 c_5)a^5}{b_1^2 + c_1^2} \tag{2.4b}$$

$$\psi_z = -\frac{2\psi b}{a} + \frac{-b_1\omega + c_1\epsilon + v\left(\frac{c_1 b}{a} - b_1\psi\right) - (b_1 c_3 + b_3 c_1)a^2 - (b_1 c_5 + b_5 c_1)a^4}{b_1^2 + c_1^2} \tag{2.4c}$$

where $\psi \equiv \phi_z$. Note that we have put the equations into a form closer to that in [5], rather than that in [11], so that (2.4) is a generalization of the traveling wave ODEs in [5] to include the quintic terms.

For future reference, we also include the fourth–order ODE system one would obtain from (2.1) using the rectangular representation

$$A(x,t) = e^{-i\omega t}\hat{A}(x-vt) = e^{-i\omega t}[\alpha(z) + i\beta(z)] \tag{2.5}$$

with $z$ given by (2.3). Using (2.5) in (2.1) yields the system:

$$-c_1\delta_z + b_1\gamma_z = \Gamma_1 \tag{2.6a}$$

$$b_1\delta_z + c_1\gamma_z = \Gamma_2 \tag{2.6b}$$

where $\gamma = \alpha'$, $\delta = \beta'$, $' = \mathrm{d}/\mathrm{d}z$, and $\Gamma_1, \Gamma_2$ are given below. This may be written as a first order system

$$\begin{aligned} \alpha' &= \gamma \\ \beta' &= \delta \\ (b_1^2 + c_1^2)\gamma' &= b_1\Gamma_1 + c_1\Gamma_2 \\ (b_1^2 + c_1^2)\delta' &= b_1\Gamma_2 - c_1\Gamma_1 \end{aligned} \tag{2.7}$$

with

$$\Gamma_1 = \omega\beta - v\gamma - \epsilon\alpha + (b_3\alpha + c_3\beta)(\alpha^2+\beta^2) + (b_5\alpha + c_5\beta)(\alpha^2+\beta^2)^2 \tag{2.8a}$$

and

$$\Gamma_2 = -\omega\alpha - v\delta - \epsilon\beta + (b_3\beta - c_3\alpha)(\alpha^2+\beta^2) + (b_5\beta - c_5\alpha)(\alpha^2+\beta^2)^2. \tag{2.8b}$$

### 2.1.2 Fixed Points and Plane (Continuous) Wave Solutions

From (2.2), a fixed point $(a_0, 0, \psi_0)$ of (2.4) corresponds to a plane wave solution

$$A(x,t) = a_0 e^{i(\psi_0 z - \omega t) + i\theta} \tag{2.9}$$

with $\theta$ an arbitrary constant.

The fixed points of (2.4a)–(2.4c) may be obtained by setting $b = 0$ (from (2.4a)) in the right hand sides of the last two equations, solving the last one for $\psi$, and substituting this in the second yielding the quartic equation

$$\alpha_4 x^4 + \alpha_3 x^3 + \alpha_2 x^2 + \alpha_1 x + \alpha_0 = 0 \tag{2.10}$$

with

$$x = a^2, \tag{2.11a}$$

$$\alpha_4 = \frac{(b_1 c_5 + b_5 c_1)^2}{b_1^2 v^2} \tag{2.11b}$$

$$\alpha_3 = \frac{2(b_1 c_3 + b_3 c_1)(b_1 c_5 + b_5 c_1)}{b_1^2 v^2} \tag{2.11c}$$

$$\alpha_2 = \frac{b_3^2 c_1^2 + 2 b_1 b_3 c_1 c_3 - 2 b_5 c_1^2 \epsilon}{b_1^2 v^2} + \frac{b_5 v^2 + b_1(c_3^2 + 2 c_5 \omega) + 2 c_1 (b_5 \omega - c_5 \epsilon)}{b_1 v} \tag{2.11d}$$

$$\alpha_1 = \frac{b_3}{b_1} + \frac{2(b_1\omega - c_1\epsilon)(b_1 c_3 + b_3 c_1)}{b_1^2 v^2} \tag{2.11e}$$

$$\alpha_0 = \frac{(c_1\epsilon - b_1\omega)^2}{b_1^2 v^2} - \frac{\epsilon}{b_1}\,. \tag{2.11f}$$

Thus, with $a_0 = \sqrt{x}$ for $x$ any of the four roots of (2.10), we have a plane wave solution of the form (2.9).

The fixed points of the system (2.7) are given by $\gamma = \delta = 0$ and $\Gamma_1 = \Gamma_2 = 0$. They may be obtained by eliminating the $\alpha$ and $\beta$ terms by solving $\Gamma_1 = \Gamma_2 = 0$ simultaneously yielding:

$$\alpha^2 + \beta^2 = 0$$

or

$$\alpha^2 + \beta^2 = \frac{b_5\omega + c_5\epsilon}{b_3c_5 - b_5c_3}.$$

Resubstituting these into the $\Gamma_1 = \Gamma_2 = 0$ yields only the trivial fixed point

$$\alpha = \beta = 0. \tag{2.12}$$

Thus, the system (2.7) has no non-trivial plane wave solutions.

In the next section, we begin the consideration of the stability, co–existence and bifurcations of the plane wave states of (2.1) (the fixed points of (2.4a)– (2.4c)).

### 2.2 Stability Analysis for Individual Plane Wave Solutions

In this section, we conduct a stability analysis of individual plane wave solutions using regular phase plane techniques. This was already done for the alternative formulation of the traveling wave ODEs given in [11]. We provide a brief derivation for our system (2.4a)–(2.4c) for completeness and future use. However, a much more complex question is the issue of categorizing and elucidating the possible existence of, and transitions among, multiple plane

wave states which may co–exist for the same parameter values in (2.1) (corresponding to the same operating conditions of the underlying system). Such behavior is well–documented in systems such as the Continuous Stirred Tank Reactor System [22, 26]. For a system such as (2.1) and the associated ODEs (2.4a)–(2.4c), the large number of parameters makes a comprehensive parametric study of co–existing states bewilderingly complex, if not actually impracticable. This more complex issue is addressed in the next section.

For each of the four roots $x_i, i = 1, \ldots, 4$ of (2.10) corresponding to a fixed point of (2.4a)– (2.4c) or a plane wave $\sqrt{x_i}\ e^{i(\psi_i z - wt) + i\theta_i}$, the stability may be determined using regular phase–plane analysis. The characteristic polynomial of the Jacobian matrix of a fixed point $x_i = a_i^2$ of (2.4a)–(2.4c) may be expressed as

$$\lambda^3 + \delta_1\lambda^2 + \delta_2\lambda + \delta_3 = 0 \tag{2.13}$$

where

$$\delta_1 = \frac{2b_1 v}{b_1^2 + c_1^2} \tag{2.14a}$$

$$\begin{aligned}\delta_2 = \frac{1}{b_1^2 + c_1^2}\big[&3a^2(c_1c_3 - b_1b_3) + 5a^4(c_1c_5 - b_1b_5) \\ &+ (b_1\epsilon + c_1\omega) + 3(b_1^2 + c_1^2)\psi^2 + v(v - 3c_1\psi)\big]\end{aligned} \tag{2.14b}$$

$$\begin{aligned}\delta_3 = &\frac{4a^2\psi[(b_1c_3 + b_3c_1) + 2a^2(b_1c_5 + b_5c_1)]}{b_1^2 + c_1^2} \\ &+ \frac{1}{(b_1^2 + c_1^2)^2}\Big\{b_1c_1\psi v^2 - v\Big[a^2\Big(2b_3(b_1^2 + c_1^2) + b_1(b_1b_3 - c_1c_3)\Big) \\ &+ a^4\Big(4b_5(b_1^2 + c_1^2) + b_1(b_1b_5 - c_1c_5)\Big) - b_1\Big((b_1\epsilon + c_1\omega) - \psi^2(b_1^2 + c_1^2)\Big)\Big]\Big\},\end{aligned} \tag{2.14c}$$

where the fixed point values $(a_i, \psi_i) = (\sqrt{x_i}, \psi_i)$ are to be substituted in terms of the system parameters of Section 2.1. Note that $\psi_i$ is obtained by setting $a = a_i = \sqrt{x_i}$, and $b = 0$ in the right side of (2.4c).

Using the Routh–Hurwitz conditions, the corresponding fixed point is stable for

$$\delta_1 > 0, \quad \delta_3 > 0, \quad \delta_1\delta_2 - \delta_3 > 0. \tag{2.15}$$

Equation (2.15) is thus the condition for stability of the plane wave corresponding to $x_i$.

On the contrary, one may have the onset of instability of the plane wave solution occurring in one of two ways. In the first, one root of (2.13) (or one eigenvalue of the Jacobian) becomes non–hyperbolic by going through zero for

$$\delta_3 = 0. \tag{2.16}$$

Equation (2.16) is thus the condition for the onset of "static" instability of the plane wave. Whether this bifurcation is a pitchfork or transcritical one, and its subcritical or supercritical nature, may be readily determined by deriving an appropriate canonical system in the vicinity of (2.16) using any of a variety of normal form or perturbation methods [23, 24, 25].

One may also have the onset of dynamic instability ("flutter" in the language of Applied Mechanics) when a pair of eigenvalues of the Jacobian become purely imaginary. The consequent Hopf bifurcation at

$$\delta_1\delta_2 - \delta_3 = 0 \tag{2.17}$$

leads to the onset of periodic solutions of (2.4a)–(2.4c) (dynamic instability or "flutter"). These periodic solutions for $a(z)$ and $\psi(z)$, which may be stable or unstable depending on

the super– or subcritical nature of the bifurcation, correspond via (2.2) to solutions

$$A(x,t) = a(z)e^{i\left(\int \psi dz - \omega t\right)} \tag{2.18}$$

of the CGLE (2.1) which are, in general, quasiperiodic wavetrain solutions. This is because the period of $\psi$ and $\omega$ are typically incommensurate. Eq. (2.18) is periodic if $\omega = 0$.

Here, we change gears to address the more difficult question of the possible coexistence of, and transitions among, multiple plane wave states for the same parameter sets.

## 2.3 Co–existing and Competing Plane Waves

As mentioned earlier, for a multiparameter system like (2.1), and the associated ODEs (2.4a)–(2.4c), a comprehensive parametric study of co–existing states is forbiddingly complex, if not actually impracticable. Theoretical guidance is needed to determine all the multiplicity features in various parameter domains, as well as the stability of, and mutual transitions among, coexisting plane waves in each domain.

In this section, we use Singularity Theory [22] to comprehensively analyze such multiplicity features for (2.1), (2.4a)–(2.4c). In particular, we shall derive the existence conditions on the eight coefficients of the CGLE under which the steady state equation (2.10) assumes either (a) all possible quartic normal forms (the quartic fold, and an unnamed form), or (b) all distinct cubic normal forms (the pitchfork or the winged cusp) for singularities of codimension up to three. In addition, given that the most degenerate singularities or bifurcations tend to be the primary organizing centers for the dynamics, we also consider the even higher

codimension singularities leading to various quadratic normal forms. Clearly, the most degenerate singularities for a particular parameter set would "organize" the dynamics in the sense that local behavior in its vicinity predicts actual quasi–global results. In fact, since we employ the actual governing equations, the ensuing results are not just locally valid, as is often the case, but they have global applicability.

First, denoting (2.10) as

$$g(x, \alpha_i) = \alpha_4 x^4 + \alpha_3 x^3 + \alpha_2 x^2 + \alpha_1 x + \alpha_0 = 0 \tag{2.19}$$

where $g$ denotes the "germ" and the $\alpha_i$ are given in terms of system parameters by (2.11), all points of bifurcation (where the Implicit Function Theorem fails) satisfy

$$g_x = 0. \tag{2.20}$$

Given a germ satisfying (2.19) and (2.20), the general Classification Theorem in [22] provides a comprehensive list of all possible distinct normal forms to which it may be reduced for bifurcations of codimension less than or equal to three.

For our $g$, which is already in polynomial form, it is particularly straightforward to reduce it to each of these normal forms in turn and this is what we shall do next. Following this, we shall consider the general form (2.19) itself. We start first with the possible distinct quartic normal forms viz., the "Quartic Fold" and an unnamed form, and then proceed systematically to lower order normal forms. In the standard manner, the so–called "recognition problem" or identification of each normal form yields certain defining conditions and non–degeneracy conditions and we check these first for each form. Each normal form has a well–known

"universal unfolding" or canonical form under any possible perturbation [22]. This is so under certain other non–degeneracy conditions (the conditions for the solution of the so–called recognition problem) which we next satisfy. Once the universal unfolding is established, we next need to consider the various parameter regions (for the parameters in the unfolding) where distinct behaviors for the solutions $x$ occur. The boundaries of these regions are the so–called "transition varieties" across which these behaviors change or are non–persistent. We consider these next. The final step involves detailing in each region delimited by two adjacent "transition variety" curves the bifurcation diagram for $x$, i.e., the possible co–existing steady states of (2.4a)–(2.4c) (or plane waves of (2.1)) and their stability.

### 2.3.1 The Quartic Fold

We perform the steps mentioned above for the first quartic normal form, viz. the Quartic Fold

$$h_1(x,\lambda) = \overline{\epsilon}x^4 + \delta\lambda. \tag{2.21}$$

Clearly, our germ (2.19) has this form for

$$\begin{aligned} &\alpha_4 = \overline{\epsilon}, \\ &\alpha_3 = \alpha_2 = \alpha_1 = 0 \\ &\alpha_0 = \delta\lambda. \end{aligned} \tag{2.22}$$

For the normal form (2.21), the universal unfolding is

$$G_1(x,\lambda) = \bar{\epsilon}x^4 + \delta\lambda + \alpha x + \beta x^2 \tag{2.23}$$

with defining conditions

$$g_{xx} = g_{xxx} = 0, \tag{2.24}$$

non–degeneracy conditions

$$\bar{\epsilon} = \text{sgn}\left(\frac{\partial^4 h_1}{\partial x^4}\right), \quad \delta = \text{sgn}\left(\frac{\partial h_1}{\partial \lambda}\right)$$

and provided the condition for the solution of the recognition problem

$$\begin{vmatrix} g_\lambda & g_{\lambda x} & g_{\lambda xx} \\ G_{1\alpha} & G_{1\alpha x} & G_{1\alpha xx} \\ G_{1\beta} & G_{1\beta x} & G_{1\beta xx} \end{vmatrix} \neq 0 \tag{2.25}$$

is satisfied. Given (2.19) and (2.22), the conditions (2.23) are automatically satisfied, while (2.25) yields the condition

$$\delta \neq 0. \tag{2.26}$$

The transition varieties across which the $(\lambda, x)$ bifurcation diagrams change character are:

i. The Bifurcation Variety

$$\mathcal{B} = \{\vec{\alpha} \in R^k : (x,\lambda) \text{ such that } G = G_x = G_\lambda = 0 \text{ at } (x,\lambda,\alpha)\}. \tag{2.27}$$

ii. The Hysteresis Variety

$$\mathcal{H} = \{\vec{\alpha} \in R^k : (x, \lambda) \text{ such that } G = G_x = G_{xx} = 0 \text{ at } (x, \lambda, \alpha)\}. \tag{2.28}$$

iii. The Double Limit Variety

$$\mathcal{D} = \{\vec{\alpha} \in R^k : (x_1, x_2, \lambda), x_1 \neq x_2 \text{ such that } G = G_x = 0 \text{ at } (x_i, \lambda, \alpha), i = 1, 2\}. \tag{2.29}$$

We compute these here since the derivations are not given in [22]. For $\mathcal{B}$, we need

$$G_{1x} = 4\bar{\epsilon}x^3 + \alpha + 2\beta x = 0$$

and

$$G_{1\lambda} = \delta = 0.$$

However, $\delta \neq 0$ by (2.26), and hence the bifurcation set is just the null set

$$\mathcal{B} = \varnothing. \tag{2.30}$$

For $\mathcal{H}$, we need

$$G_{1x} = 4\bar{\epsilon}x^3 + \alpha + 2\beta x = 0$$

$$G_{1xx} = 12\bar{\epsilon}x^2 + 2\beta = 0$$

which yield

$$\mathcal{H} = \left\{ \left(\frac{\alpha}{8\bar{\epsilon}}\right)^2 = -\left(\frac{\beta}{6\bar{\epsilon}}\right)^3, \ \ \beta \leq 0 \right\}. \tag{2.31}$$

Similarly, using (2.29), it is straightforward to derive the double limit set

$$\mathcal{D} = \{\alpha = 0, \beta \leq 0\}. \tag{2.32}$$

In the $(\alpha, \beta)$ plane, the $(\lambda, x)$ bifurcation diagrams change character across the curves (2.30)–(2.32), so that there are different multiplicities of steady–states in the regions they delimit. We shall consider this in detail in the next section.

### 2.3.2 A Second Quartic Normal Form

Repeating the above steps for the other possible distinct normal form

$$h_2(x, \lambda) = \bar{\epsilon} x^4 + \delta \lambda x, \tag{2.33}$$

our germ (2.19) takes this form for

$$\begin{aligned} &\alpha_4 = \bar{\epsilon} \\ &\alpha_3 = \alpha_2 = \alpha_0 = 0 \\ &\alpha_1 = \delta \lambda. \end{aligned} \tag{2.34}$$

For the normal form (2.33), the universal unfolding is

$$G_2(x, \lambda) = \bar{\epsilon} x^4 + \delta \lambda x + \alpha + \beta \lambda + \gamma x^2 \tag{2.35}$$

with defining conditions

$$g_{xx} = g_{xxx} = g_\lambda = 0, \tag{2.36}$$

non–degeneracy conditions which are automatically satisfied, and the solution of the recognition problem yielding the condition

$$\begin{vmatrix} 0 & 0 & g_{x\lambda} & 0 & g_{xxxx} \\ 0 & g_{\lambda x} & g_{\lambda\lambda} & g_{\lambda xx} & g_{\lambda xxx} \\ G_{2\alpha} & G_{2\alpha x} & G_{2\alpha\lambda} & G_{2\alpha xx} & G_{2\alpha xxx} \\ G_{2\beta} & G_{2\beta x} & G_{2\beta\lambda} & G_{2\beta xx} & G_{2\beta xxx} \\ G_{2\gamma} & G_{2\gamma x} & G_{2\gamma\lambda} & G_{2\gamma xx} & G_{2\gamma xxx} \end{vmatrix} \neq 0. \tag{2.37}$$

For (2.19)/(2.34), (2.36) is satisfied, while (2.37) yields

$$\bar{\epsilon}\delta \neq 0, \quad \text{or} \quad \alpha_1\alpha_4 \neq 0. \tag{2.38}$$

We derive the transition varieties for this case since derivations are not provided in [22].

For $\mathcal{B}$:

$$G_{2x} = 4\bar{\epsilon}x^3 + \delta\lambda + 2\gamma x = 0$$

$$G_{2\lambda} = \delta x + \beta = 0$$

which, together with (2.35), yield

$$\mathcal{B} : \frac{\bar{\epsilon}\beta^4}{\delta^4} + \frac{\gamma\beta^2}{\delta^2} + \alpha = 0. \tag{2.39}$$

For $\mathcal{H}$:

$$G_{2xx} = 0 \Rightarrow \gamma = -6\bar{\epsilon}x^2$$

and

$$G_{2x} = 0 \Rightarrow \delta\lambda = 8\bar{\epsilon}x^3.$$

Together, these yield

$$\lambda^2 = -\Big(\frac{2\gamma}{3}\Big)^3 \frac{1}{\delta^2\overline{\epsilon}}.$$

Using these in (2.35) yields the hysteresis curve:

$$\mathcal{H} : \Big(\alpha + \frac{\gamma^2}{12\overline{\epsilon}}\Big)^2 + \frac{8\gamma^3\beta^2}{27\delta^2\overline{\epsilon}} = 0. \tag{2.40}$$

Similarly, the double limit curve $\mathcal{D}$ is:

$$\mathcal{D} : 4\alpha = \gamma^2, \quad \gamma \leq 0. \tag{2.41}$$

In the next two subsections, we summarize similar results for the two distinct cubic normal forms, but omit the details. Then we briefly mention the four possible quadratic normal forms for even more degenerate cases, before concluding the section with the general, least degenerate case.

### 2.3.3 The Pitchfork

For our germ (2.19) to have the cubic normal form for the well–known pitchfork bifurcation

$$h_3(x, \lambda) = \overline{\epsilon}x^3 + \delta\lambda x \tag{2.42}$$

we require

$$\alpha_4 = \alpha_2 = \alpha_0 = 0$$

$$\alpha_3 = \overline{\epsilon},$$

$$\alpha_1 = \delta\lambda. \tag{2.43}$$

This will have a universal unfolding [22]

$$G_3 = \bar{\epsilon}x^3 + \delta\lambda x + \alpha + \beta x^2 \tag{2.44}$$

provided

$$\begin{vmatrix} 0 & 0 & h_{3x\lambda} & h_{3xxx} \\ 0 & h_{3\lambda x} & h_{3\lambda\lambda} & h_{3\lambda xx} \\ G_{3\alpha} & G_{3\alpha x} & G_{3\alpha\lambda} & G_{3\alpha xx} \\ G_{3\beta} & G_{3\beta x} & G_{3\beta\lambda} & G_{3\beta xx} \end{vmatrix} = \delta \neq 0.$$

The well–known transition varieties, generalized to our notation, are:

$$\mathcal{B}: \quad \alpha = 0 \tag{2.45}$$

$$\mathcal{H}: \quad \alpha = \frac{\beta^3}{27\bar{\epsilon}^2} \tag{2.46}$$

$$\mathcal{D}: \quad \varnothing. \tag{2.47}$$

### 2.3.4 The Winged Cusp

The other distinct cubic normal form

$$h_4(x, \lambda) = \bar{\epsilon}x^3 + \delta\lambda^2 \tag{2.48}$$

requires

$$\alpha_4 = \alpha_2 = \alpha_1 = 0$$

$$\alpha_3 = \bar{\epsilon},$$

$$\alpha_0 = \delta\lambda^2. \tag{2.49}$$

This has a universal unfolding [22]

$$G_4(x,\lambda) = \bar{\epsilon}x^3 + \delta\lambda^2 + \alpha + \beta x + \gamma\lambda x \tag{2.50}$$

provided

$$\begin{vmatrix} 0 & 0 & h_{4x\lambda} & h_{4xxx} \\ 0 & h_{4\lambda x} & h_{4\lambda\lambda} & h_{4\lambda xx} \\ G_{4\alpha} & G_{4\alpha x} & G_{4\alpha\lambda} & G_{4\alpha xx} \\ G_{4\beta} & G_{4\beta x} & G_{4\beta\lambda} & G_{4\beta xx} \end{vmatrix} = -12\delta\epsilon \neq 0.$$

The transition varieties, for our unfolding $G_4$, are:

$$\mathcal{B}: \quad \alpha = 2x^3 - \frac{\gamma^2}{4}x^2, \quad \beta = -3x^2 + \frac{\gamma^2 x}{2} \tag{2.51}$$

$$\mathcal{H}: \quad \alpha\gamma^2 + \beta^2 = 0, \quad \alpha \leq 0 \tag{2.52}$$

$$\mathcal{D}: \quad \varnothing. \tag{2.53}$$

### 2.3.5 Quadratic Normal Forms

Since our system of ODEs has many parameters, we may clearly have more degenerate (higher codimension) cases corresponding to any of the distinct quadratic normal forms

$$h_5(x,\lambda) = \bar{\epsilon}x^2 + \delta\lambda \tag{2.54}$$

$$h_6(x,\lambda) = \bar{\epsilon}(x^2 - \lambda^2) \tag{2.55}$$

$$h_7(x,\lambda) = \bar{\epsilon}(x^2 + \lambda^2) \tag{2.56}$$

$$h_8(x,\lambda) = \bar{\epsilon}x^2 + \delta\lambda^3 \tag{2.57}$$

or

$$h_9(x,\lambda) = \overline{\epsilon}x^2 + \delta\lambda^4 \tag{2.58}$$

Each of these is obtained by matching our germ (2.19) to the appropriate form, with the defining and non–degeneracy conditions automatically being satisfied (because (2.19) is polynomial). Solving the recognition problem [22], the corresponding unfoldings are respectively

$$G_5(x,\lambda) = \overline{\epsilon}x^2 + \delta\lambda \tag{2.59}$$

$$G_{6,7}(x,\lambda) = \overline{\epsilon}(x^2 + \delta\lambda^2 + \alpha) \tag{2.60}$$

(with $\delta < 0$ for (2.55) and $\delta > 0$ for (2.56))

$$G_8(x,\lambda) = \overline{\epsilon}x^2 + \delta\lambda^3 + \alpha + \beta\lambda \tag{2.61}$$

$$G_9(x,\lambda) = \overline{\epsilon}x^2 + \delta\lambda^4 + \alpha + \beta\lambda + \gamma\lambda^2 \tag{2.62}$$

with determinant conditions [22] for the cases (2.61) and (2.62) which may be straightforwardly enforced as in previous cases. The $\mathcal{B}$, $\mathcal{H}$, and $\mathcal{D}$ curves for these cases are straightforward generalizations of those given in [22], and they may be derived as for the quartic and cubic cases.

### 2.3.6 General Case

Finally, we include the most general possibility where, for arbitrary parameters in the CGLE (2.1), we have the germ (2.19) with all $\alpha_i$ non–zero. Treating (2.19) itself as the unfolding,

with $\alpha_0$ the bifurcation parameter $\lambda$, the transition varieties in the $(\alpha_1, \alpha_2)$ plane are:

$$\mathcal{B} \ : \ \varnothing \tag{2.63}$$

$$\mathcal{H} \ : \ \alpha_2 = -6\alpha_4 x^2 - 3\alpha_3 x$$

$$\alpha_1 = 8\alpha_4 x^3 + 3\alpha_3 x^2 \tag{2.64}$$

$$\mathcal{D} \ : \ \text{identical to } \mathcal{H} \text{ (see Theorem 1)} \tag{2.65}$$

**Theorem 1.** *The Double Limit Variety for* (2.19) *is identical to the Hysteresis Variety of* (2.64).

*Proof.* Using (2.19) and (2.29), $\mathcal{D}$ is defined by the equations

$$G(x_1, \lambda) = 0 \tag{2.66a}$$

$$G(x_2, \lambda) = 0 \tag{2.66b}$$

$$G_x(x_1, \lambda) = 0 \tag{2.66c}$$

$$G_x(x_2, \lambda) = 0. \tag{2.66d}$$

Canceling the trivial solution $x_1 = x_2$, the equations obtained from the difference of (2.66a) and (2.66b), and of (2.66c) and (2.66d), yield respectively

$$\alpha_1 = -a(2b - a^2)\alpha_4 - b\alpha_3 - a\alpha_2 \tag{2.67a}$$

$$\alpha_2 = -\frac{1}{2}(4b\alpha_4 + 3a\alpha_3) \tag{2.67b}$$

where $a \equiv x_1 + x_2^2$, $b \equiv x_1^2 + x_1 x_2 + x_2^2$. Using (2.67b) in (2.67a), these yield

$$\alpha_1 = \Big(\frac{3a^2}{2} - b\Big)\alpha_3 + a^3\alpha_4 \tag{2.68a}$$

$$\alpha_2 = -\frac{3a}{2}\alpha_3 - 2b\alpha_4. \tag{2.68b}$$

The Eqts. (2.66a) and (2.66b) may be considered to define the bifurcation parameter $\alpha_0$ which we do not require here. However, (2.66c) and (2.66d) independently define $\alpha_1$ and thus far only their difference has been used. In order to incorporate $\alpha_1$, we consider the sum of (2.66c) and (2.66d) written in terms of a and b as:

$$4\alpha_4 a(3b - 2a^2) + 3\alpha_3(2b - a^2) + 2\alpha_2 a + 2\alpha_1 = 0.$$

Using (2.68) in this equation and simplifying yields

$$b = \frac{3a^2}{4}. \tag{2.69}$$

Using this in (2.68) yields the parametric equations for $\mathcal{D}$:

$$\alpha_1 = a^2\Big(\frac{3\alpha_3}{4} + \alpha_4 a\Big) \tag{2.70a}$$

$$\alpha_2 = -\frac{3a}{2}\Big(\alpha_3 + \alpha_4 a\Big). \tag{2.70b}$$

The re–parametrization $a = 2x$ puts this into exactly the form (2.64) of the hysteresis variety, thus proving the claim. □

Note that the $\mathcal{H}$ curve is parametrized in terms of $x$ (with $\alpha_3, \alpha_4$ being chosen values). Also, given the non–degenerate nature of this general case, it is not surprising that there is only one distinct transition variety.

## 2.4 Bifurcation Diagrams and Effects on the Dynamics

Having mapped out the $\mathcal{B}$, $\mathcal{H}$, and $\mathcal{D}$ curves for the various possible distinct quartic and cubic normal forms, we now proceed in this section to consider the various bifurcation diagrams in

the regions which they define in $(\alpha, \beta)$ space. These will then give us the multiplicities and stabilities of the various co–exisitng steady states of (2.4a)–(2.4c) (or plane wave solutions of (2.1)) in each region. In turn, these also enable us to consider dynamic features of the plane wave solutions. The dynamics will include hysteretic behaviors among co–existing plane waves. We will also find regimes of *isolated* plane wave behavior, both for a plane wave branch which co–exists with other branches but cannot interact with them, as well as those which actually occur only in isolation.

We first list examples of representative sets of parameters for which we may have the various degenerate cases considered in Section 2.3.

a. For the Quartic Fold of Section 2.3.1, typical parameters are:

   i. $b_1 = 0.0845$, $b_3 = -0.0846$, $b_5 = 0.0846$, $c_1 = c_3 = -c_5 = 1$, $\epsilon = 0.5$, $v = 0.1$, $\omega = 0$.

   ii. $b_1 = b_5 = 0.01696$, $b_3 = -0.0206$, $c_1 = 1$, $c_3 = 1.25$, $c_5 = -1$, $\epsilon = 0.5$, $v = 0.1$, $\omega = 0$.

b. For the Quartic Normal form of Section 2.3.2:

   i. $b_1 = 2.035$, $b_3 = 29.274$, $b_5 = 9.8496$, $c_1 = -0.1$, $c_3 = -1$, $c_5 = 0.08$, $\epsilon = 0.3$, $v = 0.3$, $\omega = 0.1$.

c. For the Pitchfork case of Section 2.3.3:

i. $b_1 = 0.0904$, $b_3 = 0.0679$, $b_5 = 0.1811$, $c_1 = -0.4$, $c_3 = 0.35$, $c_5 = 0.8$, $\epsilon = 0.2$, $v = 0.01$, $\omega = -0.9$.

ii. $b_1 = 0.0904$, $b_3 = 0.0823$, $b_5 = -0.1808$, $c_1 = -0.4$, $c_3 = 0.35$, $c_5 = -0.8$, $\epsilon = 0.2$, $v = 0.01$, $\omega = -0.9$.

d. For the Winged Cusp of Section 2.3.4:

i. $b_1 = 0.000923$, $b_3 = +.00005548$, $b_5 = 0.0013$, $c_1 = 0.5$, $c_3 = -0.03$, $c_5 = -0.7$, $\epsilon = 0.01$, $v = 0.1$, $\omega = 0.15$.

For the winged cusp unfolding (2.50) in the particular form

$$G_1(x, \lambda) = x^3 + \lambda^2 + \alpha + \beta x + \gamma \lambda x = 0,$$

the transition varieties (2.51) and (2.52) are shown in the $(\alpha, \beta)$ plane in Fig 2.1(1–3)for $\gamma < 0$, $\gamma = 0$, and $\gamma > 0$, respectively. They divide the $(\alpha, \beta)$ space into seven distinct regions. As mentioned earlier, the $(\lambda, x)$ bifurcation diagrams are isomorphous or "persistent" or of similar form within each region, and they change form across the transition varieties (or "nonpersistence" curves) as one crosses into an adjacent region. The representative bifurcation diagrams in each of the seven regions are shown in Fig. 2.2, and they give us a comprehensive picture of the co–existing plane wave solutions of (2.1) and their stability (given by the eigenvalues of the Jacobian, or here just the sign of $G_x$) in each region. Hence, as we shall consider next, one also has a clear picture of the ensuing dynamics from the plane wave interactions.

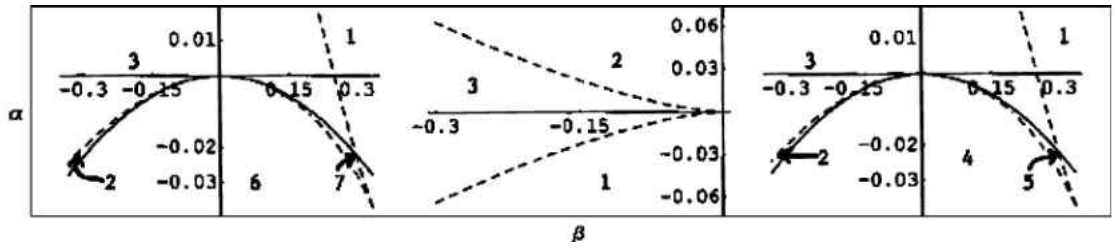


Figure 2.1: Transition varieties for the winged cusp (2.50) with $\bar{\epsilon} = 1 = \delta$ for the cases $\gamma < 0$, $\gamma = 0$, and $\gamma > 0$, respectively. $\mathcal{H}$ is in solid lines, and $\mathcal{B}$ is dashed.

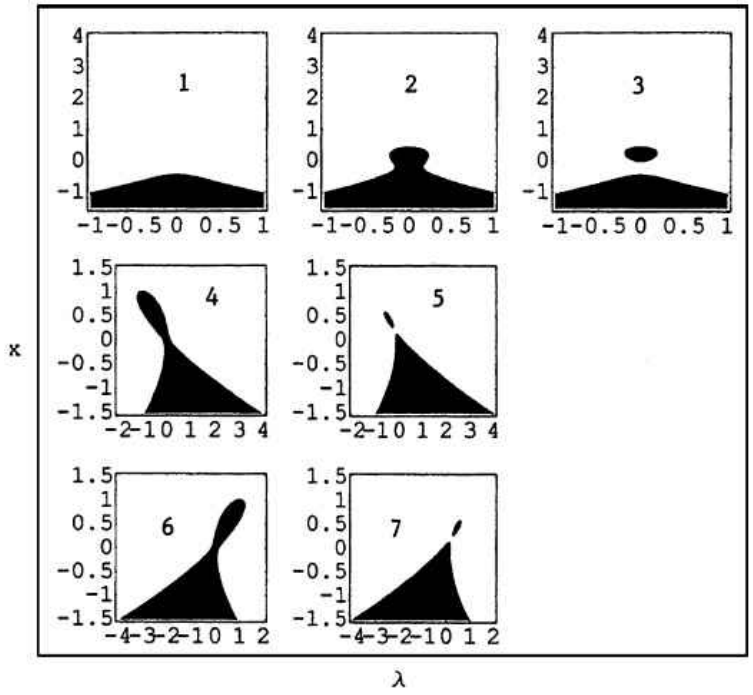


Figure 2.2: The $(\lambda, x)$ bifurcation diagrams in the regions 1–7 of Fig. 2.1, respectively.

First, note the mushroom shaped bifurcation diagram in Fig. 2.2(2) for region 2 of Fig. 2.1. Clearly, there are two distinct ranges of $\lambda$ (at the two ends of the mushroom) where three plane waves co-exist (with the central one being unstable). Thus the dynamics exhibits hysteresis. For instance, if $\lambda$ is decreased from large values, one stays on the lower branch until point A before jumping to the upper branch. If $\lambda$ is then increased, one stays on the

upper branch until B and then jumps back down to the lower one. Similar hysteresis occurs in regions 4–7 of Fig. 2.1 as seen in the corresponding bifurcation diagrams of Fig. 2.2(4–7). In each case, hysteresis occurs between the upper and lower fixed points in the range of $\lambda$ with three co–existing solutions (the central one is always unstable).

Another type of behavior is the isola, i.e., an isolated branch of solutions unconnected to the primary solution (the one at $\lambda \to \pm\infty$). Such isola type behavior is seen in Fig. 2.2(3,5,7) corresponding to regions 3,5,7 of Fig. 2.1 . In each case, the isola co–exists with the primary solution branch and is the chosen branch or not according to the initial conditions. However, once chosen, the dynamics is on the isola while $\lambda$ is in the domain of its existence once we leave this domain, the solution cannot jump to the primary branch and just disappears.

Next, we consider the normal form (2.33) in Section 2.3.2. Considering the unfolding (2.35) in the particular form

$$G_2(x, \lambda) = x^4 - \lambda x + \alpha + \beta\lambda + \gamma x^2 = 0,$$

the transition varieties (2.39)–(2.41) are shown in Fig. 2.3(1–3) for the cases $\gamma > 0$, $\gamma = 0$, and $\gamma < 0$ respectively. Note in particular, a significant correction to [3] in the $\mathcal{H}$ curve of Fig. 2.3(3). The $\mathcal{H}$ curve (2.40) represents a pair of straight lines in the $(\alpha, \beta)$ plane, rather than the incorrect form

$$\alpha + \frac{\gamma^2}{12\overline{\epsilon}} + \frac{8\gamma^3\beta^2}{27\delta^2\overline{\epsilon}} = 0$$

in [22]. In Fig. 2.3(3), one consequence is two new regions or domains 13 and 14 of the $(\alpha, \beta)$ space. Also, the bifurcation plots in the domains 3,4,5 and 8 are significantly modified from those given in [22] for the corresponding regions.

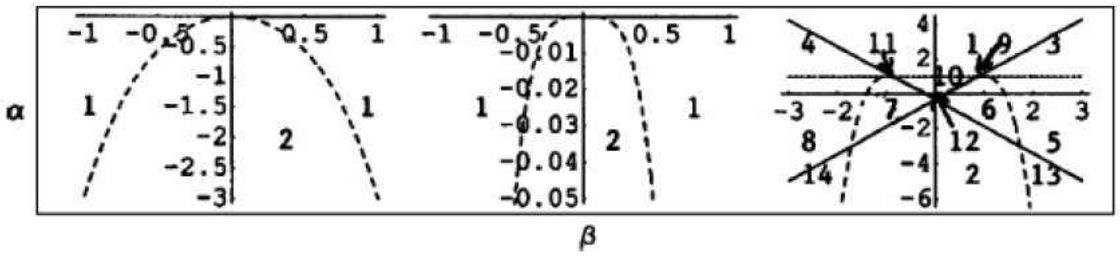


Figure 2.3: The transition varieties for the quartic normal form (2.35) with $\delta = -1$ for the cases $\gamma > 0$, $\gamma = 0$, and $\gamma < 0$, respectively. $\mathcal{H}$ is in solid lines, $\mathcal{B}$ is dashed and the double limit curve $\mathcal{D}$ is in fine dashing. The regions 1–14 which they delimit are shown.

The bifurcations plots in the fourteen regions in Fig. 2.3(3) (Fig. 2.3(1 and 2) feature only some of the regions) are shown in Figs. 2.4 and 2.5. Note that there are no regions of isola behavior. In regions 3,4,5 and 8, there is only one branch of solutions, rather than two as shown in Fig. 2.4 (case 10) of [22]. Of these, the segments BC and DE are unstable in cases 3 and 5, so that the hysteretic behavior of the solutions will consist of transitions from the stable plane waves on branch AB to those on branch CD as $\lambda$ is increased past point B, and a reverse transition when it is decreased through C. Similarly, in regions 4 and 8 where only segment BC is unstable, hysteresis occurs with a transition from the plane wave on branch DE to branch AB if $\lambda$ is decreased through D, a transition from branch CD to branch AB when $\lambda$ is decreased through D, and a transition from CD to either AB or DE (depending on system bias, noise et cetera) as $\lambda$ is increased through C. Analogous hysteresis behavior is clearly possible in regions 7 and 11, while regions 9, 10, and 12 feature hysteresis between co–existing stable plane wave solutions on *distinct* solution branches. In the two new regions 13 and 14 of Fig. 2.3(3) (which were missing in [22]), the bifurcation plots in Figs. 2.5(11 and 12) show only two co–existing plane wave solutions in each $\lambda$ range, unlike

the adjacent regions 5 and 8 of Fig. 2.3(3) where the bifurcation plots Fig. 2.4(5 and 8) have $\lambda$ ranges with four coeval solutions.

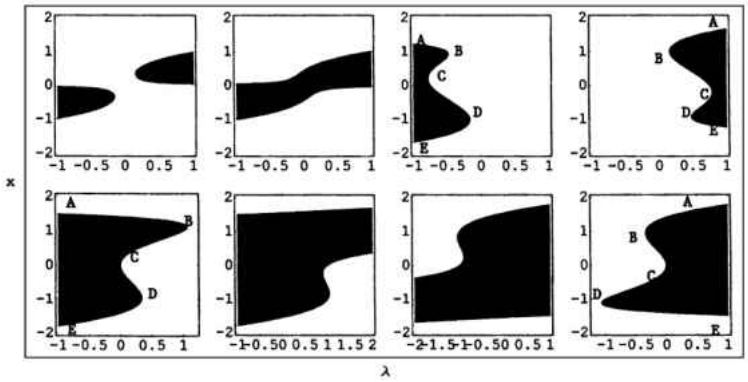


Figure 2.4: Bifurcation diagrams in the regions 1–8 of Fig. 2.3(3).

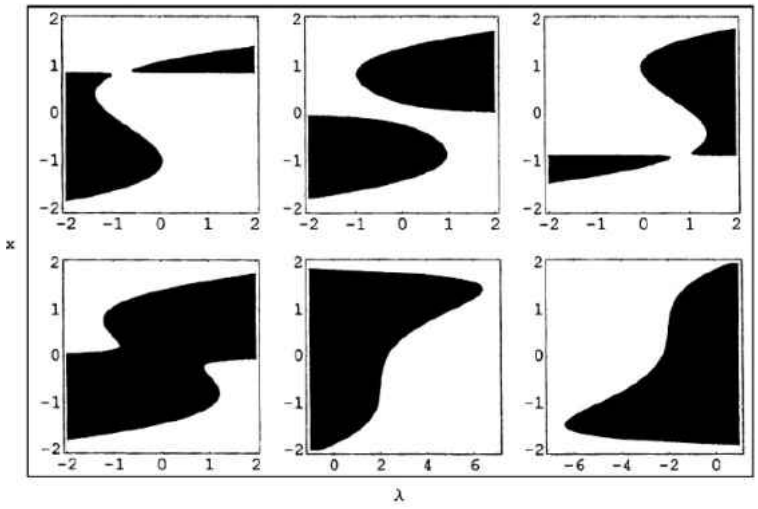


Figure 2.5: Bifurcation diagrams in the regions 9–14 of Fig. 2.3(3).

For the very degenerate cases discussed in Section 2.3.5 and corresponding to quadratic normal forms, the corresponding transition varieties as well as the bifurcation plots and resulting dynamics in the regions of $(\alpha, \beta)$ which they delimit may be deduced from the rele-

vant cases in Figures 4.1–4.3 of [22]. In particular, cases (2.60)–(2.62) show isola, hysteresis, and double isola behaviors respectively.

Let us consider the general case in Section 2.3.6 next. Since the results are entirely new, we need to consider the issue of the stability of the $(\lambda, x) \equiv (\alpha_0, x)$ bifurcation diagrams in various regions of the $(\alpha_1, \alpha_2)$ plane. Using (2.19),

$$\frac{\mathrm{d}G}{\mathrm{d}\lambda} \equiv \frac{\mathrm{d}G}{\mathrm{d}\alpha_0} = \frac{\partial G}{\partial x}\frac{\mathrm{d}x}{\mathrm{d}\lambda} + \frac{\partial G}{\partial \lambda} = 0,$$

so that

$$\frac{\partial G}{\partial x} = -\frac{1}{(\mathrm{d}x/\mathrm{d}\lambda)}. \tag{2.71}$$

Thus, the Jacobian and its eigenvalue $G_x$ (these are identical for a one-dimensional system such as (2.19)) are negative, and the corresponding fixed–point branch of the $(\lambda, x)$ plane is stable, for segments of the bifurcation plot where

$$\frac{\mathrm{d}x}{\mathrm{d}\lambda} > 0, \quad \text{stable.} \tag{2.72}$$

Conversely, segments with $\frac{\mathrm{d}x}{\mathrm{d}\lambda} < 0$ are unstable.

Finally, let us consider the dynamics and interactions of plane waves for the most general case of Section 2.3.6. The coincident transition varieties $\mathcal{H}$ and $D$ in (2.64),(2.65) are shown in Fig. 2.6(1–8) for various combinations of $(\alpha_3, \alpha_4)$ values. As is readily apparent, the configurations in Fig. 2.6(1–3) are the independent ones corresponding to centered and off-centered cusps and a parabolic variety curve respectively – the other cases are simple reflections of these. For Fig. 2.6(1) with $(\alpha_3, \alpha_4) = (0, 1)$, the transition variety divides the

$(\alpha_1, \alpha_2)$ space into two distinct regions 1 and 2. The bifurcation plots in the two regions are shown in Fig. 2.7(1 and 2). As per (2.71), the segment(s) with $\frac{\mathrm{d}x}{\mathrm{d}\lambda} > 0$ are stable, so that there is a unique stable plane wave for Fig. 2.7(1) in region 1 of Fig. 2.6(1). By contrast, there are co–existing stable plane wave states in regions BC and DE of Fig. 2.7(2) for region 2 of Fig. 2.6(1). Thus, hysteretic dynamics occurs with a transition from BC to DE as $\lambda \equiv \alpha_0$ is decreased through C, and a reverse transition as $\lambda$ is increased on DE through D. For Fig. 2.6(2) with $(\alpha_3, \alpha_4) = (1, 1)$, the bifurcation plots in regions 1 and 2 are shown in Fig. 2.8(1 and 2) respectively. Once gain, per (2.71), the segments of these plots with positive slope correspond to stable plane waves. Thus, only the segment corresponding to DE in Fig. 2.8(1) is a unique stable plane wave solution in region 1 of Fig. 2.6(2). For region 2 of Fig. 2.6(2), Fig. 2.8(2) shows hysteresis between the stable plane wave branches BC and DE. For regions 1 and 2 of Fig. 2.6(3) corresponding to $(\alpha_3, \alpha_4) = (1, 0)$, the bifurcation plots in regions 1 and 2 are shown in Fig. 2.9(1 and 2). For the former, as per (2.71), no stable plane waves exist. For the latter, there is a unique stable plane wave solution in the range of $\lambda(\alpha_0)$ corresponding to segment BC.

Finally, for the sake of completeness, we mention an alternative interpretation of the general case using Catastrophe Theory [27] (see [22] for a discussion of the connection between this and the Singularity Theory approach). Treating (2.19) in a manner analogous to the Cusp Catastrophe,

$$\begin{aligned} G_x &= 4\alpha_4 x^3 + 3\alpha_3 x^2 + 2\alpha_2 x + \alpha_1 \\ &\equiv 4\alpha_4 (x^3 + \Gamma_2 x^2 + \Gamma_1 x + \Gamma_0) = 0 \end{aligned} \tag{2.73}$$

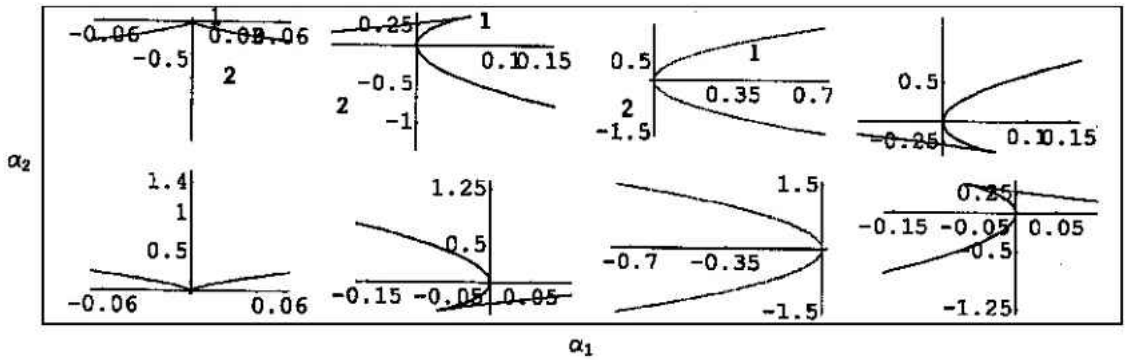


Figure 2.6: Transition varieties for the general case (2.19) treated in Section 2.3. There is no $\mathcal{B}$ curve, and $\mathcal{H}$ and $\mathcal{D}$ are coincident. The regions they delimit are shown. The figures correspond respectively to $(\alpha_3, \alpha_4)$ values $(0,1)$, $(1,1)$, $(1,0)$, $(-1,1)$, $(-1,0)$, $(-1,-1)$, $(0,-1)$, and $(1,-1)$.

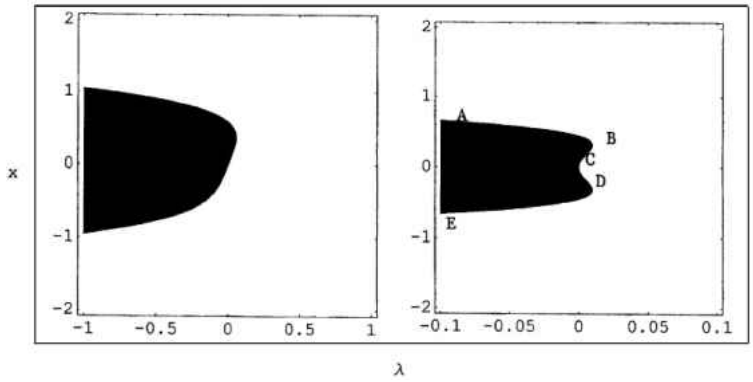


Figure 2.7: Bifurcation diagrams in regions 1 and 2 of Fig. 2.6(1), respectively.

with

$$\Gamma_2 = \frac{3\alpha_3}{4\alpha_4},$$

$$\Gamma_1 = \frac{\alpha_2}{2\alpha_4},$$

$$\Gamma_0 = \frac{\alpha_1}{\alpha_4}. \tag{2.74}$$

Defining

$$q = \frac{1}{3}\Gamma_1 - \frac{1}{9}\Gamma_2^2$$
$$r = \frac{1}{6}(\Gamma_1\Gamma_2 - 3\Gamma_0) - \frac{\Gamma_2^3}{27}, \tag{2.75}$$

the transition cusp curve between domains with one and three real solutions is given by

$$q^3 + r^2 = 0. \tag{2.76}$$

For $(\alpha_3, \alpha_4) = (1, 1)$ corresponding to Figs. 2.6(2) and 2.8, the catastrophe surface (2.73) showing regions of one/three real solutions in the $(\alpha_1, \alpha_2)$ plane shown in Fig. 2.9(1). Fig. 2.9(2) shows the corresponding cusp surface (2.76) in $(\alpha_1, \alpha_2)$ space. As mentioned, [22] discusses the relationship between these plots and the Singularity Theory plots given in Figs. 2.6(2) and 2.8 for this case.

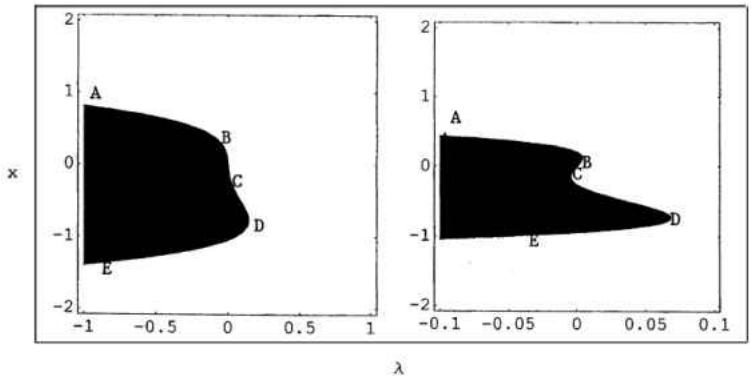


Figure 2.8: Bifurcation diagrams in regions 1 and 2 of Fig. 2.6(2), respectively.

In concluding, we have comprehensively analyzed the co–existing plane wave solutions in various parameter regimes for the CGLE (2.1). This includes transitions among co–existing states involving up to two domains with hysteresis, isolated parameter regimes with

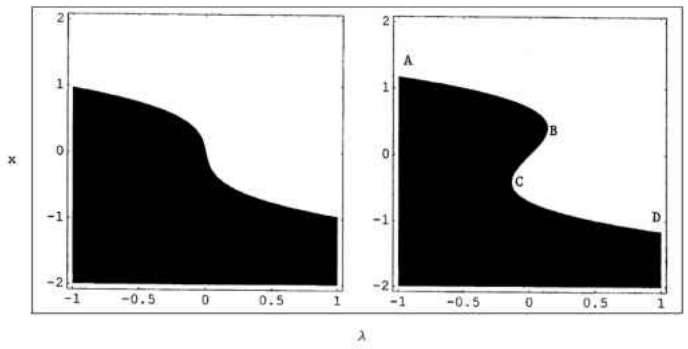


Figure 2.9: Bifurcation diagrams in regions 1 and 2 of Fig. 2.6(3), respectively.

isola behavior, and the resulting dynamics. We should also stress that, since our governing equation (2.19) is of polynomial form, all the results in Sections 2.3 and 2.4 are globally (and not just locally) valid in their respective regimes, as of course are the results for the general case.

# CHAPTER THREE: TRAVELING WAVETRAINS IN THE CGLE: HOPF BIFURCATIONS

In this chapter we begin by using a traveling wave reduction or a so–called spatial approximation to investigate the periodic solutions of the CGLE. The primary tool used here is the Hopf bifurcation theory and perturbation theory.

Immediately following the Hopf bifurcations we construct the periodic orbits by using the method of multiple scales. The remainder of the chapter is organized as follows. We first analyze the stability of fixed points in Section 3.1 and the onset of instability via a Hopf bifurcation, which may be either supercritical or subcritical. Then stability of periodic orbits is presented in Section 3.2 where we derive analytical expressions for the periodic orbits resulting from this Hopf bifurcation, and for their stability coefficients, by employing the multiple scales method. Section 3.3 considers numerical solutions and discusses the results.

## 3.1 Stability Analysis of Fixed Points

In this section, we conduct a stability analysis of individual plane wave solutions using regular phase–plane techniques. This was already done for the alternative formulation of the traveling wave ODEs given in [11]. We provide a brief derivation for our system (3.1a)–(3.1c) for completeness and future use. However, a much more complex question is the issue of categorizing and elucidating the possible existence of, and transitions among, multiple plane

wave states which may co–exist for the same parameter values in (2.1) (corresponding to the same operating conditions of the underlying system). Such behavior is well–documented in systems such as the Continuous Stirred Tank Reactor System [22, 26]. For a system such as (2.1) and the associated ODEs (3.1a)–(3.1c), the large number of parameters makes a comprehensive parametric study of co–existing states bewilderingly complex, if not actually impracticable. This more complex issue is addressed in the next section.

Proceeding as in Section 2.1.1, the system (2.4a)–(2.4c) can be written in the new form

$$a_z = b \tag{3.1a}$$

$$b_z = a\psi^2 - \gamma_1\Big[\gamma_2 a + v\Big(b_1 b + c_1\psi a\Big) - \gamma_3 a^3 - \gamma_4 a^5\Big] \tag{3.1b}$$

$$\psi_z = -\frac{2\psi b}{a} + \gamma_1\Big[\gamma_5 + v\Big(\frac{c_1 b}{a} - b_1\psi\Big) - \gamma_6 a^2 - \gamma_7 a^4\Big] \tag{3.1c}$$

where the constant terms $\gamma_1 - \gamma_7$ are given as functions of the system parameters in the following manner:

$$\gamma_1 = \frac{1}{b_1^2 + c_1^2}$$

$$\gamma_2 = b_1\epsilon + c_1\omega$$

$$\gamma_3 = b_1 b_3 - c_1 c_3$$

$$\gamma_4 = b_1 b_5 - c_1 c_5$$

$$\gamma_5 = -b_1\omega + c_1\epsilon$$

$$\gamma_6 = b_1 c_3 + c_1 b_3$$

$$\gamma_7 = b_1 c_5 + c_1 b_5\ .$$

From (2.2), a fixed point $(a_0, 0, \psi_0)$ of (3.1a) corresponds to a plane wave solution

$$A(x,t) = a_0 e^{i(\psi_0 z - \omega t) + i\theta} \tag{3.2}$$

with $\theta$ an arbitrary constant.

The fixed points of (3.1a)–(3.1c) may be obtained by setting $b = 0$ (from (3.1a)) in the right hand sides of the last two equations, solving the last one for $\psi$, and substituting this in the second yielding the quartic equation

$$\alpha_4 x^4 + \alpha_3 x^3 + \alpha_2 x^2 + \alpha_1 x + \alpha_0 = 0 \tag{3.3}$$

with

$$x = a^2, \tag{3.4a}$$

$$\alpha_4 = \frac{\gamma_7^2}{b_1^2 v^2} \tag{3.4b}$$

$$\alpha_3 = \frac{2\gamma_6\gamma_7}{b_1^2 v^2} \tag{3.4c}$$

$$\alpha_2 = \frac{\gamma_6^2 - 2\gamma_5\gamma_7}{b_1^2 v^2} + \frac{\gamma_1(b_1\gamma_4 + c_1\gamma_7)}{b_1} \tag{3.4d}$$

$$\alpha_1 = \gamma_1\big(\gamma_3 + \frac{c_1\gamma_6}{b_1}\big) - \frac{2\gamma_5\gamma_6}{b_1^2 v^2} \tag{3.4e}$$

$$\alpha_0 = \frac{\gamma_5^2}{b_1^2 v^2} - \frac{\gamma_1}{b_1}\big(b_1\gamma_2 + c_1\gamma_5\big)\ . \tag{3.4f}$$

Thus, with $a_0 = \sqrt{x}$ for $x$ any of the four roots of (3.3), we have a plane wave solution of the form (3.2). For each of the four roots $x_i, i = 1, \ldots, 4$ of (3.3) corresponding to a fixed point of (3.1a)–(3.1c) or a plane wave $\sqrt{x_i}\ e^{i(\psi_i z - wt) + i\theta_i}$, the stability may be determined using regular phase–plane analysis. The characteristic polynomial of the Jacobian matrix of

a fixed point $x_i = a_i^2$ of (3.1a)–(3.1c) may be expressed as

$$\lambda^3 + \delta_1\lambda^2 + \delta_2\lambda + \delta_3 = 0 \tag{3.5}$$

where

$$\delta_1 = 2b_1 v\gamma_1 \tag{3.6a}$$

$$\delta_2 = 3\psi^2 + \gamma_1[\gamma_2 - a^2(3\gamma_3 + 5a^2\gamma_4) - v(3c_1\psi - v)] \tag{3.6b}$$

$$\begin{aligned}\delta_3 = {} & -2a^2\gamma_1(\gamma_6 + 2a^2\gamma_7)(-2\psi + c_1\gamma_1 v) \\ & + b_1\gamma_1 v[-\psi^2 + \gamma_1(\gamma_2 - 3a^2\gamma_3 - 5a^4\gamma_4 + c_1\psi v)]\end{aligned} \tag{3.6c}$$

where the fixed point values $(a_i, \psi_i) = (\sqrt{x_i}, \psi_i)$ are to be substituted in terms of the system parameters. Note that $\psi_i$ is obtained by setting $a = a_i = \sqrt{x_i}$, and $b = 0$ in the right side of (3.1c).

For $(a_0, 0, \psi_0)$ to be a stable fixed point within the linearized analysis, all the eigenvalues must have negative real parts. Using the Routh–Hurwitz criterion, the necessary and sufficient conditions for (3.5) to have $Re(\lambda_{1,2,3}) < 0$ are:

$$\delta_1 > 0, \quad \delta_3 > 0, \quad \delta_1\delta_2 - \delta_3 > 0. \tag{3.7}$$

Equation (3.7) is thus the condition for stability of the plane wave corresponding to $x_i$.

On the contrary, one may have the onset of instability of the plane wave solution occurring in one of two ways. In the first, one root of (3.5) (or one eigenvalue of the Jacobian) becomes non–hyperbolic by going through zero for

$$\delta_3 = 0. \tag{3.8}$$

Equation (3.8) is thus the condition for the onset of "static" instability of the plane wave. Whether this bifurcation is a pitchfork or transcritical one, and its subcritical or supercritical nature, may be readily determined by deriving an appropriate canonical system in the vicinity of (3.8) using any of a variety of normal form or perturbation methods [23, 24, 25].

One may also have the onset of dynamic instability ("flutter" in the language of Applied Mechanics) when a pair of eigenvalues of the Jacobian become purely imaginary. The consequent Hopf bifurcation at

$$\delta_1\delta_2 - \delta_3 = 0 \tag{3.9}$$

leads to the onset of periodic solutions of (3.1a)–(3.1c) (dynamic instability or "flutter"). These periodic solutions for $a(z)$ and $\psi(z)$, which may be stable or unstable depending on the super- or subcritical nature of the bifurcation, correspond via (2.2) to solutions

$$A(x,t) = a(z)e^{i\left(\int \psi dz - \omega t\right)} \tag{3.10}$$

of the CGLE (2.1) which are, in general, quasiperiodic wavetrain solutions. This is because the period of $\psi$ and $\omega$ are typically incommensurate. Eq. (3.10) is periodic if $\omega = 0$.

## 3.2 Stability Analysis of Periodic Orbits

In this section we will use the method of multiple scales to construct analytical approximations for the periodic orbits arising through Hopf bifurcation of the fixed point of the CGLE equation. For the systems of differential equations given by (3.1a)–(3.1c), the physically

relevant point is given by $(a_0, 0, \psi_0)$ where $\psi_i$ is obtained by setting $a = a_i = \sqrt{x_i}$, in

$$\psi_i = \frac{\gamma_5 - a_i^2(\gamma_6 + a_i^2\gamma_7)}{b_1 v} \tag{3.11}$$

and $x_i$ is one of the roots of the fixed point equation (3.3). We will choose the parameter $\epsilon$ which represents the linear gain or loss as the control parameter. The limit cycle is determined by expanding about the fixed point using progressively slower spatial scales. In the standard way, we write the various or multiple scales as $z = Z_0$, $Z_1 = \delta Z_0$, $Z_2 = \delta^2 Z_0$, ..., where $\delta$ is the usual multiple scales expansion parameter. We shall expand in powers of $\delta$, to separate the various scales, and then set $\delta = 1$ at the end in the usual way. The expansion takes the form

$$a = a_0 + \sum_{n=1}^{3} \delta^n a_n(Z_0, Z_1, Z_2) + \ldots, \tag{3.12}$$

$$b = B_0 + \sum_{n=1}^{3} \delta^n B_n(Z_0, Z_1, Z_2) + \ldots, \tag{3.13}$$

$$\psi = \psi_0 + \sum_{n=1}^{3} \delta^n \psi_n(Z_0, Z_1, Z_2) + \ldots. \tag{3.14}$$

Using the chain rule, the spatial derivative becomes

$$\frac{\mathrm{d}}{\mathrm{d}Z} = D_0 + \delta D_1 + \delta^2 D_2 + \ldots, \tag{3.15}$$

where $D_n = \partial/\partial Z_n$. The delay parameter $\epsilon$ is ordered as

$$\epsilon = \epsilon_0 + \delta^2 \epsilon_2, \tag{3.16}$$

where $\epsilon_0$ is the critical value such that (3.7) is not satisfied, (i.e. $\epsilon_0$ is a solution of (3.9). This is standard for this method, as it allows the influence from the nonlinear terms and the control parameter to occur at the same order.

Using (3.12)–(3.16) in (3.1a)–(3.1c) and equating like powers of $\delta$ yields equations at $\mathrm{O}(\delta^i)$, $i = 1, 2, 3$ of the form:

$$L_1(a_i, B_i, \psi_i) = S_{i,1}, \tag{3.17}$$

$$L_2(a_i, B_i, \psi_i) = S_{i,2}, \tag{3.18}$$

$$L_3(a_i, B_i, \psi_i) = S_{i,3}, \tag{3.19}$$

where, the $L_i$, $i = 1, 2, 3$ are the differential operators

$$L_1(a_i, B_i, \psi_i) = D_0 a_i - B_i \equiv S_{i,1}, \tag{3.20}$$

$$\begin{aligned} L_2(a_i, B_i, \psi_i) &= D_0 B_i - \psi_0^2 a_i - 2a_0\psi_0\psi_i \\ &\quad + \gamma_1\{\gamma_{20} a_i + v[b_1 B_i + c_1(\psi_0 a_i + a_0\psi_i)] \\ &\quad - 3\gamma_{30} a_0^2 a_i - 5\gamma_{40} a_0^4 a_i\} \equiv S_{i,2}, \end{aligned} \tag{3.21}$$

$$\begin{aligned} L_3(a_i, B_i, \psi_i) &= a_0(D_0\psi_i) + 2(\psi_0 B_i + B_0\psi_i) \\ &\quad - \gamma_1\{\gamma_{50} a_i + v[c_1 B_i - b_1(\psi_0 a_i + a_0\psi_i)] \\ &\quad - 3\gamma_{60} a_0^2 a_i - 5\gamma 70 a_0^4 a_i\} \equiv S_{i,3}, \end{aligned} \tag{3.22}$$

where $\gamma_p = \gamma_{p0} + \delta^2\gamma_{p2}$ with $p = 2, 3, \ldots, 7$, the source terms $S_{i,j}$ for $i, j = 1, 2, 3$ at $\mathrm{O}(\delta)$, $\mathrm{O}(\delta^2)$, and $\mathrm{O}(\delta^3)$ are given by the following:

$$\mathrm{O}(\delta):$$

$$S_{1,1} = 0 \tag{3.23}$$

$$S_{1,2} = 0 \tag{3.24}$$

$$S_{1,3} = 0. \tag{3.25}$$

$$\mathrm{O}(\delta^2):$$

$$S_{2,1} = -D_1 a_1 \tag{3.26}$$

$$S_{2,2} = -D_1 B_1 + a_0\psi_1^2 + 2\psi_0 a_1\psi_1 - \gamma_1(\gamma_{22}a_0 + vc_1\psi_1 a_1 - 3\gamma_{30}a_0 a_1^2$$
$$- \gamma_{32}a_0^3 - 10\gamma_{40}a_0^3 a_1^2 - \gamma_{42}a_0^5) \tag{3.27}$$

$$S_{2,3} = -a_0 D_1\psi_1 - a_1 D_0\psi_1 - 2\psi_1 B_1 + \gamma_1[(\gamma_{52}a_0 - vb_1\psi_1 a_1)$$
$$- (3\gamma_{60}a_0 a_1^2 + \gamma_{62}a_0^3) - (10\gamma_{70}a_0^3 a_1^2 + \gamma_{72}a_0^5)]. \tag{3.28}$$

$$\mathrm{O}(\delta^3):$$

$$S_{3,1} = -D_1 a_2 - D_2 a_1 \tag{3.29}$$

$$S_{3,2} = -D_1 B_2 - D_2 B_1 + 2a_2\psi_0\psi_1 + a_1(2\psi_0\psi_2 + \psi_1^2) + 2a_0\psi_1\psi_2$$
$$- \gamma_1\{\gamma_{22}a_1 + vc_1(\psi_1 a_2 + \psi_2 a_1) - [\gamma_{30}(a_1^3 + 6a_0 a_1 a_2) + 3\gamma_{32}a_0^2 a_1]$$
$$- [\gamma_{40}(10a_0^2 a_1^3 + 20a_0^3 a_1 a_2) + 5\gamma_{42}a_0^4 a_1]\} \tag{3.30}$$

$$S_{3,3} = -D_1\psi_2 - D_2\psi_1 - a_1(D_1\psi_1 + D_0\psi_2) - a_2 D_0\psi_1 - 2(\psi_1 B_2 + \psi_2 B_1)$$
$$+ \gamma_1\{\gamma_{52}a_1 - vb_1(\psi_1 a_2 + \psi_2 a_1) - [\gamma_{60}(a_1^3 + 6a_0 a_1 a_2)$$
$$+ 3\gamma_{62}a_0^2 a_1] - [\gamma_{70}(10a_0^2 a_1^3 + 20a_0^3 a_1 a_2) + 5\gamma_{72}a_0^4 a_1]\}. \tag{3.31}$$

Also, (3.17) may be solved for $B_i$ in terms of $a_i$ and $\psi_i$. Using this in (3.18) yields $\psi_i$

$$\psi_i = \frac{\theta_i}{\phi_1}, \tag{3.32}$$

where

$$\theta_i = -D_0 S_{i,1} + D_0^2 a_i - \psi_0^2 + \gamma_1\{\gamma_{20} a_i - 3\gamma_{30} a_0^2 a_i - 5\gamma_{40} a_0^4 a_i$$

$$+ v[b_1(-S_{i,1} + D_0 a_i) + c_1]\} - S_{i,2} \tag{3.33}$$

and

$$\phi_1 = 2a_0\psi_0 - v\gamma_1 c_1 a_0. \tag{3.34}$$

Using (3.32) and the equation for $B_i$ in (3.20) yields the composite equation:

$$L_c a_i \equiv \Gamma_i, \tag{3.35}$$

where

$$\Gamma_i \equiv S_{i,3} - \frac{a_0}{\phi_1}\Big(D_0\zeta_i\Big) - \frac{2B_0}{\phi_1}\zeta_i - \gamma_1 v b_1 a_0 \frac{\zeta_i}{\phi_1} + (2\psi_0 - \gamma_1 v c_1) S_{i,1}, \tag{3.36}$$

$$\zeta_i = -D_0 S_{i,1} - \gamma_1 v b_1 S_{i,1} - S_{i,2}. \tag{3.37}$$

We shall now use (3.36) and (3.37) to systematically identify and suppress secular terms in the solutions of (3.20)–(3.22). Let us now turn to finding the solutions of (3.20)–(3.22). In what follows , we shall detail the solution of the above system of equations for the case $\epsilon_0 = \epsilon_{01}$. In order to achieve that we must find first the fixed points. The characteristic polynomial of the Jacobian matrix of a fixed point of (3.1a)–(3.1c) may be expressed as

$$\lambda^3 + \delta_1\lambda^2 + \delta_2\lambda + \delta_3 = 0, \tag{3.38}$$

as in (3.5), and the fixed point values $(a_i, \psi_i)$ are to be substituted in terms of the system parameters.

The condition $\delta_1\delta_2 - \delta_3 = 0$ yields an involved equation in $\epsilon$ which actually can be solved easily numerically for $\epsilon_0$ by the root method .

For O($\delta$) the Eqns. (3.23)–(3.25) give $S_{i,1} = S_{i,2} = S_{i,3} = 0$, and hence we may pick a solution for the first order as

$$a_1 = \alpha(Z_1, Z_2)e^{\lambda_1 Z_0} + \beta(Z_1, Z_2)e^{\lambda_2 Z_0} + \gamma(Z_1, Z_2)e^{\lambda_3 Z_0}, \tag{3.39}$$

where $\beta = \bar{\alpha}$ is the complex conjugate of $\alpha$ and $\lambda_2 = \lambda_1$. As evident for the Routh–Hurwitz condition, the $\alpha$ and $\beta$ modes correspond to the center manifold where $\lambda_{1,2}$ are purely imaginary and where the Hopf bifurcation occurs, while $\gamma$ corresponds to the attractive direction or the stable manifold. Since we wish to construct and analyze the stability of the periodic orbits which lie in the center manifold, we should take $\gamma = 0$ so (3.39) becomes

$$a_1 = \alpha(Z_1, Z_2)e^{i\omega Z_0} + \beta(Z_1, Z_2)e^{-i\omega Z_0}. \tag{3.40}$$

Using (3.23)–(3.25) for $i = 1$, then the first order fields $(a_1, B_1, \psi_1)$ are

$$B_1 = D_0 a_1 = i\omega\alpha e^{i\omega Z_0} - i\omega\beta e^{-i\omega Z_0}, \tag{3.41}$$

and (3.32) becomes

$$\begin{aligned}\psi_1 = \frac{1}{\phi_1}\Big[ -\omega^2 - \psi_0^2 + \gamma_1\Big(\gamma_{20} + vc_1\psi_0 - 3\gamma_{30}a_0^2 - 5\gamma_{40}a_0^4\Big)\Big]\Big(\alpha e^{i\omega Z_0} + \beta e^{-i\omega Z_0}\Big) \\ + \frac{\gamma_1 v b_1}{\phi_1}\Big(i\omega\alpha e^{i\omega Z_0} - i\omega\beta e^{-i\omega Z_0}\Big).\end{aligned} \tag{3.42}$$

Now that the first order solutions (3.40)–(3.42) are known, the second order sources $S_{21}$, $S_{22}$, $S_{23}$ may be evaluated via (3.26)–(3.28). Using these sources in (3.36) we obtain $\Gamma_2$

which may be written as

$$\Gamma_2 = \Gamma_2^{(0)} + \Gamma_2^{(1)} e^{i\omega Z_0} + \Gamma_2^{(2)} e^{2i\omega Z_0} + c.c. \tag{3.43}$$

Setting the coefficients of the secular $e^{i\omega Z_0}$ terms (which are the solutions of the homogeneous equation for $i = 1$) to zero, i.e. $\Gamma_2^{(1)} = 0$ yields

$$\begin{aligned} D_1\alpha &= \frac{\partial \alpha}{\partial Z_1} = 0, \\ D_1\beta &= \frac{\partial \beta}{\partial Z_1} = 0. \end{aligned} \tag{3.44}$$

Using (3.44), the second–order sources, and assuming a second–order particular solution for $a_2$ of the form:

$$a_2 = a_2^{(0)} + a_2^{(2)} e^{2i\omega Z_0}, \tag{3.45}$$

having the standard form of a DC or time–independent term plus second–harmonic terms, the composite equations (3.35)–(3.37) for $i = 2$, yield

$$L_c a_2 = \Gamma_2^{(0)} + \Gamma_2^{(2)} e^{2i\omega Z_0}, \tag{3.46}$$

which will be solved for the particular solution $a_2^{(0)}$, and $a_2^{(2)}$ by equating both sides of the expression (3.46). In terms of the composit operator $L_c$ which is obtained from (3.36), the

particular solution takes the form:

$$a_2^{(0)} = -\Gamma_2^{(0)}\big[a_0(vc_1\gamma_1 - 2\psi_0)\big]\Big\{2B_0\big[-\psi_0^2 + \gamma_1(\gamma_{20} - 3a_0^2\gamma_{30} - 5a_0^4\gamma_{40} + vc_1\psi_0)\big]$$
$$+ a_0\gamma_1\big\{(\gamma_{50} - 3a_0^2\gamma_{60} - 5a_0^4\gamma_{70})(vc_1\gamma_1 - 2\psi_0)$$
$$+ vb_1[\gamma_1(\gamma_{20} - 3a_0^2\gamma_{30} - 5a_0^4\gamma_{40}) + \psi_0^2]\big\}\Big\}^{-1}, \tag{3.47}$$

$$a_2^{(2)} = -\Gamma_2^{(2)}\big[a_0(vc_1\gamma_1 - 2\psi_0)\big]\Big\{6a_0^2B_0\gamma_1\gamma_{30} + 10a_0^4B_0\gamma_1\gamma_{40}$$
$$+ 3a_0^3\gamma_1\big[\gamma_{30}(2i\omega + vb_1\gamma_1) + \gamma_{60}(vc_1\gamma_1 - 2\psi_0)\big]$$
$$+ 5a_0^5\gamma_1\big[\gamma_{40}(2i\omega + vb_1\gamma_1) + \gamma_{70}(vc_1\gamma_1 - 2\psi_0)\big]$$
$$+ 2B_0\big[4\omega_2 - 2iv\omega b_1\gamma_1 + \psi_0^2 - \gamma_1(\gamma_{20} + vc_1\psi_0)\big]$$
$$+ a_0\big\{8i\omega^3 - 2iv^2\omega b_1^2\gamma_1^2 - 6i\omega\psi_0^2 + 2\gamma_1\psi_0(3iv\omega c_1 + \gamma_{50})$$
$$+ \gamma_1[-2i\omega(v^2c_1^2\gamma_1 + \gamma_{20}) - vc_1\gamma_1\gamma_{50}] - vb_1\gamma_1(-8\omega_2 + \gamma_1\gamma_{20} + \psi_0^2)\big\}\Big\}^{-1}. \tag{3.48}$$

Using (3.32), the second–order sources, and the equation for $B_i$ in (3.20) with $i = 2$, then we can find the second–order fields $B_2$ and $\psi_2$. Substituting them into the Eqts. (3.29)–(3.31) we find the third order sources and we may evaluate the coefficients of the secular term $e^{i\omega Z_0}$ in the composite source $\Gamma_3$ of (3.36). Suppressing again the secular terms to obtain uniform expansions yields the final equation for the evolution of the coefficients in the linear solutions (3.40)-(3.42) on the slow second–order spatial scales

$$\frac{\partial\alpha}{\partial Z_2} = S_1\alpha^2\beta + S_2\alpha. \tag{3.49}$$

Writing $\alpha = \frac{1}{2}Ae^{i\theta}$ and separating (3.49) into real and imaginary parts, yields

$$\frac{\partial A}{\partial Z_2} = \frac{S_{1r}A^3}{4} + S_{2r}A, \tag{3.50}$$

where $S_{1r}$ and $S_{2r}$ represent the real parts of $S_1$ and $S_2$ respectively. In the usual way, the fixed points of (3.50), $(A_1, A_{2,3})$ where

$$\begin{aligned} A_1 &= 0, \\ A_{2,3} &= \pm 2\sqrt{-\frac{S_{2r}}{S_{1r}}} \end{aligned} \tag{3.51}$$

give the amplitude of the solution $\alpha = \frac{1}{2}Ae^{i\theta}$, with $A_{2,3}$ corresponding to the bifurcation periodic orbits. Clearly $A_{2,3}$ are real fixed points whenever

$$\frac{S_{2r}}{S_{1r}} < 0, \tag{3.52}$$

and the Jacobian of the right hand side of (3.50) evaluated at $A_{2,3}$ is $J|_{A_{2,3}} = -2S_{2r}$, where $J(A) = \frac{\partial(\frac{S_{1r}A^3}{4} + S_{2r}A)}{\partial A}$. Clearly, a necessary condition for stability is to have $S_{2r} > 0$, and for instability $S_{2r} < 0$. Thus, the system undergoes:

a. supercritical Hopf bifurcations when

$$S_{2r} > 0, \qquad S_{1r} < 0, \tag{3.53}$$

b. subcritical Hopf bifurcations when

$$S_{2r} < 0, \qquad S_{1r} > 0. \tag{3.54}$$

## 3.3 Discussion of Results

In this section, we consider the numerical results which follow from the analysis in the previous sections. The fixed point Eq. (3.3) can be solved analytically for each fixed point

$x_i$ using the program Mathematica, for $i = 1, \ldots, 4$. Since all coefficients $\alpha_i$, for $i = 1, \ldots, 4$ depend on the nine system parameters, we fix $b_1 = 0.08$, $b_3 = -0.65$, $b_5 = 0.1$, $c_1 = 0.5$, $c_3 = 1$, $c_5 = -0.07$, $\omega = 0$, and $v = 0.01$. The possibility of bounded chaotic solitons depends on the system being fairly strongly dissipative near the fixed points $(a_0, 0, \psi_0)$ in a significant part of the phase space, with the strong dissipativity ruling out the appreciable volume expansion associated with an attractor at infinity, as well as volume–conserving quasiperiodic behavior. The trace of the Jacobian matrix for this sets of values at the fixed point $(a_0, 0, \psi_0)$, which gives the local logarithmic rate of change of $(a, b, \psi)$ phase–space volume $V$ is $\frac{1}{V}\frac{\mathrm{d}v}{\mathrm{d}t} = J(a_0, 0, \psi_0) = -0.0062$, so we may anticipate that the orbits may go to an attractor at infinity, since the dissipation is weak.

The four fixed points can be analytically found as a function of only one parameter, in our case we chose $\epsilon$ as being the free parameter. By choosing "the right fixed point", the Hopf curve $\alpha_1\alpha_2 - \alpha_3 = 0$ may be solved numerically for $\epsilon$, which gives $\epsilon_0 = -0.0000807$. The idea is to find the "right" $\epsilon$ which will give rise to the condition for Hopf bifurcation, (i.e. $\alpha_1 > 0$, $\alpha_2 > 0$, $\alpha_3 > 0$ and $\alpha_1\alpha_2 - \alpha_3 < 0$).

We obtain $\alpha_1 = 0.006$, $\alpha_2 = 0.001$, $\alpha_3 = 0.0001$ and $\alpha_1\alpha_2 - \alpha_3 = -1.01\ 10^{-6}$ for an $\epsilon = -0.008$, i.e. $\epsilon < \epsilon_0$.

Now we will analyze the multiple scales method to construct the analytical approximations for the periodic orbits arising through the Hopf bifurcations of the fixed point. The delay parameter $\epsilon$ (or the bifurcation parameter) is ordered as $\epsilon = \epsilon_0 + \delta^2\epsilon_2$, where $\epsilon_0 = -0.0000807$, and $\epsilon_2 = -0.1$. This method allows the influence from the nonlinear terms

and the control parameter to occur at the same order. For the system parameters chosen above, at the fixed points, we get $(a_0, 0, \psi_0) = (0.0121663, 0, -0.00514)$.

From (3.35) and by the method presented in Section 3.1, the final equation for the evolution coefficients in the linear solutions, on the slow second–order time scale is

$$\frac{\partial \alpha(Z_1, Z_2)}{\partial Z_2} = S_1 \alpha^2(Z_1, Z_2)\beta(Z_1, Z_2) + S_2 \alpha(Z_1, Z_2), \tag{3.55}$$

where $S_1 = -3235.55 + 295.279i$ and $S_2 = 297.074 - 32.26i$. Since $S_{2r} = Re(S_2) > 0$, and $S_{1r} = Re(S_1) < 0$, then this situation will correspond to a supercritical Hopf bifurcation.

Figs. 3.1–3.3 show the time behaviors of $a(z)$, $b(z)$, and $\psi(z)$ for $\epsilon = -0.00008$ (the supercritical regime). Note that, as anticipated from before, there is a stable limit cycle attractor at $\epsilon$, the solution remains positive and bounded while it stays periodic.

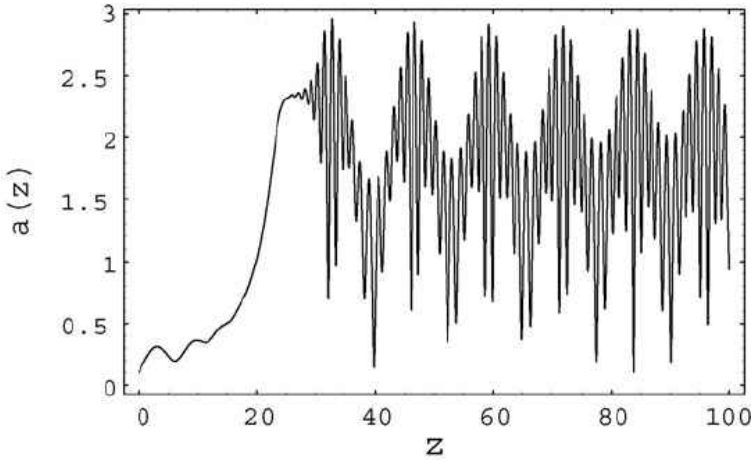


Figure 3.1: Stable periodic oscillations on the limit cycle $a(z)$ vs. $z$

Clearly, similar stable periodic solutions may be obtained for many other parameter sets. For each case, the overall solution $A(x, t)$ of the CGLE is, via (3.10), a quasiperiodic solution.

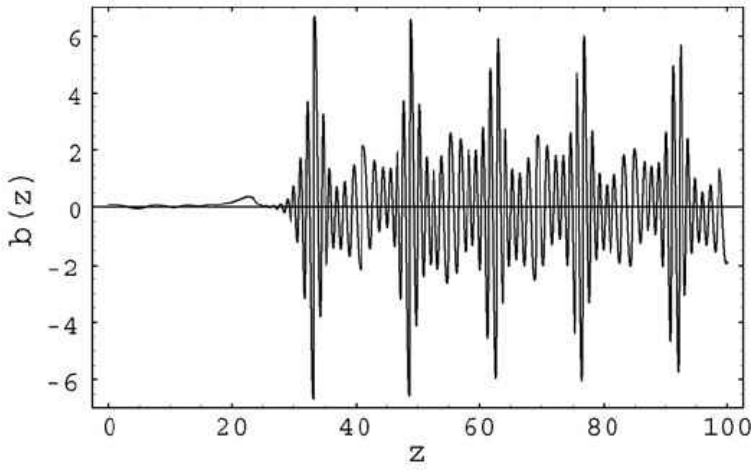


Figure 3.2: $b(z) = a_z$ vs. $z$

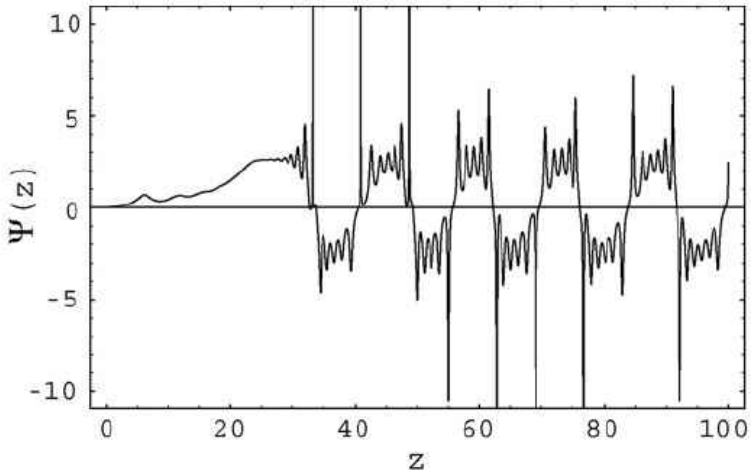


Figure 3.3: $\psi(z) = \phi_z$ vs. $z$

One may also use the above approach to both explain, and extend, the numerical treatment by Brusch et al. [5, 6] of the periodic traveling waves of the CGLE using the bifurcation software AUTO [31]. However, the solutions in Brusch et al. do not appear to be clearly correlated to the dissipative solitons of the CGLE in Akhmediev at al [26]. Hence, we shall move on next to briefly consider possible generalizations of the above treatment.

# CHAPTER FOUR: REMARKS ON GENERALIZED HOPF BIFURCATIONS AND EMERGENCE OF GLOBAL STRUCTURE

One may pursue the line of inquiry based on the traveling waves or spatial ODEs even further to track the emergence of global structure. We have done preliminary work along these lines which is outlined in this chapter. However, although there is well–established roadmap and it has been implemented in detail for the well–known Continuous Stirred Tank Reactor System [27, 28], we are not convinced of its relevance to the actual numerical simulations of dissipative solitons. Hence, we present it here as a possible future direction before moving into fully spatiotemporal approaches in the subsequent chapters.

For completeness, let us first consider more degenerate cases where more than one root of the Jacobian is non–hyperbolic. In such cases the non–hyperbolic eigenvalues of the Jacobian matrix, may consist of either:

(a) a double zero: $\lambda_{1,2} = 0$, $\lambda_3 \in \Re$

(b) one zero and a complex conjugate pair:$\lambda_1 = 0$, $\lambda_2 = \bar{\lambda}_3$

(c) a triple zero: $\lambda_{1,2,3} = 0$

For the above situations, we have the following sub–cases of the so–called "degenerate Hopf" ($H1$) bifurcation. Each sub–case is given a name:

$$\mathrm{F}_1: \qquad \lambda_{1,2} = 0, 0 \tag{4.1}$$

$$\mathrm{F}_2: \qquad \lambda_{1,2,3} = \pm i\omega_0, 0 \tag{4.2}$$

$$\mathrm{G}_1: \qquad \lambda_{1,2,3} = 0, 0, 0 \tag{4.3}$$

In these cases, [28, 32, 33, 34, 35, 36], these ($H1$) bifurcations may lead to global structure including homoclinic orbits, invariant tori, and period doubling to chaos at the ($H1$) points. One may also work perturbatively [32] near these ($H1$) points as done by Keener for the well–known Continuous Stirred Tank Reactor problem.

Two other degenerate/generalized Hopf bifurcation scenarios are possible. As seen in Chapter 3 (3.50), the normal form for the Hopf bifurcation may be written as

$$\dot{r} = r\left[\alpha(\mu) + c_1(\mu)r^2 + c_2(\mu)r^4 + ...\right] \tag{4.4}$$

$$\dot{\theta} = \omega_0 + O(\mu, r^2) \tag{4.5}$$

where we have made the identification $A \to r$, $S_{1r}/4 \to c_1$, $S_{2r} \to \alpha$, and higher order nonlinear terms are included.

The first kind of possible degeneracy (the ($H2$) kind) occurs if

$$\alpha = \alpha' = ... = \alpha^{(k)} = 0$$

$$\alpha^{(k+1)} \neq 0. \tag{4.6}$$

This is the so–called $\mathrm{k}^{\mathrm{th}}$ order ($H2$) degeneracy and it gives rise to multiple Hopf points and multiple periodic orbits. The resulting structure is thus similar to that resulting from

a regular Hopf bifurcation, and much less complex than the structure produced by $(H1)$ bifurcation.

A second possible degeneracy in the normal form (4.4) corresponds to

$$c_1 = c_2 = ... = c_m = 0$$

$$c_{m+1} \neq 0. \tag{4.7}$$

This so–called $\mathrm{m}^{\mathrm{th}}$ order $(H3)$ degeneracy results in isolated branches of periodic solutions unconnected to the main branch.

When the $\mathrm{k}^{\mathrm{th}}$ order $(H2)$ degeneracy and the $\mathrm{m}^{\mathrm{th}}$ order $(H3)$ degeneracy occur simultaneously, the normal form (4.4) may be rescaled to the form:

$$\dot{r} = r\left[r^{2m+2} + ... \pm \mu^{k+1}\right] \tag{4.8}$$

This is the so–called $H_{mk}$ degeneracy.

In the case of the $(H2)$ degeneracy, the complex conjugate eigenvalues $\pm i\omega$ at the Hopf point cross the imaginary axis tangentially leading, after additional analysis, to multiple periodic orbits.

For $(H3)$ degeneracy, one may obtain isolated branches (isolas) of periodic orbits unconnected to the main branch.

However, of greatest interest are the $(H1)$ bifurcations where the Jacobian has more than one non–hyperbolic eigenvalue and global structure emerges.

As mentioned, we have investigated these in preliminary fashion. However, the connections to the actual bifurcations of dissipative solitons are hard to see, and this approach

appears to be of dubious value. Hence, we shall now change track and switch to fully spatiotemporal approaches for the remainder of this dissertation.

# CHAPTER FIVE: THE GENERALIZED VARIATIONAL FORMULATION

In this chapter, we develop a general variational formulation to address four of the five classes of dissipative solitons, viz. the pulsating, creeping, snake, and chaotic solitons on all parameter ranges. As mentioned in Chapter 1 in general terms, we shall need to generalize previous variational approaches in several crucial ways.

First, the starting formulation of the Lagrangian for dissipative NLPDEs is relatively of recent vintage [30] and neither widely known or widely explored. We are grateful to David Kaup for digging into his encyclopedic body of work and pointing us to this. An alternative, complex formulation of the Lagrangian for dissipative NLPDEs has been recently employed by Skarka [37] to investigate conventional stationary solitons only. We are also in touch with Vladimir Skarka in order to obtain a write–up on this other formulation.

This chapter is organized as follows. Section 5.1 details the recent variational formulation for dissipative systems, as well as the novel generalized trial functions to be employed in modeling the pulsating solitary waves. Section 5.2 outlines the framework of investigation of the pulsating and snake solitons. Periodic evolution of the trial function parameters on stable periodic attractors resulting from supercritical Hopf bifurcations, when substituted back into the trial function, yield pulsating solitary waves. Within this framework, we also comprehensively explore:

(a) the cascade of period doubling bifurcations observed in the simulations of the CGLE, and

(b) the effect of the various parameters in the CGLE on the shape (amplitude, width and period) and domain of existence of the pulsating solitary waves. In Section 5.3 we use the method of multiple scales to construct analytical approximations for the periodic orbits arising through Hopf bifurcation of the fixed point of the Euler–Lagrange equations (5.14) or (5.18). Sections 5.4 and 5.5 provide numerical work for the pulsating and snakes solitons. In Section 5.6 we elucidate the new mechanism responsible for the various classes of pulsating solitary wave solutions in dissipative systems, viz. the possibility of Hopf bifurcations. This also explains the absence of pulsating solitary waves in Hamiltonian and integrable systems.

## 5.1 The Generalized Variational Formulation

In this section we develop a general variational formulation to address the pulsating solitons on all parameter ranges. As mentioned earlier, we shall need to generalize previous variational approaches in several crucial ways.

First, the starting formulation of the Lagrangian for dissipative NLPDEs is relatively of recent vintage [30] and neither widely known or widely explored. We are grateful to David Kaup for digging into his encyclopedic body of work and pointing us to this. An alternative, complex formulation of the Lagrangian for dissipative NLPDEs has been recently employed by Skarka [37] to investigate conventional stationary solitons only.

### 5.1.1 Formulation

Proceeding as in [30], the Lagrangian for the cubic–quintic CGLE (2.1) may be written as

$$\begin{aligned}\mathcal{L} &= r^*\left[\partial_t A - \epsilon A - (b_1 + ic_1)\partial_x^2 A + (b_3 - ic_3)|A|^2 A + (b_5 - ic_5)|A|^4 A\right] \\ &+ r\left[\partial_t A^* - \epsilon A^* - (b_1 - ic_1)\partial_x^2 A^* + (b_3 + ic_3)|A|^2 A^* + (b_5 + ic_5)|A|^4 A^*\right] \end{aligned} \tag{5.1}$$

Here $r$ is the usual auxiliary equation employed in [30] and it satisfies a perturbative evolution equation dual to the CGLE with all non–Hamiltonian terms reversed in sign.

The second key assumption involves the trial functions $A(t)$ and $r(t)$ which have been generalized considerably over conventional ones to keep the shape relatively simple and the trial functions integrable. To this end, we choose single–humped trial functions of the form:

$$A(x,t) = A_1(t)e^{-\sigma_1(t)^2[x-\phi_1(t)]^2}e^{i\alpha_1(t)} \tag{5.2}$$

$$r(x,t) = e^{-\sigma_2(t)^2[x-\phi_2(t)]^2}e^{i\alpha_2(t)} \tag{5.3}$$

Here, the $A_1(t)$ is the amplitude, the $\sigma_i(t)$'s are the inverse widths, $\phi_i(t)$'s are the positions (with $\phi_i(t)/t$ being phase speeds, $\dot{\phi}_i(t)$ the speed) and $\alpha_i(t)$'s are the phases of the solitons. All are allowed to vary arbitrarily in time. For now, the chirp terms are omitted for simplicity.

Substituting (5.2) in (5.1) the effective or averaged Lagrangian is

$$
\begin{aligned}
L_{EFF} = \int_{-\infty}^{\infty} \mathcal{L} dx = 2\sqrt{\pi}\Bigg\{ & - \frac{e^{-\frac{\sigma_1(t)^2\sigma_2(t)^2[\phi_1(t)-\phi_2(t)]^2}{\sigma_1(t)^2+\sigma_2(t)^2}}}{[\sigma_1(t)^2+\sigma_2(t)^2]^{\frac{1}{2}}} \epsilon A_1(t)\cos[\alpha_1(t)-\alpha_2(t)] \\
& + \frac{e^{-\frac{3\sigma_1(t)^2\sigma_2(t)^2[\phi_1(t)-\phi_2(t)]^2}{3\sigma_1(t)^2+\sigma_2(t)^2}}}{\Big[3\sigma_1(t)^2+\sigma_2(t)^2\Big]^{\frac{1}{2}}} A_1(t)^3 \Big[ b_3\cos[\alpha_1(t)-\alpha_2(t)] + c_3\sin[\alpha_1(t)-\alpha_2(t)] \Big] \\
& + \frac{e^{-\frac{5\sigma_1(t)^2\sigma_2(t)^2[\phi_1(t)-\phi_2(t)]^2}{5\sigma_1(t)^2+\sigma_2(t)^2}}}{\Big[5\sigma_1(t)^2+\sigma_2(t)^2\Big]^{\frac{1}{2}}} A_1(t)^5 \Big[ b_5\cos[\alpha_1(t)-\alpha_2(t)] + c_5\sin[\alpha_1(t)-\alpha_2(t)] \Big] \\
& + \frac{e^{-\frac{\sigma_1(t)^2\sigma_2(t)^2[\phi_1(t)-\phi_2(t)]^2}{\sigma_1(t)^2+\sigma_2(t)^2}}}{\Big[\sigma_1(t)^2+\sigma_2(t)^2\Big]^{\frac{5}{2}}} \Bigg[ \cos[\alpha_1(t)-\alpha_2(t)][\sigma_1(t)^2+\sigma_2(t)^2]^2 \dot{A}_1(t) \\
& + A_1(t)\Bigg( - 2\sigma_1(t)^2\sigma_2(t)^2\Big[ b_1\cos[\alpha_1(t)-\alpha_2(t)] - c_1\sin[\alpha_1(t)-\alpha_2(t)] \Big]\Big[ -\sigma_2(t)^2 \\
& + \sigma_1(t)^2[-1+2\sigma_2(t)^2[\phi_1(t)-\phi_2(t)]^2] \Big] - \dot{\alpha_1}(t)\sin[\alpha_1(t)-\alpha_2(t)][\sigma_1(t)^2+\sigma_2(t)^2]^2 \\
& - \sigma_1(t)\dot{\sigma_1}(t)\cos[\alpha_1(t)-\alpha_2(t)]\Big[\sigma_1(t)^2+\sigma_2(t)^2+2\sigma_2(t)^4[\phi_1(t)-\phi_2(t)]^2\Big] \\
& - 2\dot{\phi_1}(t)\sigma_1(t)^2\sigma_2(t)^2[\phi_1(t)-\phi_2(t)][\sigma_1(t)^2+\sigma_2(t)^2]\cos[\alpha_1(t)-\alpha_2(t)]\Bigg)\Bigg]\Bigg\}
\end{aligned}
\tag{5.4}
$$

Since (5.4) reveals that only the relative phase $\alpha(t) = \alpha_1(t) - \alpha_2(t)$ of $A(x,t)$ and $r(x,t)$ is relevant, we henceforth take

$$
\begin{aligned}
\alpha_1(t) &= \alpha(t) \\
\alpha_2(t) &= 0
\end{aligned}
\tag{5.5}
$$

with no loss of generality.

Also, for algebraic tractability, we have found it necessary to assume

$$
\sigma_2(t) = m\sigma_1(t) \equiv m\sigma(t). \tag{5.6}
$$

While this ties the widths of the $A(x,t)$ and $r(x,t)$ fields together, the loss of generality is acceptable since the field $r(x,t)$ has no real physical significance.

For reasons of algebraic simplicity, we may also scale the positions according to:

$$\phi_1(t) = \phi(t)$$
$$\phi_2(t) = 0, \tag{5.7}$$

although this assumption may easily be relaxed. In fact, we may expect that it may be necessary to relax (5.7) for certain classes of dissipative solitons.

Finally, for real solutions (note that the numerical results in [20, 26] pertain to $|A(x,t)|$), we may make the additional assumption

$$\alpha(t) = 0 \tag{5.8}$$

when desired, although this too may be easily relaxed.

Hence, using all assumptions, (i.e. (5.5)–(5.7) in (5.4)), the effective Lagrangian (5.4) may be written in a simpler but still general form

$$\begin{aligned} L_{EFF} \;=\; & 2\sqrt{\pi}\Bigg\{\frac{A_1(t)}{\sigma(t)}\Bigg[-\frac{e^{-\frac{m^2\sigma(t)^2\phi(t)^2}{1+m^2}}}{[1+m^2]^{\frac{1}{2}}}\epsilon\cos\alpha(t) \\ & +\frac{e^{-\frac{3m^2\sigma(t)^2\phi(t)^2}{3+m^2}}}{[3+m^2]^{\frac{1}{2}}}A_1(t)^2\Big[b_3\cos\alpha(t)+c_3\sin\alpha(t)\Big] \\ & +\frac{e^{-\frac{5m^2\sigma(t)^2\phi(t)^2}{5+m^2}}}{[5+m^2]^{\frac{1}{2}}}A_1(t)^4\Big[b_5\cos\alpha(t)+c_5\sin\alpha(t)\Big]\Bigg] \\ & +\frac{e^{-\frac{m^2\sigma(t)^2\phi(t)^2}{1+m^2}}}{[1+m^2]^{\frac{5}{2}}\sigma(t)^2}\Bigg[(1+m^2)^2\cos\alpha(t)\sigma(t)\dot{A}_1(t) \end{aligned}$$

$$
\begin{aligned}
&-A_1(t)\Bigg(4m^4\sigma(t)^5\phi(t)^2\Big[b_1\cos\alpha(t)-c_1\sin\alpha(t)\Big]\\
&+(1+m^2)^2\sigma(t)\dot{\alpha}(t)\sin\alpha(t)+(1+m^2)\dot{\sigma}(t)\cos\alpha(t)\\
&-2m^2(1+m^2)\sigma(t)^3\Big[b_1\cos\alpha(t)-c_1\sin\alpha(t)\Big]\\
&+2m^4\dot{\sigma}(t)\sigma(t)^2\phi(t)^2+\dot{\phi}(t)\phi(t)\cos\alpha(t)\Bigg)\Bigg]\Bigg\}
\end{aligned}
\tag{5.9}
$$

## 5.2 Framework for Investigation of Euler–Lagrange Equations for Pulsating and Snake Solitons

### 5.2.1 Variational Equations

Pulsating Solitons

For plain pulsating solitons, the speed is always zero [20, 26] and we take

$$\phi_1(t)=\phi_2(t)=0. \tag{5.10}$$

However, we need *not*, in general invoke (5.8), since the solution of (2.1) must be complex. Therefore, the trial functions (5.2) and (5.3) become

$$A(x,t)=A_1(t)e^{-\sigma(t)^2x^2}e^{i\alpha(t)} \tag{5.11}$$

$$r(x,t)=e^{-\sigma(t)^2} \tag{5.12}$$

Substituting the last two equations into (5.9), and by choosing $m = 1$, the simplified effective Lagrangian becomes

$$\begin{aligned} L_{EFF} &= \frac{\sqrt{\pi}}{6\sigma(t)^2}\Bigg[6A_1(t)^3\sigma(t)\big(b_3\cos\alpha(t)+c_3\sin\alpha(t)\big) \\ &\quad +\sqrt{2}\Bigg(2\sqrt{3}A_1(t)^5\sigma(t)\big(b_5\cos\alpha(t)+c_5\sin\alpha(t)\big) \\ &\quad +6\dot{A}_1(t)\sigma(t)\cos\alpha(t)-6A_1(t)\sigma(t)\sin\alpha(t)\big(c_1\sigma(t)^2+\dot{\alpha}(t)\big) \\ &\quad -3A_1(t)\cos\alpha(t)\big(\dot{\sigma}(t)+2\epsilon\sigma(t)-2b_1\sigma(t)^3\big)\Bigg)\Bigg] \end{aligned} \tag{5.13}$$

We are left with three parameters $A_1(t)$, $\sigma(t)$ and $\alpha(t)$ in $L_{EFF}$. Varying these parameters, we obtain the following Euler–Lagrange equations

$$\frac{\partial L_{EFF}}{\partial \star\,(t)} - \frac{\mathrm{d}}{\mathrm{dt}}\Big(\frac{\partial L_{EFF}}{\partial \dot{\star}(t)}\Big) = 0,$$

where $\star$ refers to $A_1$, $\sigma$, or $\alpha$. Solving for $\dot{\star}(t)$ as a system of three ODEs,

$$\begin{aligned} \dot{A}_1(t) &= f_1[A_1(t),\sigma(t),\alpha(t)] \\ \dot{\sigma}(t) &= f_2[A_1(t),\sigma(t),\alpha(t)] \\ \dot{\alpha}(t) &= f_3[A_1(t),\sigma(t),\alpha(t)], \end{aligned} \tag{5.14}$$

where the $f_i$, $i = 1,\cdots,3$ are complicated nonlinear functions of the arguments and are given in the Appendix.

Snake Solitons

For this class of solutions, we require the position $\phi_1(t)$ (and phase–speed $\frac{\phi_1(t)}{t}$) to vary. Hence, as a first approach, we could use (5.6)–(5.8) (and relax (5.8) later if needed). Thus,

the Eqn. (5.2) becomes

$$A(x,t) = A_1(t)e^{-\frac{4}{\phi(t)^2}[x-\phi(t)]^2}e^{i\alpha(t)} \tag{5.15}$$

$$r(x,t) = e^{-\frac{4}{\phi(t)^2}x^2} \tag{5.16}$$

Substituting the last two into (5.9), and by choosing again $m = 1$ and $\sigma(t) = \frac{2}{\phi(t)}$, the new simplified effective Lagrangian becomes

$$\begin{aligned} L_{EFF} \;=\; & \frac{\sqrt{\pi}}{12e^{\frac{10}{3}}\phi(t)}\Bigg[6e^{\frac{1}{3}}A_1(t)^3\phi(t)^2\big(b_3\cos\alpha(t)+c_3\sin\alpha(t)\big) \\ & +2\sqrt{6}A_1(t)^5\phi(t)^2\big(b_5\cos\alpha(t)+c_5\sin\alpha(t)\big) \\ & -3\sqrt{2}e^{-\frac{4}{3}}\Bigg(-2A_1(t)\sin\alpha(t)\big(-12c_1+\phi(t)^2\dot{\alpha(t)}\big) \\ & +\cos\alpha(t)\big(-2\phi^2(t)\dot{\alpha}(t)+A_1(t)(24b_1+2\epsilon\phi^2(t)+3\phi(t)\dot{\phi}(t))\big)\Bigg)\Bigg] \end{aligned} \tag{5.17}$$

As in the previous case, we are left with three parameters $A_1(t)$, $\phi(t)$ and $\alpha(t)$ in $L_{EFF}$. Varying these parameters (5.4), we obtain

$$\frac{\partial L_{EFF}}{\partial \star(t)} - \frac{\mathrm{d}}{\mathrm{dt}}\Big(\frac{\partial L_{EFF}}{\partial \dot{\star}(t)}\Big) = 0,$$

where $\star$ refers to $A_1$, $\phi$, or $\alpha$. Solving for $\dot{\star}(t)$ as a system of three ODEs,

$$\begin{aligned} \dot{A}_1(t) &= f_4[A_1(t),\phi(t),\alpha(t)] \\ \dot{\phi}(t) &= f_5[A_1(t),\phi(t),\alpha(t)] \\ \dot{\alpha}(t) &= f_6[A_1(t),\phi(t),\alpha(t)], \end{aligned} \tag{5.18}$$

where the $f_i$, $i = 4,\cdots,6$ are complicated nonlinear functions of the arguments and are given in the Appendix.

Regimes of supercritical Hopf bifurcations identified by Multiple Scales analysis then yield stable periodic solutions for $\sigma(t)$, $A_1(t)$ and $\phi(t)$. The soliton (5.2) would now "snake" or wiggle as its position varies periodically. Note that the amplitude $|A(t)|$ varies periodically as $A_1(t)$ varies, but there would be additional amplitude modulation due to the periodic variation of $\phi(t) \equiv \phi_1(t)$.

### 5.2.2 Hopf Bifurcations

The general strategy for investigating pulsating solitons and their bifurcations within the variational framework is as follows. The Euler–Lagrange equations (5.14) are treated in a completely novel way. Rather than consider the stable fixed points which correspond to the well–known stationary solitons or plain pulses, we use Hopf bifurcation theory to focus on periodic attractors. Periodic evolution of the trial function parameters on stable periodic attractors yield the pulsating soliton whose amplitude is non–stationary or time dependent.

We derive the conditions for the temporal Hopf bifurcations of the fixed points. The conditions for supercritical temporal Hopf bifurcations, leading to stable periodic orbits of $A_1(t)$, $\sigma(t)$, and $\alpha(t)$ will be evaluated using the method of Multiple Scales in Section 4. These are the conditions or parameter regimes where exhibit stable periodic oscillations, and hence stable pulsating solitons will exist within our variational formulation. Note that, as is easy to verify numerically, periodic oscillations of $A_1(t)$, $\sigma(t)$, and $\alpha(t)$, correspond to a spatiotemporal pulsating soliton structure of the $|A(x,t)|$ given by (5.2).

The fixed points of (5.14) are given by a complicated system of transcendental equations. These are solved numerically to obtain results for each particular case.

For a typical fixed point, the characteristic polynomial of the Jacobian matrix of a fixed point of (5.14) may be expressed as

$$\lambda^3 + \delta_1\lambda^2 + \delta_2\lambda + \delta_3 = 0 \tag{5.19}$$

where $\delta_i$ with $i = 1, \ldots, 3$ depend on the system parameters and the fixed points. Since these are extremely involved, we omit the actual expressions, and evaluate them numerically where needed.

To be a stable fixed point within the linearized analysis, all the eigenvalues must have negative real parts. Using the Routh–Hurwitz criterion, the necessary and sufficient conditions for (5.19) to have $Re(\lambda_{1,2,3}) < 0$ are:

$$\delta_1 > 0, \quad \delta_3 > 0, \quad \delta_1\delta_2 - \delta_3 > 0. \tag{5.20}$$

On the contrary, one may have the onset of instability of the plane wave solution occurring in one of two ways. In the first, one root of (5.14) (or one eigenvalue of the Jacobian) becomes non–hyperbolic by going through zero for

$$\delta_3 = 0. \tag{5.21}$$

Eq. (5.21) is thus the condition for the onset of "static" instability of the plane wave. Whether this bifurcation is a pitchfork or transcritical one, and its subcritical or supercritical nature, may be readily determined by deriving an appropriate canonical system in the vicinity of (5.21) using any of a variety of normal form or perturbation methods.

One may also have the onset of dynamic instability ("flutter" in the language of Applied Mechanics) when a pair of eigenvalues of the Jacobian become purely imaginary. The consequent Hopf bifurcation at

$$\delta_1\delta_2 - \delta_3 = 0 \tag{5.22}$$

leads to the onset of periodic solutions of (5.14) (dynamic instability or "flutter").

### 5.2.3 Effects of system parameters on shape of the Pulsating Soliton

Also, within the regimes of stable periodic solutions, we comprehensively investigate:
(a) the effects of the nonlinearity/dispersion/linear and nonlinear gain/loss spectral filtering on the shape and structure of the pulsating solitons given by (5.2), and
(b) the period doubling sequences of the pulsating solitons given by (5.2) as the above system parameters are varied.

To study the effects of system parameters on the shape and the stability of the Pulsating Soliton, we integrate Eqns. (5.14), (5.18) numerically in Mathematica for different sets of the various system parameters within the regime of stable periodic solutions. The resulting periodic time series for $A_1(t)$, $\sigma(t)$ and $\alpha(t)$ and are then simply inserted in (5.2) whose spatiotemporal structure ($|A(x,t)|$ versus $x$ and $t$) may be plotted. As the various system parameters within the stable regime are varied, the effects of the pulsating soliton amplitude, width, and phase will be studied.

### 5.2.4 Investigation of period doubling

Pulsating solitons can exhibit more complicated behaviors as one of the parameters changes. Simple pulsations can be transformed by period doubling and period quadrupling as the parameter changes further. This phenomena occurs due to the bifurcations at certain boundaries in the parameter space.

To study the period doubling bifurcation sequences of the pulsating solitons, we will use the standard numerical diagnostics [38]. In other words, a stable pulsating soliton will be constructed as above for a set of parameters in the stable regime. One parameter (the "distinguished bifurcation parameter") will then be varied and the effect on the periodic orbits for $A_1(t)$, $\sigma(t)$ and $\alpha(t)$ will be studied. If these period double (or subharmonics appear in the power spectral density [38]), note that this would result in an approximate temporal period doubling of $|A(t)|$ given by (5.2). This is precisely what is observed in the numerical simulations of Akhmediev et al [20], as we can see in Figs. 5.1 and 5.2. In his simulations, as $b_3$ is varied the plane pulsating soliton experienced almost period doubling. Further varying of $b_3$ produced almost period quadrupling.

In the next section we shall implement the above procedure and also will make detailed comparisons between our work that of Akhmediev et al. [20, 26].

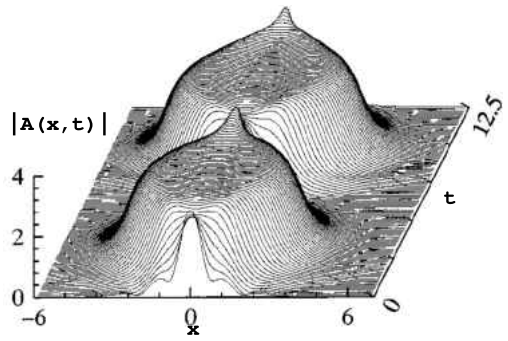


Figure 5.1: Plain pulsating soliton that shows period doubling, $b_3 = -0.785$

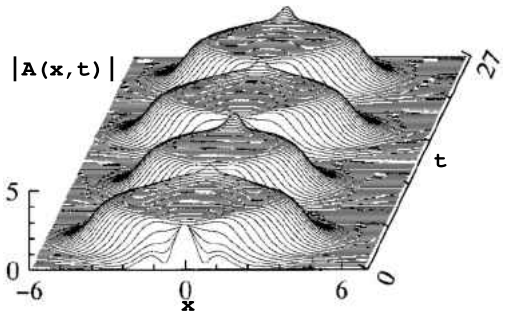


Figure 5.2: Plain pulsating soliton that shows period quadrupling, $b_3 = -0.793$

### 5.3 Stability Analysis of Periodic Orbits

In this section we will use the method of multiple scales to construct analytical approximations for the periodic orbits arising through Hopf bifurcation of the fixed point of the Euler–Lagrange equations (5.14). For the systems of differential equations given by (5.14), the limit cycle is determined by expanding the amplitude $A_1(t)$, the inverse width $\sigma(t)$, and phase $\alpha(t)$, using progressively slower spatial scales. In the standard way, we write the various or multiple scales as $z = Z_0$, $Z_1 = \delta Z_0$, $Z_2 = \delta^2 Z_0$, ..., where $\delta$ is the usual multiple scales expansion parameter. We shall expand in powers of $\delta$, to separate the various scales,

and then set $\delta = 1$ at the end in the usual way. We will choose the parameter $b_3$, which stands for cubic gain when negative, as the control or distinguished bifurcation parameter. The expansion takes the form

$$A_1 = A_{11}(Z_0, Z_1, Z_2) + \delta A_{12}(Z_0, Z_1, Z_2) + \delta^2 A_{13}(Z_0, Z_1, Z_2) \ldots, \tag{5.23}$$

$$\sigma = \sigma_1(Z_0, Z_1, Z_2) + \delta \sigma_2(Z_0, Z_1, Z_2) + \delta^2 \sigma_3(Z_0, Z_1, Z_2) \ldots, \tag{5.24}$$

$$\alpha = \alpha_1(Z_0, Z_1, Z_2) + \delta \alpha_2(Z_0, Z_1, Z_2) + \delta^2 \alpha_3(Z_0, Z_1, Z_2) \ldots. \tag{5.25}$$

Using the chain rule, the spatial derivative becomes

$$\frac{\mathrm{d}}{\mathrm{d}Z} = D_0 + \delta D_1 + \delta^2 D_2 + \ldots, \tag{5.26}$$

where $D_n = \partial/\partial Z_n$. The delay parameter $b_3$ is ordered as

$$b_3 = b_{30} + \delta^2 b_{32}, \tag{5.27}$$

where $b_{30}$ is the critical value such that (5.20) is not satisfied, (i.e. $b_{30}$ is a solution of (5.22)). This is standard for this method [1], as it allows the influence from the nonlinear terms and the control parameter to occur at the same order. Using (5.23)–(5.27) in (5.14) and equating like powers of $\delta$ yields equations at $\mathrm{O}(\delta^i)$ of the form:

$$\frac{d}{dZ_0}\vec{x}_i + \begin{pmatrix} f_{1v} & f_{2v} & f_{3v} \\ f_{1w} & f_{2w} & f_{3w} \\ f_{1z} & f_{2z} & f_{3z} \end{pmatrix} \vec{x}_i = \vec{S}_{i,j} \tag{5.28}$$

where, $i = 1, \ldots, 3$, represents the order, and $j = 1, \ldots, 3$ represents the equations, and $S_{i,j}$ is the source or inhomogeneous term for the $j^{\text{th}}$ equation at $\mathrm{O}(\delta^i)$,

$$\vec{x}_i = \begin{pmatrix} A_{1i}(Z_0, Z_1, Z_2) \\ \sigma_i(Z_0, Z_1, Z_2) \\ \alpha_i(Z_0, Z_1, Z_2) \end{pmatrix}.$$

Here,

$$\begin{pmatrix} f_{1v} & f_{2v} & f_{3v} \\ f_{1w} & f_{2w} & f_{3w} \\ f_{1z} & f_{2z} & f_{3z} \end{pmatrix} = J\Big[\frac{\partial f_1, \partial f_2, \partial f_3}{\partial A_1, \partial \sigma, \partial \alpha}\Big] \tag{5.29}$$

where $J$ is the Jacobian matrix of (5.14), numerically evaluated at the fixed points. For all orders, the structure of the equations is the same, only the source terms $S_{i,j}$ are different, and they are represented below order by order.

$$\mathrm{O}(\delta^1):$$

$$S_{1,j} = 0 \tag{5.30}$$

$$\mathrm{O}(\delta^2):$$

$$\begin{aligned} S_{2,1} = {} & \frac{1}{2}(f_{1vv}A_{11}^2 + f_{1ww}\sigma_1^2 + f_{1zz}\alpha_1^2) \\ & + f_{1vw}A_{11}\sigma_1 + f_{1vz}A_{11}\alpha_1 + f_{1wz}\sigma_1\alpha_1 - 2D_1A_{11} \end{aligned} \tag{5.31}$$

$$\begin{aligned} S_{2,2} = {} & \frac{1}{2}(f_{2vv}A_{11}^2 + f_{2ww}\sigma_1^2 + f_{2zz}\alpha_1^2) \\ & + f_{2vw}A_{11}\sigma_1 + f_{2vz}A_{11}\alpha_1 + f_{2wz}\sigma_1\alpha_1 - 2D_1\sigma_1 \end{aligned} \tag{5.32}$$

$$S_{2,3} = \frac{1}{2}(f_{3vv}A_{11}^2 + f_{3ww}\sigma_1^2 + f_{3zz}\alpha_1^2) \tag{5.33}$$
$$+ f_{1vw}A_{31}\sigma_1 + f_{3vz}A_{11}\alpha_1 + f_{3wz}\sigma_1\alpha_1 - 2D_1\alpha_1$$

$$\mathrm{O}(\delta^3) :$$

$$S_{3,1} = \frac{1}{6}(f_{1vvv}A_{11}^3 + f_{1www}\sigma_1^3 + f_{1zzz}\alpha_1^3) \tag{5.34}$$
$$+ \frac{1}{2}(f_{1vvw}A_{11}^2\sigma_1 + f_{1vvz}A_{11}^2\alpha_1 + f_{1wwz}\sigma_1^2\alpha_1 + f_{1vzz}A_{11}\alpha_1^2 + f_{1wzz}\sigma_1\alpha_1^2 + f_{1vww}A_{11}\sigma_1^2)$$
$$+ g_{1v}A_{11} + g_{1w}\sigma_1 + g_{1z}\alpha_1 + f_{1vv}A_{11}A_{12} + f_{1ww}\sigma_1\sigma_2 + f_{1zz}\alpha_1\alpha_2$$
$$+ f_{1vz}(A_{11}\alpha_2 + A_{12}\alpha_1) + f_{1vw}(A_{11}\sigma_2 + A_{12}\sigma_1) + f_{1wz}(\sigma_1\alpha_2 + \sigma_2\alpha_1)$$
$$+ f_{1wz}A_{11}\sigma_1\alpha_1 - D_2A_{11} - D_1A_{12}$$

$$S_{3,2} = \frac{1}{6}(f_{2vvv}A_{11}^3 + f_{2www}\sigma_1^3 + f_{2zzz}\alpha_1^3) \tag{5.35}$$
$$+ \frac{1}{2}(f_{2vvw}A_{11}^2\sigma_1 + f_{2vvz}A_{11}^2\alpha_1 + f_{2wwz}\sigma_1^2\alpha_1 + f_{2vzz}A_{11}\alpha_1^2 + f_{2wzz}\sigma_1\alpha_1^2 + f_{2vww}A_{11}\sigma_1^2)$$
$$+ g_{2v}A_{11} + g_{2w}\sigma_1 + g_{2z}\alpha_1 + f_{2vv}A_{11}A_{12} + f_{2ww}\sigma_1\sigma_2 + f_{2zz}\alpha_1\alpha_2$$
$$+ f_{2vz}(A_{11}\alpha_2 + A_{12}\alpha_1) + f_{2vw}(A_{11}\sigma_2 + A_{12}\sigma_1) + f_{2wz}(\sigma_1\alpha_2 + \sigma_2\alpha_1)$$
$$+ f_{2wz}A_{11}\sigma_1\alpha_1 - D_2\sigma_1 - D_1\sigma_2$$

$$S_{3,3} = \frac{1}{6}(f_{3vvv}A_{11}^3 + f_{3www}\sigma_1^3 + f_{3zzz}\alpha_1^3) \tag{5.36}$$
$$+ \frac{1}{2}(f_{3vvw}A_{11}^2\sigma_1 + f_{3vvz}A_{11}^2\alpha_1 + f_{3wwz}\sigma_1^2\alpha_1 + f_{3vzz}A_{11}\alpha_1^2 + f_{3wzz}\sigma_1\alpha_1^2 + f_{3vww}A_{11}\sigma_1^2)$$
$$+ g_{3v}A_{11} + g_{1w}\sigma_1 + g_{3z}\alpha_1 + f_{3vv}A_{11}A_{12} + f_{3ww}\sigma_1\sigma_2 + f_{3zz}\alpha_1\alpha_2$$
$$+ f_{3vz}(A_{11}\alpha_2 + A_{12}\alpha_1) + f_{3vw}(A_{11}\sigma_2 + A_{12}\sigma_1) + f_{3wz}(\sigma_1\alpha_2 + \sigma_2\alpha_1)$$
$$+ f_{3wz}A_{11}\sigma_1\alpha_1 - D_2\alpha_1 - D_1\alpha_2$$

Here, the $g_i$ functions are obtained by using (5.27) in $f_i$ as this variation will introduce additional terms of higher order. i.e. $f_i \to f_i + \delta^2 g_i$. So the new $f_i$ will contain $b_{30}$ terms and represents the fact that we are situated on the Hopf bifurcation curve, while $g_i$s contain $b_{32}$ terms, and shows how far we are from the curve.

Now we will proceed to solve (5.28) order by order. Since the sources for the first order system are identically zero, we may assume the first order solution of (5.28) to be

$$\vec{x}_1 = \begin{pmatrix} \beta_1 \\ \gamma_1 \\ \eta_1 \end{pmatrix} e^{-i\omega_0 Z_0} + c.c., \tag{5.37}$$

and substituting back this solution into (5.28), we obtain the eigenvalue problem which gives the eigenvalue $\omega_0$, and corresponding eigenvector $\vec{x}_1$. By looking at the characteristic polynomial of the Jacobian matrix of (5.19) we obtain that

$$\delta_2 = \omega_0^2 = -f_{1w}f_{2v} + f_{1v}f_{2w} - f_{1z}f_{3v} + f_{1v}f_{3z} + f_{2w}f_{3z}. \tag{5.38}$$

Hence, the first order solution of (5.28), $\vec{x}_1$ can be written as

$$A_{11} = (a+ib)\theta(Z_1, Z_2)e^{i\omega_0 Z_0} + (a-ib)\bar{\theta}(Z_1, Z_2)e^{-i\omega_0 Z_0} \tag{5.39}$$

$$\sigma_1 = (c+id)\theta(Z_1, Z_2)e^{i\omega_0 Z_0} + (c-id)\bar{\theta}(Z_1, Z_2)e^{-i\omega_0 Z_0} \tag{5.40}$$

$$\alpha_1 = \theta(Z_1, Z_2)e^{i\omega_0 Z_0} + \bar{\theta}(Z_1, Z_2)e^{-i\omega_0 Z_0}, \tag{5.41}$$

where $\eta_1$ is taken to be 1, $\beta_1 \equiv a + ib$, and $\gamma_1 \equiv c + id$. Now, since the first order solutions (5.39)–(5.41) are known, the second order sources $S_{2,j}$ may be evaluated via (5.31)–(5.33).

In the standard way, these take the form

$$\vec{S}_{2,j} = \begin{pmatrix} S_{2,1}^{(0)} \\ S_{2,2}^{(0)} \\ S_{2,3}^{(0)} \end{pmatrix} + \begin{pmatrix} S_{2,1}^{(1)} \\ S_{2,2}^{(1)} \\ S_{2,3}^{(1)} \end{pmatrix} e^{i\omega_0 Z_0} + \begin{pmatrix} S_{2,1}^{(2)} \\ S_{2,2}^{(2)} \\ S_{2,3}^{(2)} \end{pmatrix} e^{2i\omega_0 Z_0} + c.c., \tag{5.42}$$

Setting the coefficients of the secular first harmonic or $e^{i\omega_0 Z_0}$ terms (which are the solutions of the homogeneous equation) to zero, i.e. $\vec{S}_{2,j}^{(1)} = \vec{0}$ yields

$$\begin{aligned} D_1\theta &= \frac{\partial\theta}{\partial Z_1} = 0 \\ D_1\bar{\theta} &= \frac{\partial\bar{\theta}}{\partial Z_1} = 0. \end{aligned} \tag{5.43}$$

Using (5.43), (5.39)–(5.42), and the second order sources (5.42), and by assuming a second order particluar solution of (5.28) of the type

$$\vec{x}_2 = \begin{pmatrix} A_{12}^{(0)} \\ \sigma_2^{(0)} \\ \alpha_2^{(0)} \end{pmatrix} + \begin{pmatrix} A_{12}^{(2)} \\ \sigma_2^{(2)} \\ \alpha_2^{(2)} \end{pmatrix} e^{2i\omega_0 Z_0} + c.c., \tag{5.44}$$

we can solve the system (5.28) by elementary linear algebra for the unknowns $A_{12}^{(0)}$, $\sigma_2^{(0)}$, and $\alpha_2^{(0)}$, by looking at the homogeneous system, and for the unknowns $A_{12}^{(2)}$, $\sigma_2^{(2)}$, and $\alpha_2^{(2)}$, by looking at the inhomogeneous system (5.28). Using the full second order solution $\vec{x}_2$, which includes the DC terms and the 2$^{\text{nd}}$ harmonic terms, and the previously found first order solution $\vec{x}_1$, we can find the third order sources via (5.34)–(5.36). By writing the third order sources as

$$\vec{S}_{3,j} = \begin{pmatrix} S^{(0)}_{3,1} \\ S^{(0)}_{3,2} \\ S^{(0)}_{3,3} \end{pmatrix} + \begin{pmatrix} S^{(1)}_{3,1} \\ S^{(1)}_{3,2} \\ S^{(1)}_{3,3} \end{pmatrix} e^{i\omega_0 Z_0} + \begin{pmatrix} S^{(2)}_{3,1} \\ S^{(2)}_{3,2} \\ S^{(2)}_{3,3} \end{pmatrix} e^{2i\omega_0 Z_0} + \begin{pmatrix} S^{(3)}_{3,1} \\ S^{(3)}_{3,2} \\ S^{(3)}_{3,3} \end{pmatrix} e^{3i\omega_0 Z_0} + c.c., \quad (5.45)$$

we can find the coefficient of the secular terms $e^{i\omega_0 Z_0}$ terms, i.e. $\vec{S}^{(1)}_{3,j}$. Now, the evolution equation can be found by solving (5.46).

$$\begin{pmatrix} f_{1v} + i\omega_0 & f_{2v} & f_{3v} \\ f_{1w} & f_{2w} + i\omega_0 & f_{3w} \\ f_{1z} & f_{2z} & f_{3z} + i\omega_0 \end{pmatrix} \vec{x}_3 = \vec{S}^{(1)}_{3,j} \quad (5.46)$$

This system can be written in the compact form

$$(\mathbf{A} - \lambda \mathbf{I})\vec{x}_3 = \vec{S}^{(1)}_{3,j}, \quad (5.47)$$

where $\lambda = \pm i\omega_0$ are the eigenvalues of $\mathbf{A}$. By the Fredholm alternative, (5.47) has solution iff $\vec{S}^{(1)}_{3,j} \in Range(\mathbf{A} - \lambda \mathbf{I})$. The final evolution equation for the coefficients in the linear solutions of (5.28) my be obtained more directly [38] using Cramer's rule as

$$\begin{vmatrix} S^{(1)}_{3,1} & f_{2v} & f_{3v} \\ S^{(1)}_{3,2} & f_{2w} + i\omega_0 & f_{3w} \\ S^{(1)}_{3,3} & f_{2z} & f_{3z} + i\omega_0 \end{vmatrix} = 0 \quad (5.48)$$

From (5.48), we have the evolution equation on the slow second order $Z_2$ scale

$$\frac{\partial \theta}{\partial Z_2} = S_1 \theta^2 \bar{\theta} + S_2 \theta. \quad (5.49)$$

Writing $\theta = \frac{1}{2}Ae^{i\zeta}$ and separating (5.49) into real and imaginary parts, yields

$$\frac{\partial A}{\partial Z_2} = \frac{S_{1r}A^3}{4} + S_{2r}A, \tag{5.50}$$

where $S_{1r}$ and $S_{2r}$ represent the real parts of $S_1$ and $S_2$ respectively. In the usual way, the fixed points of (5.48), $(A_1, A_{2,3})$ where

$$\begin{aligned} A_1 &= 0, \\ A_{2,3} &= \pm 2\sqrt{-\frac{S_{2r}}{S_{1r}}} \end{aligned} \tag{5.51}$$

give the amplitude of the solution $\theta = \frac{1}{2}Ae^{i\zeta}$, with $A_{2,3}$ corresponding to the bifurcation periodic orbits. Clearly $A_{2,3}$ are real fixed points whenever

$$\frac{S_{2r}}{S_{1r}} < 0, \tag{5.52}$$

and the Jacobian of the right hand side of (5.52) evaluated at $A_{2,3}$ is $J|_{A_{2,3}} = -2S_{2r}$, where $J(A) = \frac{\partial(\frac{S_{1r}A^3}{4} + S_{2r}A)}{\partial A}$. Clearly, a necessary condition for stability is to have $S_{2r} > 0$, and for instability $S_{2r} < 0$. Thus, the system undergoes:

(a) supercritical Hopf bifurcations when

$$S_{2r} > 0, \qquad S_{1r} < 0, \tag{5.53}$$

(b) subcritical Hopf bifurcations when

$$S_{2r} < 0, \qquad S_{1r} > 0. \tag{5.54}$$

We will use (5.53) next to identify regimes of supercritical bifurcations where the solutions of the Euler–Lagrange equations (5.14) or (5.18) for pulsating or snake solitons will result in

oscillations of $A_1(t)$, $\sigma(t)$ or $\phi(t)$ and $\alpha(t)$ that when substituted into trial function (5.2) or (5.15) will lead to pulsating or snake solitary wave solitons.

## 5.4 Results for the General Plane Pulsating Soliton

An example of a plain pulsating soliton, obtained by us via independent simulations on (2.1), is shown in Fig. 5.3 using the trial functions (5.11) and (5.12). It has a different shape at each time $t$, since it evolves, but it recovers its exact initial shape after a period. To derive

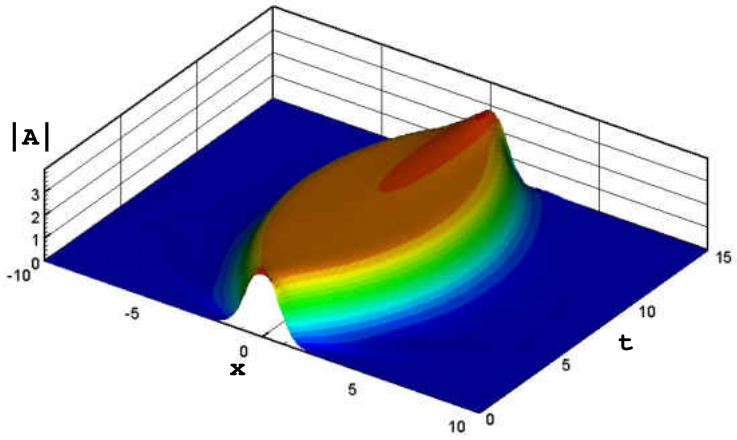


Figure 5.3: Plain pulsating soliton for $b_3 = -0.66$ and $\epsilon = -0.1$

the conditions for occurrence of stable periodic orbits of $A_1(t)$, $\sigma(t)$, and $\alpha(t)$, we proceed as follows.

First, we fix a set of system parameters $b_1 = 0.08$, $b_5 = 0.1$, $c_1 = 0.5$, $c_3 = 1$, $c_5 = -0.1$. Then, we solve numerically the system of transcendental equations (5.14), which are the equations of the fixed points. By the Ruth–Hurwitz conditions, the Hopf curve is defined as

$\delta_1\delta_2 - \delta_3 = 0$. This condition, along with the equations of the fixed points leads to onset of periodic solutions of (5.14) as we will see next.

On the Hopf bifurcation curve we obtain that $b_3 = -0.216825$, and $\epsilon = -0.345481$, while the fixed points are $A_1(0) = 0.954712$, $\sigma(0) = 0.917093$, and $\alpha(0) = -0.181274$. Using these values of $b_3$ and $\epsilon$ , we integrate numerically the systems of three ODEs (5.14), using as initial conditions the three values of the fixed points. Hopf bifurcations occur in this system leading to periodic orbits.

Next, we may plot the time series of the periodic orbit for the amplitude $A_1(t)$, and, as expected, we noticed that the amplitude was very small, since it is proportional to the square root of the distance from the Hopf curve.

To construct pulsating solitons with amplitudes large enough, we had to move away from the Hopf curve, as much as possible, but at the same time to be sure not to be outside of the parameters ranges for the existence of the pulsating soliton. That could be achieved by varying one or more of the system parameters. First, we varied $\epsilon$ slowly away from the Hopf curve. Repeating the above procedure to construct a plane pulsating soliton, we noticed that the pulsating soliton still had very small amplitudes $A_1(t)$, of magnitude only of $10^{-4}$. Therefore, we decided to vary another parameter, $b_3$, which stands for the cubic gain when negative. We found that the domain of existence for the pulsating soliton as a function of $b_3$ was $[-0.2531943, -0.1424]$, passing through the Hopf curve value of $b_3 = -0.216825$. Within this range, we varied $b_3$, and studied the effects on the shape and the stability, as well as the various bifurcations that lead potentially to period doubling and quadrupling. For the

largest value of $b_3$, i.e. $b_3 = -0.1424$, we numerically integrate in Mathematica the three differential equations (5.14), and we plot the periodic orbit, which is shown in Fig. 5.4.

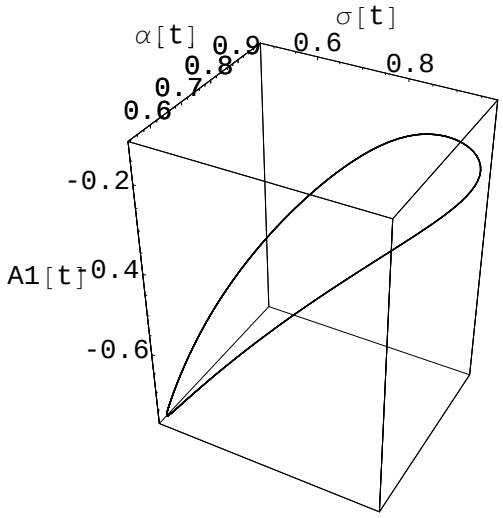


Figure 5.4: The periodic orbit for $b_3 = -0.1424$

The resulting periodic time series for $A_1(t)$, $\sigma(t)$, and $\alpha(t)$ from Fig. 5.5 are then simply inserted in (5.11) whose spatiotemporal structure ($|A(x,t)|$ or phase $A(x,t)$ versus $x$ and $t$) is plotted in Fig. 5.6. As the various system parameters $c_1$, $c_3$, $c_5$, $b_1$, $b_5$ within the stable regime are varied, the effects of the pulsating soliton amplitude, width, position, phase speed (and, less importantly, phase) may also be studied, and this is discussed subsequently. Repeating the above, we also show the orbit and the plane pulsating soliton for the smallest value of $b_3 = -0.2531943$ in Figs. 5.7 and 5.8.

Next, we consider the detailed effects of varying the parameter $b_3$. For the chosen values of the system parameters of $b_1 = 0.08$, $b_5 = 0.1$, $c_1 = 0.5$, $c_3 = 1$, $c_5 = -0.1$, and $\epsilon = -0.345481$,

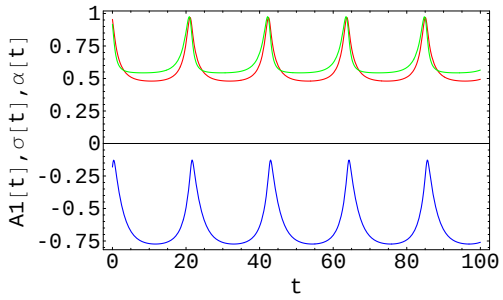


Figure 5.5: Periodic time series for $b_3 = -0.1424$

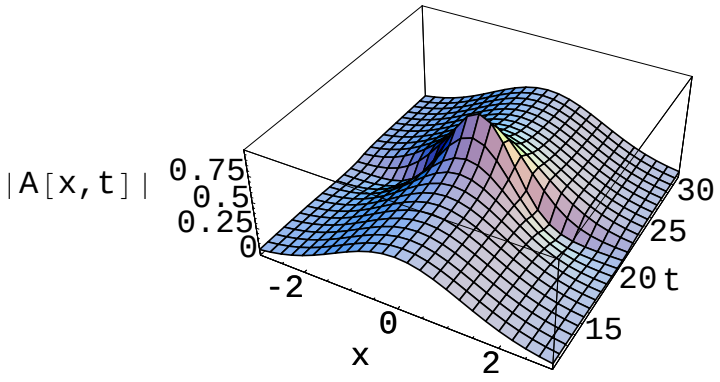


Figure 5.6: Plane pulsating soliton for $b_3 = -0.1424$

with the fixed points $A_1(0) = 0.954712$, $\sigma(0) = 0.917093$, and $\alpha(0) = -0.181274$, from (5.14) and (5.22), the Hopf bifurcation occurs at

$$b_{3Hopf} = -0.216825 \tag{5.55}$$

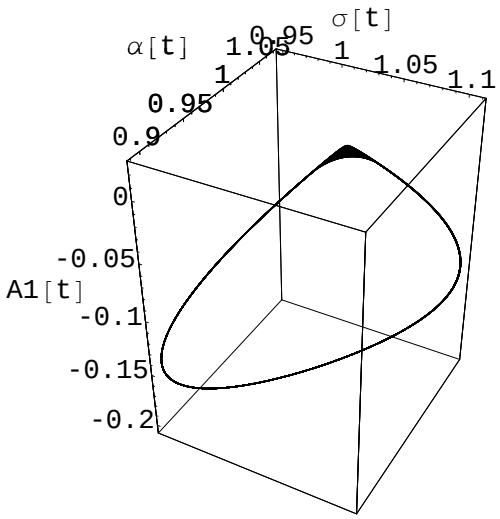


Figure 5.7: The periodic orbit for $b_3 = -0.2531943$

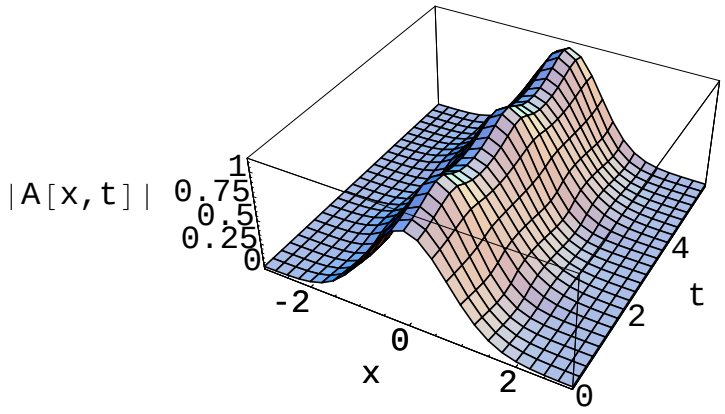


Figure 5.8: Plane pulsating soliton for $b_3 = -0.2531943$

First, let us consider values of $b_3$ greater that $b_{3Hopf}$. There is a stable and robust periodic orbit to this side which becomes larger and deforms as $b_3$ is increased up to $-0.1424$. A representative periodic orbit is shown in Fig. 5.4.

Next, moving to values smaller than $b_{3Hopf}$, we see a clean, periodic orbit which slowly grows in size as $b_3$ is made more negative. The periodic orbit, time series, and solitary waves are qualitatively similar to those for $b_3 > b_{3Hopf}$.

However, more interesting dynamics is seen as $b_3$ is decreased further. The periodic orbit goes unstable via a very rapid, complete cascade of period–doubling bifurcations between $b_3 = -0.25$, and $b_3 = -0.2516$. In Fig. 5.9 we show the period doubled orbit for $b_3 = -0.2516$. The orbit at $b_3 = -0.2531943$ after many more period doublings is shown in Fig. 5.7. The corresponding solitary wave solution is shown in Fig. 5.8. Notice that this feature agrees with the sequence of period doublings for pulsating solitons seen by Akhmediev et al. [20]. Note also that one may track the complete cascade of period doublings using software such AUTO or DERPER, or using the schemes of Holodniok and Kubicek [39]. Next, we shall consider the effect of all the various parameters in the CGLE (2.1) on the shape (amplitude, width, period) and stability of the pulsating solitary wave. This is a key feature of interest that was repeatedly mentioned by many speakers in the multi–day session on Dissipative Solitons at the $4^{\text{th}}$ IMACS Conference on Nonlinear Waves held in Athens, Georgia in April 2005, as there are no existing theoretical guidelines or predictions about this at all.

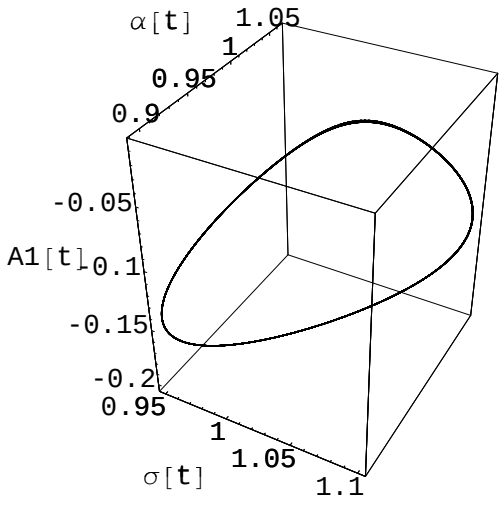


Figure 5.9: The periodic orbit for $b_3 = -0.2516$

In considering the parameter effects on the solitary wave shape and period, note that the wave is a spatially coherent structure (or a "collective coordinate" given by the trial function) whose parameters oscillate in time. Hence, the temporal period of the pulsating soliton is the same as the period $T$ of the oscillations of $A_1(t)$, $\sigma(t)$, and $\alpha(t)$ on their limit cycle. As for the peak amplitude and peak width of the pulsating wave, these are determined by the peak amplitude $A_{1p}$ of $A_1(t)$, and the *reciprocal* of the peak amplitude $\sigma_p$ of $\sigma(t)$ respectively, i.e. at any time $t$ when the amplitude is maximum, the width will be minimum, and vice versa.

Keeping the above in mind, we vary the parameters of the CGLE in turn and we observe the resulting effects on $A_{1p}$ (the peak amplitude), $\sigma_p$ (the inverse width), and $T$ (the temporal period) of the pulsating soliton:

(i) For *increased* $b_1$, the values of $A_{1p}$, $\sigma_p$, and $T$ all *increase*.

(ii) *Increasing* $b_5$ *augments* all of $A_{1p}$, $\sigma_p$, and $T$.

(iii) *Raising* $c_1$ *increases* $A_{1p}$, $\sigma_p$, and $T$.

(iv) *Incrementing* $c_3$ *decreases* all of $A_{1p}$, $\sigma_p$, and $T$.

(v) *Augmenting* $c_5$ causes a *decrease* in $A_{1p}$, $\sigma_p$, and $T$.

(vi) *Raising* $\epsilon$ causes $A_{1p}$, $\sigma_p$, and $T$ to *fall*. These results can be seen in Figs.5.10,5.11.

The results in cases (a),(c),(e) of Figs. 5.10,5.11 are to be compared with the plane pulsating soliton obtained by numerical simulations from Fig. 5.3. The results in cases (b),(d),(f) of Figs. 5.10,5.11 are to be compared with the plane pulsating soliton obtained by variational approximation from Fig. 5.8. The above constitute our detailed predictions of the various parameters in the CGLE on the amplitude, inverse width, and temporal width of the pulsating solitons. We have verified that each set of predictions (a)–(f) above agree when the corresponding parameter is varied in the solitary wave simulation for the full PDE shown in Fig. 5.3. Note also that $A_1(t)$ and $\sigma(t)$ are always in phase, so that $A_{1p}$ and $\sigma_p$ occur simultaneously. Thus, the pulsating solitons are tallest where they have least width. This is completely consistent with our simulation in Fig. 5.3, as well as those in [20, 21].

## 5.5 Results for the Snake Soliton

An example of a snake soliton, obtained by us via independent simulations on (2.1), is shown in Fig. 5.12 using the trial functions (5.15) and (5.16). The soliton would now "snake" or

wiggle as its position varies periodically. Note that the amplitude $|A(t)|$ varies periodically as $A_1(t)$ varies, but there would be additional amplitude modulation due to the periodic variation of $\phi(t)$.

To derive the conditions for occurrence of stable periodic orbits of $A_1(t)$, $\phi(t)$, and $\alpha(t)$, we proceed as follows. First, we fix a set of system parameters $b_1 = 0.08$, $b_5 = 0.11$, $c_1 = 0.5$, $c_3 = 1$, $c_5 = -0.08$. Then, we solve numerically the system of transcendental equations (5.18), which are the equations of the fixed points. By the Ruth–Hurwitz conditions, the Hopf curve is defined as $\delta_1\delta_2 - \delta_3 = 0$. This condition, along with the equations of the fixed points leads to onset of periodic solutions of (5.18) as we will see next.

On the Hopf bifurcation curve we obtain that $b_3 = -1.89646$, and $\epsilon = -0.297393$, while the fixed points are $A_1(0) = 0.583236$, $\phi(0) = 1.05969$, and $\alpha(0) = 0.185515$. Using these values of $b_3$ and $\epsilon$ , we integrate numerically the systems of three ODEs (5.14), using as initial conditions the three values of the fixed points. Hopf bifurcations occur in this system leading to periodic orbits.

Next, we may plot the time series of the periodic orbit for the amplitude $A_1(t)$, and, as expected, we noticed that the amplitude was very small, since it is proportional to the square root of the distance from the Hopf curve.

To construct snake solitons with amplitudes large enough, we had to move away from the Hopf curve, as much as possible, but at the same time to be sure not to be outside of the parameters ranges for the existence of the pulsating soliton. That could be achieved by varying one or more of the system parameters. For the value of $b_3 = -0.835$, and

$\epsilon = -0.1$ we numerically integrate in Mathematica the three differential equations (5.18). The resulting periodic time series for $A_1(t)$, $\phi(t)$, and $\alpha(t)$ are then simply inserted in (5.15) whose spatiotemporal structure ($|A(x,t)|$ or phase $A(x,t)$ versus $x$ and $t$) is plotted in Fig. 5.13. As the various system parameters $c_1$, $c_3$, $c_5$, $b_1$, $b_3$, $b_5$, and $\epsilon$ within the stable regime are varied, the effects of the snake amplitude, position, width (and, less importantly, phase) may also be studied, and this is discussed subsequently. Next, we shall consider the effect of all the various parameters in the CGLE (2.1) on the shape (amplitude, position, phase, period) and stability of the snake. As mentioned before, this is a key feature of interest that was repeatedly mentioned by many speakers in the multi–day session on Dissipative Solitons at the 4$^{\text{th}}$ IMACS Conference on Nonlinear Waves held in Athens, Georgia in April 2005, as there are no existing theoretical guidelines or predictions about this at all.

In considering the parameter effects on snake shape and period, note that the wave is a spatially coherent structure (or a "collective coordinate" given by the trial function) whose parameters oscillate in time. Hence, the temporal period of the snake is the same as the period $T$ of the oscillations of $A_1(t)$, $\phi(t)$, and $\alpha(t)$ on their limit cycle. As for the peak amplitude and peak position of the snake, these are determined by the peak amplitude $A_{1p}$ of $A_1(t)$, and the peak position $\phi_p$ of $\phi(t)$ respectively. Notice that from (5.15) we can regard the width and the amplitude of the snake as being inverse proportional with position $\phi(t)$ for the snake i.e., at any time $t$ when the amplitude is minimum, the width will be minimum, so the position is maximum and vice versa. Threfore, maximum deflection from the horizontal position $x = const.$ is obtained when the position of the snake is maximum, and hence the

width and amplitude are minimum. This can be clearly seen in Fig. 5.14. Keeping the above in mind, we vary the parameters of the CGLE in turn and we observe the resulting effects on $A_{1p}$ (the peak amplitude), $\phi_p$ (the position), and $T$ (the temporal period) of the snake soliton:

(vii) For *increased* $b_1$, the values of $A_{1p}$, $\phi_p$, and $T$ all *increase*.

(viii) *Increasing* $b_3$ *augments* all of $A_{1p}$, $\phi_p$, and $T$.

(ix) *Increasing* $b_5$ *increases* all of $A_{1p}$, $\phi_p$, and $T$.

(x) *Raising* $c_1$ *increases* $A_{1p}$, $\phi_p$, but *decreases* $T$.

(xi) *Incrementing* $c_3$ *decreases* all of $A_{1p}$, $\phi_p$, and $T$.

(xii) *Augmenting* $c_5$ causes a *decrease* in $A_{1p}$, $\phi_p$, and *increases* $T$.

(xiii) *Raising* $\epsilon$ causes $A_{1p}$, $\sigma_p$ to *rise*, but $T$ to *fall*.

An example of a snake soliton when we change $\epsilon$ is shown in Fig. 5.15. The above constitute our detailed predictions of the various parameters in the CGLE on the amplitude, position, and temporal width of the snake solitons. We have verified that each set of predictions (g)–(m) above agree when the corresponding parameter is varied in the solitary wave simulation for the full PDE shown in Fig. 5.12. Note also that $A_1(t)$ and $\phi(t)$ are always in phase, so that $A_{1p}$ and $\phi_p$ occur simultaneously. Thus, the pulsating solitons are tallest where they have most width. This is completely consistent with our simulation in Figure 5.12, as well as those in [20, 21].

## 5.6 Nonexistence of Hopf Bifurcations in Hamiltonian Systems: Connections to Pulsating Solitons

It is widely reported [21, 40] and generally accepted that Hamiltonian systems, as well as integrable systems which are a subclass, do not admit pulsating solitary wave solutions. If excited initially, pulsating solitons in Hamiltonian and integrable systems re–shape themselves and evolve into regular stationary waves. The only exceptions are pulsating structures comprising nonlinear superpositions of stationary solitons in integrable systems [22].

In addition, the regimes of the pulsating solitons in the CGLE are very far from the integrable nonlinear Schrödinger equation limit. This fact, and the great diversity of pulsating solitons in the CGLE, both indicate a new mechanism which is operative in dissipative systems in the creation of these pulsating structures.

The primary point of this section is that Hopf bifurcations are the new mechanism responsible for the occurrence of these pulsating solitons in dissipative systems, and we shall analyze both plain pulsating solitons and snakes via this mechanism. However, in order to establish that Hopf bifurcations are indeed the operative mechanism creating the various pulsating solitons in dissipative systems, we first proceed to prove their absence in Hamiltonian systems. The proof of the absence of Hopf bifurcations may possibly explain the above–mentioned absence of pulsating solitons in Hamiltonian and integrable systems.

For a Hamiltonian system with Hamiltonian $H$, the particular evolution equations may be represented in canonical form as [41].

$$i\Psi_\zeta = \frac{\delta H}{\delta \Psi^\star}$$
$$i\Psi^\star_\zeta = -\frac{\delta H}{\delta \Psi}. \tag{5.56}$$

These may be further combined into

$$i\dot{\vec{x}} = L\nabla_{\vec{x}} H(\vec{x}) \tag{5.57}$$

where $\dot{}$ denotes $\delta/\delta\zeta$,

$$\vec{x} = [\Psi, \Psi^\star], \tag{5.58}$$

$I$ is the $n \times n$ unit matrix, and $L\nabla$ is the symplectic gradient of $H(\vec{x})$

$$L = \begin{pmatrix} 0 & I \\ -I & 0 \end{pmatrix}. \tag{5.59}$$

Equation (5.57) follows from

$$i \begin{pmatrix} \dot{\Psi} \\ \dot{\Psi}^\star \end{pmatrix} = \begin{pmatrix} 0 & I \\ -I & 0 \end{pmatrix} \begin{pmatrix} \nabla_\Psi H \\ \nabla_{\Psi^\star} H \end{pmatrix}$$

which is identical to (5.56).

The fixed (or equilibrium or critical ) points of (5.57) satisfy

$$\nabla_{\vec{x}} H(\vec{x}) = 0, \tag{5.60}$$

or equivalently

$$\frac{\delta H}{\delta \Psi^\star} = 0, \qquad \frac{\delta H}{\delta \Psi} = 0.$$

Using the standard representation

$$H = \frac{1}{2}\langle \Psi_\zeta, \Psi_\zeta \rangle + V(\Psi) \tag{5.61}$$

for the Hamiltonian, this implies

$$\vec{\nabla}_\Psi V = 0$$

or

$$\frac{\delta V}{\delta \Psi} = 0. \tag{5.62}$$

At a fixed point $\vec{x}_0 = [\Psi_0, \Psi_0{}^\star]$, the Jacobian matrix of (5.57) is

$$J(\vec{x}_0) = L\mathcal{H} \tag{5.63}$$

where

$$\mathcal{H} \equiv \left[\frac{\delta^2 H}{\delta x_i \delta x_j}\right]_{\vec{x}_0} = \begin{pmatrix} \mathcal{V} & 0 \\ 0 & I \end{pmatrix} \tag{5.64}$$

from (5.60). Here

$$\mathcal{V} = \left[\frac{\delta^2 V}{\delta \Psi_i \delta \Psi_j}\right]_{\vec{x}_0} \tag{5.65}$$

Hence, we have

$$J(\vec{x}_0) = \begin{pmatrix} 0 & I \\ -I & 0 \end{pmatrix} \begin{pmatrix} \mathcal{V} & 0 \\ 0 & I \end{pmatrix} = \begin{pmatrix} 0 & I \\ -\mathcal{V} & 0 \end{pmatrix} \tag{5.66}$$

whose eigenvalues $\lambda$ satisfy the characteristic equation

$$|\mathcal{V} + \lambda^2 I| = 0 \tag{5.67}$$

Since the matrix $\mathcal{V}$ is symmetric, its eigenvalues are real and the solutions $\lambda$ of (5.67) are thus either real or purely imaginary. Thus, as claimed earlier, Hopf bifurcations cannot occur in Hamiltonian systems. The introduction of dissipation allows the occurrence of Hopf bifurcation and, as we shall model in the remainder of this dissertation, introduces the various pulsating solitary wave structures which occur in the CGLE.

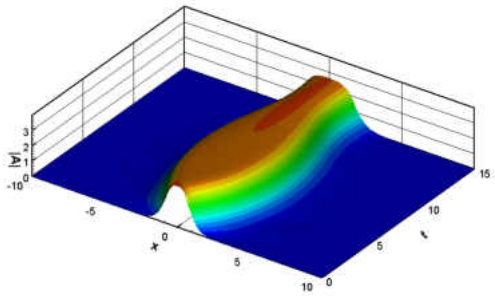

(a) Numerical simulations $b_1 = 0.2$

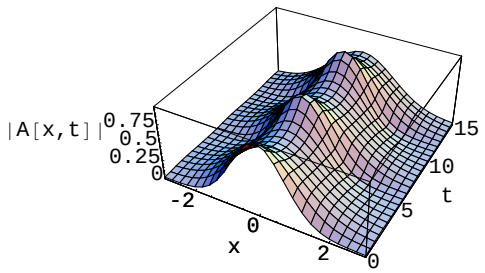


(b) Variational approximation $b_1 = 0.1$

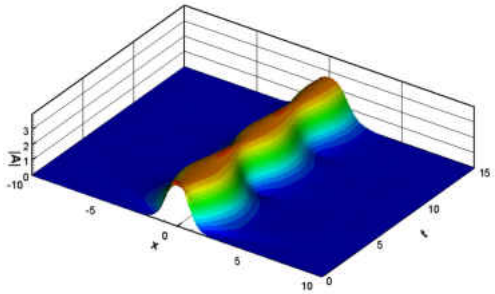

(c) Numerical simulations $b_5 = 0.11$

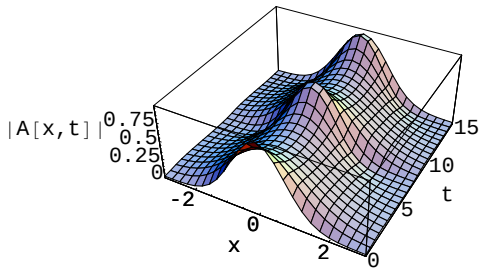


(d) Variational approximation $b_5 = 0.13$

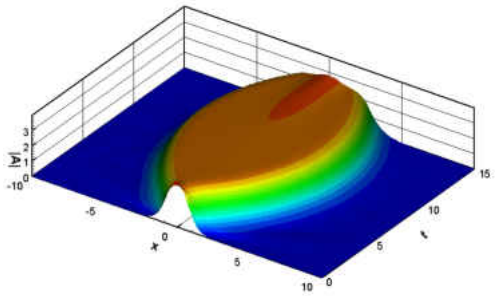

(e) Numerical simulations $c_1 = 0.6$

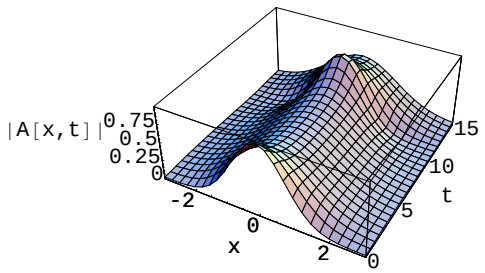


(f) Variational approximation $c_1 = 0.6$

Figure 5.10: Predictions for the plane pulsating soliton cases i–iii

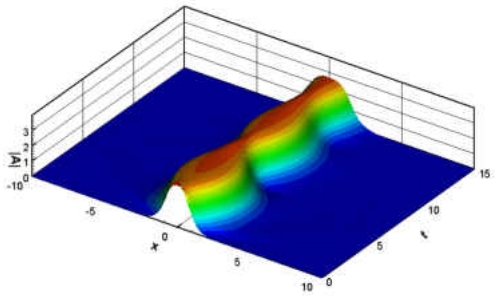

(a) Numerical simulations $c_3 = 1.05$

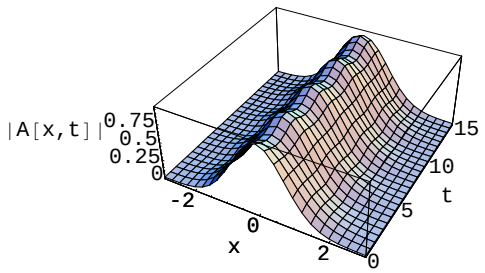


(b) Variational approximation $c_3 = 1.05$

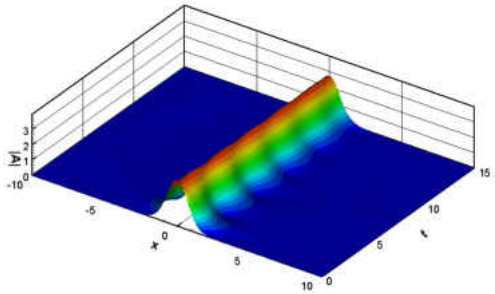

(c) Numerical simulations $c_5 = -0.075$

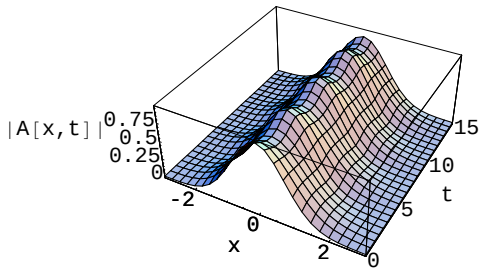


(d) Variational approximation $c_5 = -0.08$

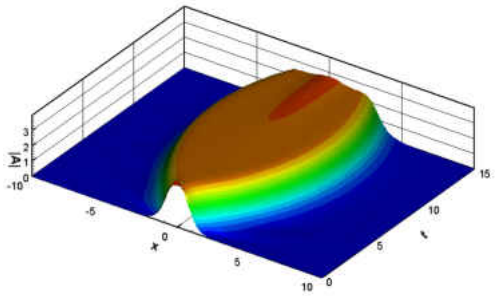

(e) Numerical simulations $\epsilon = -0.08$

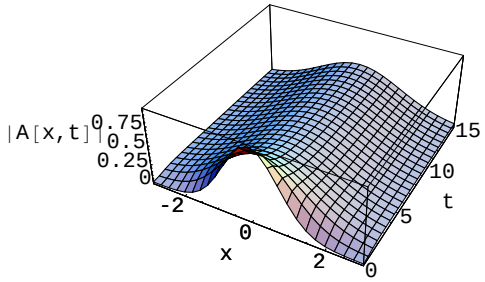


(f) Variational approximation $\epsilon = -0.06$

Figure 5.11: Predictions for the plane pulsating soliton cases iv–vi

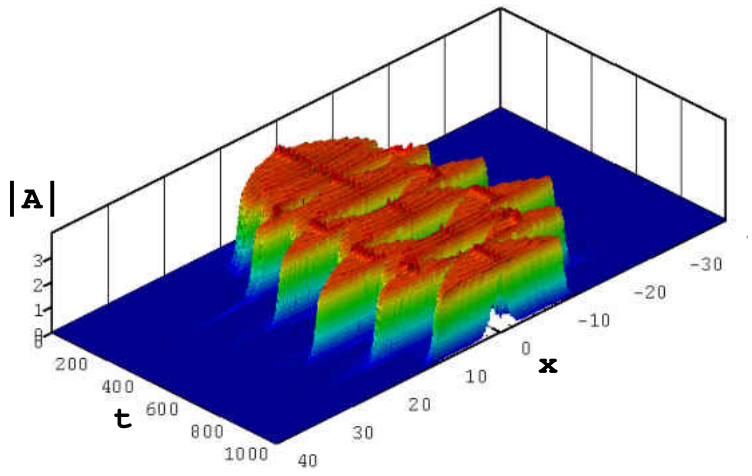


Figure 5.12: Snake soliton for $b_3 = -0.835$

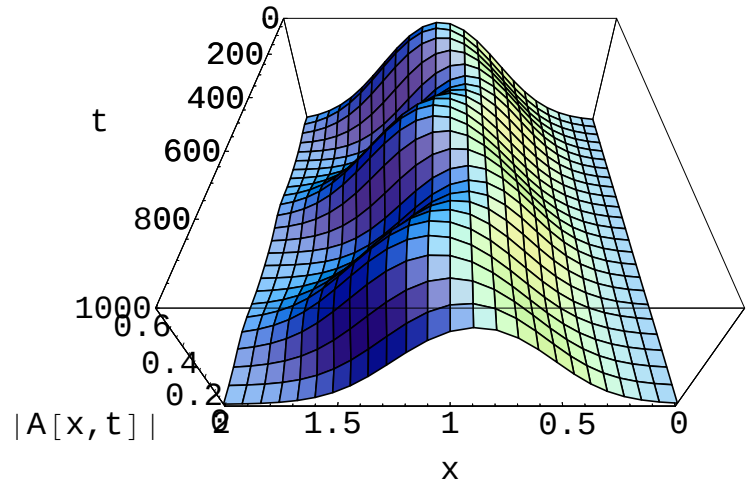


Figure 5.13: Snake soliton for $b_3 = -0.835$, and $\epsilon = -0.1$

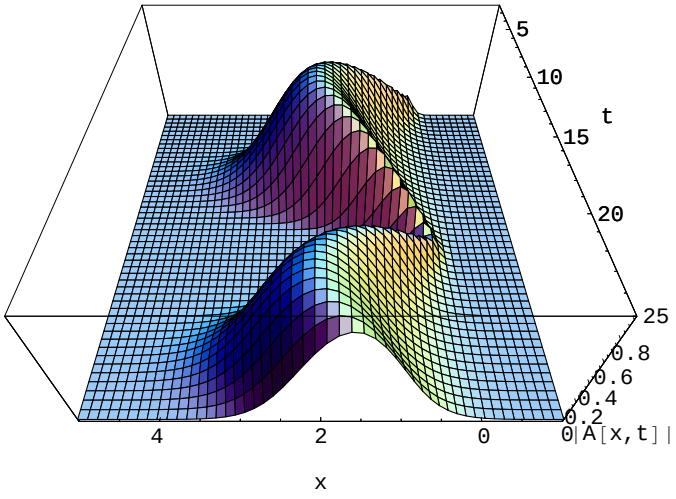


Figure 5.14: Snake soliton for $b_1 = 0.19$

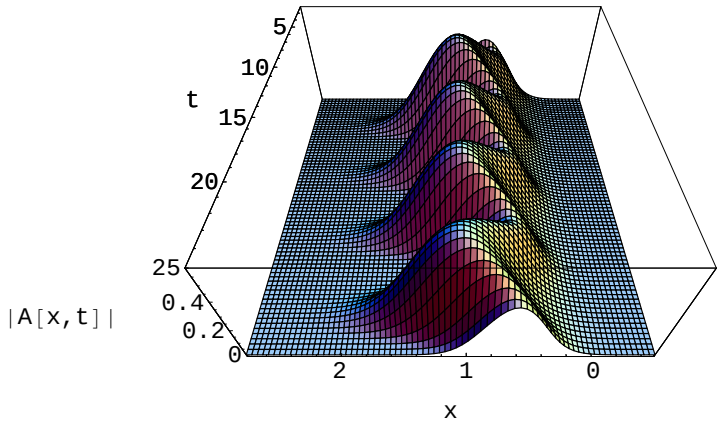


Figure 5.15: Snake soliton for $\epsilon = -0.08$

# CHAPTER SIX: PULSATING SOLITONS USING HYPERBOLIC ANSATZ

The detailed modeling in Chapter 5 elucidates many numerically observed features of pulsating and snake solitons. The one unsatisfactory feature is the somewhat narrower peaks our solitons exhibit in comparison with the plateau–like peaks of the numerical solitons. To remedy this feature, we shall consider a different class of trial functions in this chapter.

## 6.1 Framework for Investigation of Euler–Lagrange Equations for Pulsating Solitons

We choose hyperbolic trial functions of the form:

$$A(x,t) = A_1(t)\cosh^{-2}\left[\sigma(t)^2 x^2\right]e^{i\alpha(t)} \tag{6.1}$$

$$r(x,t) = e^{i\sigma(t)x} \tag{6.2}$$

This is motivated by the need for soliton shapes less steep than exponentials, as well as the standard $\mathrm{sech}^2$ solitary waves in many systems. Substituting the last two equations into (5.1), the effective Lagrangian becomes

$$\begin{aligned} L_{EFF} \;=\; & \frac{\pi}{36288\sinh(\pi/2)\sigma(t)^2}\Bigg[36288A_1(t)\cos\alpha(t)\dot{\sigma}(t)\Big(-4+\pi\coth(\pi/2)\Big) \\ & +\sigma(t)\Bigg(51408A_1(t)^3\big(b_3\cos\alpha(t)+c_3\sin\alpha(t)\big) \\ & +40885A_1(t)^5\big(b_5\cos\alpha(t)+c_5\sin\alpha(t)\big)+72576\cos\alpha(t)\dot{A}_1(t) \\ & -72576A_1(t)\Big(\cos\alpha(t)\big(\epsilon-b_1\sigma(t)^2\big)+\sin\alpha(t)\big(c_1\sigma(t)^2+\dot{\alpha}(t)\big)\Big)\Bigg)\Bigg] \end{aligned} \tag{6.3}$$

As in Chapetr 5, we are left with three parameters $A_1(t)$, $\sigma(t)$ and $\alpha(t)$ in $L_{EFF}$. Varying these parameters, we obtain the following Euler–Lagrange equations

$$\frac{\partial L_{EFF}}{\partial \star\,(t)} - \frac{\mathrm{d}}{\mathrm{dt}}\Big(\frac{\partial L_{EFF}}{\partial \dot{\star}(t)}\Big) = 0,$$

where $\star$ refers to $A_1$, $\sigma$, or $\alpha$. Solving for $\dot{\star}(t)$ as a system of three ODEs,

$$\begin{aligned}
\dot{A}_1(t) &= f_7[A_1(t), \sigma(t), \alpha(t)] \\
\dot{\sigma}(t) &= f_8[A_1(t), \sigma(t), \alpha(t)] \\
\dot{\alpha}(t) &= f_9[A_1(t), \sigma(t), \alpha(t)],
\end{aligned} \tag{6.4}$$

where the $f_i$, $i = 7, \cdots, 9$ are complicated nonlinear functions of the arguments and are given in the Appendix.

To study the effects of system parameters on the shape and the stability of the Pulsating Soliton, we integrate Eqns. (6.4) numerically in Mathematica for different sets of the various system parameters within the regime of stable periodic solutions. The resulting periodic time series for $A_1(t)$, $\sigma(t)$ and $\alpha(t)$ and are then simply inserted in (6.2) whose spatiotemporal structure ($|A(x,t)|$ versus $x$ and $t$) may be plotted. As the various system parameters within the stable regime are varied, the effects of the pulsating soliton amplitude, width, and phase will be studied.

We will use (5.53) next to identify regimes of supercritical bifurcations where the solutions of the Euler–Lagrange equations (6.4) for the pulsating soliton will result in oscillations of $A_1(t)$, $\sigma(t)$, and $\alpha(t)$ that when substituted into trial function (6.2) will lead to pulsating solitary wave solitons.

## 6.2 Results for the Plane Pulsating Soliton

To derive the conditions for occurrence of stable periodic orbits of $A_1(t)$, $\sigma(t)$, and $\alpha(t)$, we proceed as follows.

First, we fix a set of system parameters $b_1 = 0.08$, $b_5 = 0.1$, $c_1 = 0.5$, $c_3 = 1$, $c_5 = -0.1$. Then, we solve numerically the system of transcendental equations (6.4), which are the equations of the fixed points. By the Ruth–Hurwitz conditions, the Hopf curve is defined as $\delta_1\delta_2 - \delta_3 = 0$. This condition, along with the equations of the fixed points leads to onset of periodic solutions of (6.4) as we will see next.

On the Hopf bifurcation curve we obtain that $b_3 = 0.187269$, and $\epsilon = -0.638362$, while the fixed points are $A_1(0) = 1.18061$, $\sigma(0) = 0.672925$, and $\alpha(0) = -0.681909$. Using these values of $b_3$ and $\epsilon$ , we integrate numerically the systems of three ODEs (6.4), using as initial conditions the three values of the fixed points. Hopf bifurcations occur in this system leading to periodic orbits.

Next, we may plot the time series of the periodic orbit for the amplitude $A_1(t)$, and, as expected, we noticed that the amplitude was very small, since it is proportional to the square root of the distance from the Hopf curve.

To construct pulsating solitons with amplitudes large enough, we had to move away from the Hopf curve, as much as possible, but at the same time to be sure not to be outside of the parameters ranges for the existence of the pulsating soliton. That could be achieved by varying either $\epsilon$ or $b_3$ slowly and away from the Hopf curve. We found that the domain of

existence for the pulsating soliton as a function of $b_3$ was $[0.004, 0.5347]$, passing through the Hopf curve value of $b_3 = 0.1872$, and correspondingly, the domain by varying $\epsilon$ was $[-1.2148, -0.2074]$ passing through the Hopf curve value of $\epsilon = -0.6383$. Within these ranges, we varied $b_3$ or $\epsilon$ and studied the effects on the shape and the stability, as well as the various bifurcations that lead potentially to period doubling and quadrupling. For the largest value of $\epsilon$, i.e. $\epsilon = -0.2074$, we numerically integrate in Mathematica the three differential equations (6.4), and we plot the periodic orbit, which is shown in Fig. 6.1. The resulting periodic time series for $A_1(t)$, $\sigma(t)$, and $\alpha(t)$ from Fig. 6.2 are then simply inserted in (6.1) whose spatiotemporal structure ($|A(x,t)|$ versus $x$ and $t$) is plotted in Fig. 6.3. Note that the table–top structure in Fig. 6.3 is now much closer to the numerically observed shapes. As the various system parameters $c_1$, $c_3$, $c_5$, $b_1$, $b_5$ within the stable regime are varied, the effects of the pulsating soliton amplitude, width, position, phase speed (and, less importantly, phase) may also be studied, and this is discussed subsequently. Repeating the above, we also show the orbit, time series and the plane pulsating soliton for the smallest value of $b_3 = 0.003$ in Figs. 6.4–6.6.

Next, we shall consider the effect of all the various parameters in the CGLE (2.1) on the shape (amplitude, width, period) and stability of the pulsating solitary wave. This is a key feature of interest that was repeatedly mentioned by many speakers in the multi–day session on Dissipative Solitons at the $4^{\text{th}}$ IMACS Conference on Nonlinear Waves held in Athens, Georgia in April 2005, as there are no existing theoretical guidelines or predictions about this at all.

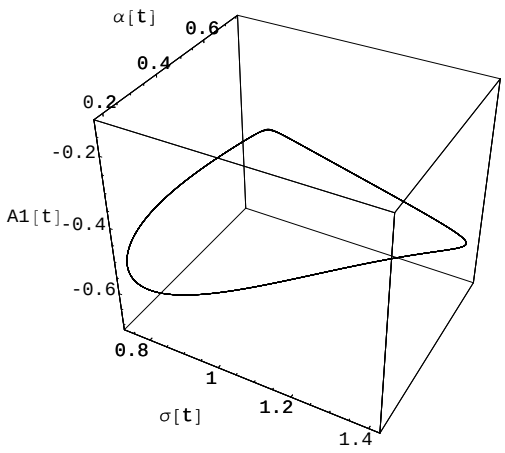


Figure 6.1: The periodic orbit for $\epsilon = -0.2074$

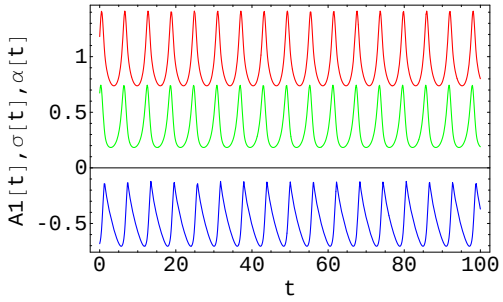


Figure 6.2: Periodic time series for $\epsilon = -0.2074$

In considering the parameter effects on the solitary wave shape and period, note that the wave is a spatially coherent structure (or a "collective coordinate" given by the trial function) whose parameters oscillate in time. Hence, the temporal period of the pulsating soliton is the same as the period $T$ of the oscillations of $A_1(t)$, $\sigma(t)$, and $\alpha(t)$ on their limit cycle. As for the peak amplitude and peak width of the pulsating wave, these are determined by the peak amplitude $A_{1p}$ of $A_1(t)$, and the *reciprocal* of the peak amplitude $\sigma_p$ of $\sigma(t)$ respectively,

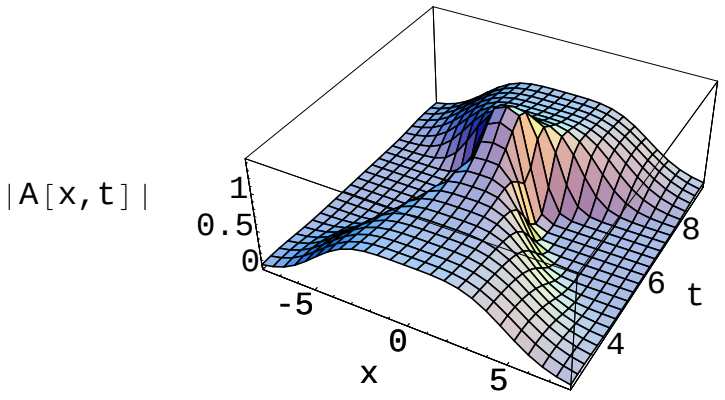


Figure 6.3: Plane pulsating soliton for $\epsilon = -0.2074$

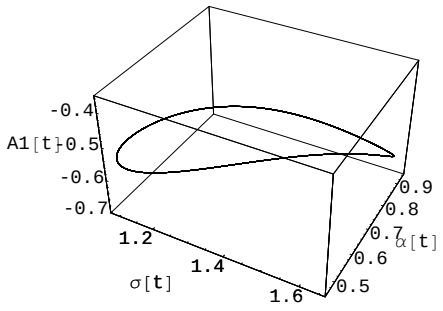


Figure 6.4: The periodic orbit for $b_3 = 0.003$

i.e. at any time $t$ when the amplitude is maximum, the width will be minimum, and vice versa.

Keeping the above in mind, we vary the parameters of the CGLE in turn and we observe the resulting effects on $A_{1p}$ (the peak amplitude), $\sigma_p$ (the inverse width), and $T$ (the temporal

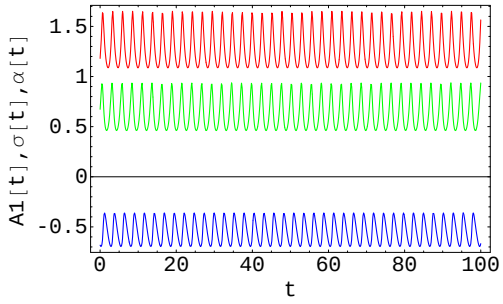


Figure 6.5: Periodic time series for $b_3 = 0.003$

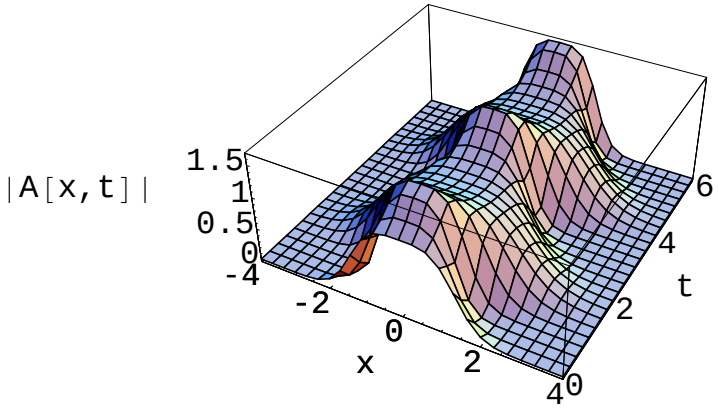


Figure 6.6: Plane pulsating soliton for $b_3 = 0.003$

period) of the pulsating soliton:

(a) For *increased* $b_1$, the values of $A_{1p}$, $\sigma_p$, and $T$ all *increase*.

(b) *Increasing* $b_5$ *augments* all of $A_{1p}$, $\sigma_p$, and $T$.

(c) *Raising* $c_1$ *increases* $A_{1p}$, $\sigma_p$, and $T$.

(d) *Incrementing* $c_3$ *decreases* all of $A_{1p}$, $\sigma_p$, and $T$.

(e) *Augmenting* $c_5$ causes a *decrease* in $A_{1p}$, $\sigma_p$, and $T$.

(f) *Raising* $\epsilon$ causes $A_{1p}$, $\sigma_p$, and $T$ to *fall*.

The above constitute our detailed predictions of the various parameters in the CGLE on the amplitude, inverse width, and temporal width of the pulsating solitons. We have verified that each set of predictions (a)–(f) above agree when the corresponding parameter is varied in the solitary wave simulation for the full PDE shown in Fig. 5.3. Note also that $A_1(t)$ and $\sigma(t)$ are always in phase, so that $A_{1p}$ and $\sigma_p$ occur simultaneously. Thus, the pulsating solitons are tallest where they have least width. This is completely consistent with our simulation in Fig. 5.3, as well as those in [20, 21].

# CHAPTER SEVEN: CONCLUSIONS AND DISCUSSIONS

In conclusion, we have developed a comprehensive theoretical framework for analyzing the full spatiotemporal structure of both pulsating and snake solitary waves in the complex, cubic–quintic Ginzburg–Landau equation. This includes elucidating the mechanism operative in creating these new classes of solitons in dissipative systems, as well as their absence in Hamiltonian and integrable systems where only stationary solitons are observed to occur.

The specific theoretical modeling includes the use of a recent variational formulation and significantly generalized trial function for the solitary waves solutions. In addition, the resulting Euler–Lagrange equations are treated in an entirely different way by looking at their stable periodic solutions (or limit cycles) resulting from supercritical Hopf bifurcations. Oscillations of their trial function parameters on these limit cycles provide the pulsations of the amplitude, width, and phase of the solitons. The model also allows for detailed predictions regarding the other issue of central interest for the pulsating and snake solitons, viz. the effect of each of the system parameters on the amplitude, width, period, and stability of the solitary waves.

Also, given the generality of the theoretical framework developed in this dissertation, it provides a platform for the detailed modeling of chaotic solitary waves as well. These will be the focus of future work in this area. Other outstanding issues which remain are the modeling of creeping and erupting solitons. These will clearly require additional features to be built into our Lagrangian formulation.

We will investigate the chaotical solitons within the same formulation as the snake by looking for chaotic attractors. These may be investigated within the same formulation (5.15) by looking for chaotic attractors of this system. In the standard way, we may look for chaotic regimes of (5.18) by enforcing that:

a. all fixed points are unstable,

b. there are no stable periodic orbits; this is harder to achieve in general, but it is often sufficient to choose system parameters to ensure:

   i. no Hopf bifurcations or

   ii. only subcritical Hopf bifurcations,

c. there are no attractors at infinity, or the solutions of (5.18) do not blow up. The general way to accomplish this is by constructing a Lyapunov function, but, if this proves intractable, an effective practical way is to choose parameters to make the system strongly dissipative or volume contracting ($Tr(J) \ll 0$) at all fixed points and thus prevent exponential growth of the volume leading to solutions flying off to infinity.

Other ways in which chaotic regimes of $A_1(t)$, $\phi(t)$, and $\alpha(t)$ may result are:

a. a subcritical Hopf bifurcation,

b. a generalized ($H1$) Hopf bifurcation,

c. repeated period doubling, and

d. bifurcations of periodic solutions.

Once all of the above are ensured, simple point, periodic, and infinite attractors for the solutions of (5.18) are precluded. Thus, $A_1(t)$, $\phi(t)$ and $\alpha(t)$ must have complex (chaotic or quasiperiodic) dynamics and this will translate, via (5.15), to a spatially localized soliton with chaotic temporal dynamics.

Other outstanding issues which remain are the modeling of creeping and erupting solitons. For the creeping soliton we may need invariants of Euler–Lagrange equations that must turn out to be equal to $\phi/t$ in the trail functions. The constant speed condition $\dot{\phi}(t) = v$ is imposed in (5.18). Eliminating $v$ in terms of $\dot{\alpha}(t)$ and $\dot{A}_1(t)$, supercritical Hopf bifurcations yield periodic solutions for $\alpha(t)$ and $A_1(t)$. The creeping speed $v$ may then be found self–consistently using $\dot{\phi}(t) = v$, $\dot{A}_1(t)$, and $\dot{\alpha}(t)$ at any one time, and, via (5.15), the $|A(x,t)|$ would be a creeping soliton.

A mathematical framework for the erupting solitons incorporating the theory of Canards into the above variational formulation is also under development.

# APPENDIX: LISTINGS OF CODE

Using the program Mathematica we show the right hand side $(f_1, \cdots, f_9)$ of the Euler–Lagrange equations (5.14), (5.18), (6.4) from Chapters 5 and 6.

We also show a notebook in which we explain how we found the pulsating soliton from Section 5.4. Using the trial functions for the pulsating soliton explained in Section 5.2 first we find the effective Lagrangian, (5.13). Then, we vary the effective Lagrangian with respect to $A_1(t)$, $\sigma(t)$ and $\alpha(t)$, and we solve the system of three ODEs (5.14). The right hand sides $f_1$, $f_2$ and $f_3$ are given above. We calculate the characteristic polynomial of the Jacobian matrix, the coefficients $\delta_1$, $\delta_2$ and $\delta_3$ and the Hopf curve condition $\delta_1\delta_2 - \delta_3 = 0$ which will depend on all system parameters and the time series. Assigning numerical values for five of the system parameters, as explained in Section 5.4, we solve numerically the equations of the fixed points on the Hopf curve. As explained before in Chapter 5, by varying one or more of the system parameters, in this case $b_3$, we numerically integrate (5.14) using as initial conditions the values obtained by the find root method. The time series are then inserted back in the ansatz and the pulsating soliton is shown in Fig. 5.6. The snakes are treated in similar fashion using the same file but different ansatz and parameters, as explained in Section 5.5.

```
fl =
  (Al[t] Sec[α[t]]
    (-2 √6 Al[t]^6 (5 b3 b5 + 17 c3 c5 + (3 b3 b5 - 19 c3 c5) Cos[2 α[t]] +
        (-2 b3 b5 + 2 c3 c5) Cos[4 α[t]] + 11 b5 c3 Sin[2 α[t]] +
        11 b3 c5 Sin[2 α[t]] - 2 b5 c3 Sin[4 α[t]] -
        2 b3 c5 Sin[4 α[t]]) -
      4 Al[t]^8 (4 b5^2 + 13 c5^2 + (2 b5^2 - 15 c5^2) Cos[2 α[t]] -
        2 (b5^2 - c5^2) Cos[4 α[t]] + 17 b5 c5 Sin[2 α[t]] -
        4 b5 c5 Sin[4 α[t]]) +
      24 c1 Sin[α[t]] (-b1 Cos[α[t]] + c1 Sin[α[t]]) σ[t]^4 +
      3 √2 Al[t]^2 (4 ϵ Cos[α[t]] (b3 Cos[α[t]] + 3 c3 Sin[α[t]]) +
        (b1 b3 - 3 c1 c3 + 2 (b1 b3 + c1 c3) Cos[2 α[t]] +
          (b1 b3 + c1 c3) Cos[4 α[t]] - 2 b3 c1 Sin[2 α[t]] +
          2 b1 c3 Sin[2 α[t]] - b3 c1 Sin[4 α[t]] + b1 c3 Sin[4 α[t]])
         σ[t]^2) +
      Al[t]^4 (-9 b3^2 - 33 c3^2 + 8 √3 b5 ϵ +
        (-6 b3^2 + 36 c3^2 + 8 √3 b5 ϵ) Cos[2 α[t]] + 3 b3^2 Cos[4 α[t]] -
        3 c3^2 Cos[4 α[t]] - 42 b3 c3 Sin[2 α[t]] +
        20 √3 c5 ϵ Sin[2 α[t]] + 6 b3 c3 Sin[4 α[t]] +
        4 √3 (b1 b5 - 3 c1 c5 + 2 (b1 b5 + c1 c5) Cos[2 α[t]] +
          (b1 b5 + c1 c5) Cos[4 α[t]] - 2 b5 c1 Sin[2 α[t]] +
          2 b1 c5 Sin[2 α[t]] - b5 c1 Sin[4 α[t]] + b1 c5 Sin[4 α[t]])
         σ[t]^2))) /
   (2
     (-1/√2
       (3 Al[t]^2 (-3 b3 Cos[α[t]] + b3 Cos[3 α[t]] - 11 c3 Sin[α[t]] +
          c3 Sin[3 α[t]]) +
        2 √3 Al[t]^4 (4 b5 Cos[α[t]] - 2 b5 Cos[3 α[t]] +
          13 c5 Sin[α[t]] - 2 c5 Sin[3 α[t]]) - 6 c1 Sin[α[t]] σ[t]^2)));
```

```
f2 =
  1/3 σ[t]
   (-9 √2 Al[t]^2 (b3 + c3 Tan[α[t]]) - 10 √3 Al[t]^4 (b5 + c5 Tan[α[t]]) +
     6 (ϵ + (-b1 + c1 Tan[α[t]]) σ[t]^2));

f3 =
  -(√6 Al[t]^6 ((b5 c3 - 3 b3 c5) Cos[α[t]] + (b5 c3 + b3 c5) Cos[3 α[t]] -
        2 (b3 b5 + c3 c5 + (b3 b5 - c3 c5) Cos[2 α[t]]) Sin[α[t]]) -
     12 c1 ϵ Cos[α[t]] σ[t]^2 +
     3 √2 Al[t]^2
      (-2 ϵ Cos[α[t]]
         (c3 Cos[2 α[t]] - 2 (c3 + b3 Cos[α[t]] Sin[α[t]])) +
        2 ((b3 c1 + 3 b1 c3) Cos[α[t]] + (b3 c1 - b1 c3) Cos[3 α[t]] +
           2 (b1 b3 - c1 c3 + (b1 b3 + c1 c3) Cos[2 α[t]]) Sin[α[t]])
         σ[t]^2) +
     4 √3 Al[t]^4
      (2 ϵ Cos[α[t]] (3 c5 - 2 c5 Cos[2 α[t]] + 2 b5 Sin[2 α[t]]) +
        3 (2 b1 c5 Cos[α[t]] + (b5 c1 - b1 c5) Cos[3 α[t]] +
           2 (b1 b5 - c1 c5 + (b1 b5 + c1 c5) Cos[2 α[t]]) Sin[α[t]])
         σ[t]^2)) /
   (-1/√2
      (3 Al[t]^2 (-3 b3 Cos[α[t]] + b3 Cos[3 α[t]] - 11 c3 Sin[α[t]] +
         c3 Sin[3 α[t]])) +
     2 √3 Al[t]^4 (4 b5 Cos[α[t]] - 2 b5 Cos[3 α[t]] + 13 c5 Sin[α[t]] -
        2 c5 Sin[3 α[t]]) - 6 c1 Sin[α[t]] σ[t]^2);
```

```
f4 =
  -(Al[t] Sec[α[t]]
      (-3456 c1 ϵ^(8/3) Sin[α[t]] (-b1 Cos[α[t]] + c1 Sin[α[t]]) +
        2 √6 ϵ^(1/3) Al[t]^6
         (5 b3 b5 + 17 c3 c5 + (3 b3 b5 - 19 c3 c5) Cos[2 α[t]] +
           (-2 b3 b5 + 2 c3 c5) Cos[4 α[t]] + 11 b5 c3 Sin[2 α[t]] +
           11 b3 c5 Sin[2 α[t]] - 2 b5 c3 Sin[4 α[t]] -
           2 b3 c5 Sin[4 α[t]]) ϕ[t]^4 +
        4 Al[t]^8 (4 b5^2 + 13 c5^2 + (2 b5^2 - 15 c5^2) Cos[2 α[t]] -
           2 (b5^2 - c5^2) Cos[4 α[t]] + 17 b5 c5 Sin[2 α[t]] -
           4 b5 c5 Sin[4 α[t]]) ϕ[t]^4 -
        6 √2 ϵ^(5/3) Al[t]^2 ϕ[t]^2
         (-6 (b1 b3 - 3 c1 c3 + 2 (b1 b3 + c1 c3) Cos[2 α[t]] +
              (b1 b3 + c1 c3) Cos[4 α[t]] - 2 b3 c1 Sin[2 α[t]] +
              2 b1 c3 Sin[2 α[t]] - b3 c1 Sin[4 α[t]] +
              b1 c3 Sin[4 α[t]]) +
           2 ϵ Cos[α[t]] (b3 Cos[α[t]] + 3 c3 Sin[α[t]]) ϕ[t]^2) +
        ϵ^(2/3) Al[t]^4 ϕ[t]^2
         (48 √3 ϵ^(2/3) (b1 b5 - 3 c1 c5 + 2 (b1 b5 + c1 c5) Cos[2 α[t]] +
              (b1 b5 + c1 c5) Cos[4 α[t]] - 2 b5 c1 Sin[2 α[t]] +
              2 b1 c5 Sin[2 α[t]] - b5 c1 Sin[4 α[t]] +
              b1 c5 Sin[4 α[t]]) +
           (9 b3^2 + 33 c3^2 - 8 √3 b5 ϵ^(2/3) ϵ +
              (6 b3^2 - 36 c3^2 - 8 √3 b5 ϵ^(2/3) ϵ) Cos[2 α[t]] -
              3 (b3^2 - c3^2) Cos[4 α[t]] + 42 b3 c3 Sin[2 α[t]] -
              20 √3 c5 ϵ^(2/3) ϵ Sin[2 α[t]] - 6 b3 c3 Sin[4 α[t]]) ϕ[t]^2))) /
    (5 ϵ^(4/3) ϕ[t]^2
      (144 c1 ϵ^(4/3) Sin[α[t]] -
        3 √2 ϵ^(1/3) Al[t]^2
         (-3 b3 Cos[α[t]] + b3 Cos[3 α[t]] - 11 c3 Sin[α[t]] +
           c3 Sin[3 α[t]]) ϕ[t]^2 +
        4 √3 Al[t]^4 (4 b5 Cos[α[t]] - 2 b5 Cos[3 α[t]] +
           13 c5 Sin[α[t]] - 2 c5 Sin[3 α[t]]) ϕ[t]^2));
```

```
f5 =
        1
  ------------------
  15 e^(4/3) φ[t]
   (-72 e^(4/3) (b1 - c1 Tan[α[t]]) +
     (-6 e^(4/3) ε + 9 √2 e^(1/3) Al[t]^2 (b3 + c3 Tan[α[t]]) +
        10 √3 Al[t]^4 (b5 + c5 Tan[α[t]])) φ[t]^2);

f6 =
  (2 (-144 c1 e^(7/3) ε Cos[α[t]] -
       √6 Al[t]^6 ((b5 c3 - 3 b3 c5) Cos[α[t]] +
          (b5 c3 + b3 c5) Cos[3 α[t]] -
          2 (b3 b5 + c3 c5 + (b3 b5 - c3 c5) Cos[2 α[t]]) Sin[α[t]]) φ[t]^2 +
       3 √2 e^(4/3) Al[t]^2
        (24 ((b3 c1 + 3 b1 c3) Cos[α[t]] + (b3 c1 - b1 c3) Cos[3 α[t]] +
             2 (b1 b3 - c1 c3 + (b1 b3 + c1 c3) Cos[2 α[t]]) Sin[α[t]]) +
          2 ε Cos[α[t]]
           (c3 Cos[2 α[t]] - 2 (c3 + b3 Cos[α[t]] Sin[α[t]])) φ[t]^2) +
       8 √3 e Al[t]^4
        (18 (2 b1 c5 Cos[α[t]] + (b5 c1 - b1 c5) Cos[3 α[t]] +
             2 (b1 b5 - c1 c5 + (b1 b5 + c1 c5) Cos[2 α[t]]) Sin[α[t]]) +
          ε Cos[α[t]] (-3 c5 + 2 c5 Cos[2 α[t]] - 2 b5 Sin[2 α[t]])
           φ[t]^2))) /
   (5 e
     (144 c1 e^(4/3) Sin[α[t]] -
       3 √2 e^(1/3) Al[t]^2
        (-3 b3 Cos[α[t]] + b3 Cos[3 α[t]] - 11 c3 Sin[α[t]] +
          c3 Sin[3 α[t]]) φ[t]^2 +
       4 √3 Al[t]^4 (4 b5 Cos[α[t]] - 2 b5 Cos[3 α[t]] +
          13 c5 Sin[α[t]] - 2 c5 Sin[3 α[t]]) φ[t]^2));
```

```
f7 =
  -(Al[t] Sec[α[t]] Sinh[π/2]
      (-2101816080 Al[t]^6
         (5 b3 b5 + 17 c3 c5 + (3 b3 b5 - 19 c3 c5) Cos[2 α[t]] +
           (-2 b3 b5 + 2 c3 c5) Cos[4 α[t]] +
           (b5 c3 + b3 c5) (11 Sin[2 α[t]] - 2 Sin[4 α[t]])) -
        1671583225 Al[t]^8
         (4 b5^2 + 13 c5^2 + (2 b5^2 - 15 c5^2) Cos[2 α[t]] +
           2 (-b5^2 + c5^2) Cos[4 α[t]] + 17 b5 c5 Sin[2 α[t]] -
           4 b5 c5 Sin[4 α[t]]) + 10534551552 c1 Sin[α[t]]
         (-b1 Cos[α[t]] + c1 Sin[α[t]]) σ[t]^4 +
        1865493504 Al[t]^2
         (4 ϵ Cos[α[t]] (b3 Cos[α[t]] + 3 c3 Sin[α[t]]) +
           (b1 b3 - 3 c1 c3 + (b1 b3 + c1 c3) (2 Cos[2 α[t]] + Cos[4 α[t]]) -
              8 (b3 c1 - b1 c3) Cos[α[t]]^3 Sin[α[t]]) σ[t]^2) +
        1233792 Al[t]^4 (-1071 (3 b3^2 + 11 c3^2) + 4810 b5 ϵ +
           (-2142 (b3^2 - 6 c3^2) + 4810 b5 ϵ) Cos[2 α[t]] +
           1071 (b3 - c3) (b3 + c3) Cos[4 α[t]] +
           (-14994 b3 c3 + 12025 c5 ϵ) Sin[2 α[t]] +
           2142 b3 c3 Sin[4 α[t]] +
           2405 (b1 b5 - 3 c1 c5 + (b1 b5 + c1 c5)
                (2 Cos[2 α[t]] + Cos[4 α[t]]) -
              8 (b5 c1 - b1 c5) Cos[α[t]]^3 Sin[α[t]]) σ[t]^2))) /
    (72576 (π Cosh[π/2] - 2 Sinh[π/2])
      (25704 Al[t]^2 (-3 b3 Cos[α[t]] + b3 Cos[3 α[t]] - 11 c3 Sin[α[t]] +
          c3 Sin[3 α[t]]) +
       40885 Al[t]^4 (-4 b5 Cos[α[t]] + 2 b5 Cos[3 α[t]] -
          13 c5 Sin[α[t]] + 2 c5 Sin[3 α[t]]) +
       72576 c1 Sin[α[t]] σ[t]^2));
```

$$f8 = \frac{1}{36288\left(-2+\pi\,\text{Coth}\left[\frac{\pi}{2}\right]\right)}$$

$$\left(\sigma[t]\left(-154224\,Al[t]^2\,(b3+c3\,\text{Tan}[\alpha[t]])-204425\,Al[t]^4\,(b5+c5\,\text{Tan}[\alpha[t]])+72576\left(\epsilon+(-b1+c1\,\text{Tan}[\alpha[t]])\,\sigma[t]^2\right)\right)\right);$$

$$f9 = \left(\text{Sinh}\left[\frac{\pi}{2}\right]\left(695045\,Al[t]^6\,((b5\,c3-3\,b3\,c5)\,\text{Cos}[\alpha[t]]+(b5\,c3+b3\,c5)\,\text{Cos}[3\,\alpha[t]]-2\,(b3\,b5+c3\,c5+(b3\,b5-c3\,c5)\,\text{Cos}[2\,\alpha[t]])\,\text{Sin}[\alpha[t]])-3483648\,c1\,\epsilon\,\text{Cos}[\alpha[t]]\,\sigma[t]^2+2467584\,Al[t]^2\left(\epsilon\,\text{Cos}[\alpha[t]]\,(2\,c3-c3\,\text{Cos}[2\,\alpha[t]]+b3\,\text{Sin}[2\,\alpha[t]])+((b3\,c1+3\,b1\,c3)\,\text{Cos}[\alpha[t]]+(b3\,c1-b1\,c3)\,\text{Cos}[3\,\alpha[t]]+(b1\,b3-3\,c1\,c3)\,\text{Sin}[\alpha[t]]+(b1\,b3+c1\,c3)\,\text{Sin}[3\,\alpha[t]])\,\sigma[t]^2\right)+1962480\,Al[t]^4\left(2\,\epsilon\,\text{Cos}[\alpha[t]]\,(3\,c5-2\,c5\,\text{Cos}[2\,\alpha[t]]+2\,b5\,\text{Sin}[2\,\alpha[t]])+3\,(2\,b1\,c5\,\text{Cos}[\alpha[t]]+(b5\,c1-b1\,c5)\,\text{Cos}[3\,\alpha[t]]+(b1\,b5-3\,c1\,c5)\,\text{Sin}[\alpha[t]]+(b1\,b5+c1\,c5)\,\text{Sin}[3\,\alpha[t]])\,\sigma[t]^2\right)\right)\Big/\left(24\left(\pi\,\text{Cosh}\left[\frac{\pi}{2}\right]-2\,\text{Sinh}\left[\frac{\pi}{2}\right]\right)\left(25704\,Al[t]^2\,(-3\,b3\,\text{Cos}[\alpha[t]]+b3\,\text{Cos}[3\,\alpha[t]]-11\,c3\,\text{Sin}[\alpha[t]]+c3\,\text{Sin}[3\,\alpha[t]])+40885\,Al[t]^4\,(-4\,b5\,\text{Cos}[\alpha[t]]+2\,b5\,\text{Cos}[3\,\alpha[t]]-13\,c5\,\text{Sin}[\alpha[t]]+2\,c5\,\text{Sin}[3\,\alpha[t]])+72576\,c1\,\text{Sin}[\alpha[t]]\,\sigma[t]^2\right)\right);$$

```
<< Graphics`Graphics`

A = Al[t] Exp[- σ[t]^2 x^2] Exp[i α[t]];

Astar = Al[t] Exp[- σ[t]^2 x^2] Exp[-i α[t]];

r = Exp[- σ[t]^2 x^2];

rstar = r;

MagAsq = A * Astar;

Axx = Simplify[D[A, {x, 2}]];

Astarxx = Simplify[D[Astar, {x, 2}]];

L = Simplify[rstar * D[A, t] + r * D[Astar, t] - ε (rstar * A + r * Astar) -
    b1 (rstar * Axx + r * Astarxx) - i c1 (rstar * Axx - r * Astarxx) +
    MagAsq (b3 (rstar * A + r * Astar) - i c3 (rstar * A - r * Astar)) +
    MagAsq^2 (b5 (rstar * A + r * Astar) - i c5 (rstar * A - r * Astar))];

Leff = FullSimplify[Integrate[L, {x, -∞, ∞},
    GenerateConditions → False, Assumptions → {σ[t] > 0}]];

dLdAl = ∂Al[t] Leff;

dLdAldot = ∂Al'[t] Leff;

EL1 = FullSimplify[dLdAl - D[dLdAldot, t], σ[t] > 0];

dLdsigma = ∂σ[t] Leff;

dLdsigmadot = ∂σ'[t] Leff;

EL2 = FullSimplify[dLdsigma - D[dLdsigmadot, t], σ[t] > 0];

dLdalph = ∂α[t] Leff;

dLdalphdot = ∂α'[t] Leff;
```

```
EL3 = FullSimplify[dLdalph - D[dLdalphdot, t], σ[t] > 0];

vf = {f1, f2, f3};

jaco = Transpose[{D[vf, Al[t]], D[vf, σ[t]], D[vf, α[t]]}];

characpoly = Det[λ IdentityMatrix[3] - jaco];

61 = Coefficient[characpoly, λ^2];

62 = Coefficient[characpoly, λ];

63 = characpoly /. {λ → 0};

hopfcurve = 61 * 62 - 63;

{numf1, numf2, numf3, numhopfcurve, num62} =
  {f1, f2, f3, hopfcurve, 62} /.
   {b1 → 0.08, b5 → 0.1, c1 → 0.5, c3 → 1, c5 → -0.1};

ans = FindRoot[{numf1 == 0, numf2 == 0, numf3 == 0, numhopfcurve == 0,
   num62 == 4}, {b3, -1.12, 0}, {ε, -0.1, -0.01}, {Al[t], -1, 1},
  {σ[t], 0.1, 0.7}, {α[t], -1, 1}, MaxIterations → 99]

{numericf1, numericf2, numericf3} =
  {numf1, numf2, numf3} /. {b3 → -0.2531943, ε → -0.3454813292210729};

sol3d =
 NDSolve[{Al'[t] == numericf1, Al[0] == 0.9547123, σ'[t] == numericf2,
   σ[0] == 0.9170931, α'[t] == numericf3, α[0] == -0.181274285},
  {Al, σ, α}, {t, 0, 300}, Method → ExplicitRungeKutta]

plot1 = ParametricPlot3D[Evaluate[{Al[t], σ[t], α[t]} /. sol3d],
  {t, 0, 100}, PlotPoints → 2000, PlotRange → All,
  AxesLabel -> {"σ[t]  ", "α[t]      ", "Al[t] "}]
```

```
evAlt = Evaluate[Al[t] /. sol3d];

evσt = Evaluate[σ[t] /. sol3d];

evαt = Evaluate[α[t] /. sol3d];

plot2 = Plot[ {evAlt, evσt, evαt}, {t, 0, 100}, PlotPoints → 20,
  Frame → True, FrameLabel → {"t", "Al[t],σ[t],α[t]", None, None},
  RotateLabel → True,
  PlotStyle → {RGBColor[1, 0, 0], RGBColor[0, 1, 0],
    RGBColor[0, 0, 1]}]

finalAlt = evAlt[[1]];

finalσt = evσt[[1]];

magnit = finalAlt * Exp[-(finalσt)^2 * x^2];

plot3 = Plot3D[magnit, {x, -3, 3}, {t, 0, 5.9},
   AxesLabel -> {"x", "t", " |A[x,t]|   "}];
```

# LIST OF REFERENCES


[1] R.K. Dodd, J.C. Eilbeck, J.D. Gibbon, and H.C. Morris. *Solitons and Nonlinear Wave Equations*. Academic, London, 1982.

[2] P.G. Drazin and W.H. Reid. *Hydrodynamic Stability*. Cambridge U. Press, Cambridge, 1981.

[3] I.S. Aranson and L.Kramer. The World of the Complex Ginzburg–Landau Equation. *Rev. Mod. Phys.*, 74:99, 2002.

[4] C.Bowman and A.C. Newell. Natural Patterns and Wavelets. *Rev. Mod. Phys.*, 70:289, 1998.

[5] L. Brusch, A. Torcini, M. van Hecke, M. G. Zimmermann, and M. Bär. Modulated amplitude waves and defect formation in the one–dimensional complex Ginzburg–Landau equation. *Phys D.*, 160:127, 2001.

[6] L. Brusch, A. Torcini, and M. Bär. Nonlinear analysis of the Eckhaus Instability: Modulated amplitude waves and phase chaos. *Phys.D*, 160:127, 2001.

[7] L.R. Keefe. Dynamics of perturbed wavetrain solutions to the Ginzburg–Landau equation. *Stud. Appl. Math.*, 73:91, 1985.

[8] M.J. Landman. Solutions of the GL equation of interest in shear flow. *Stud. Appl. Math.*, 76:187, 1987.

[9] P.K. Newton and L. Sirovich. Instabilities of the Ginzburg–Landau equation: Periodic solutions. *Quart. Appl. Math.*, XLIV:49, 1984.

[10] P.K. Newton and L. Sirovich. Instabilities of the Ginzburg–Landau equation Pt.II: Secondary bifurcations. *Quart. Appl. Math.*, XLIV:367, 1986.

[11] W. van Saarloos and P. C. Hohenberg. Fronts, pulses, sources and sinks in generalized complex Ginzburg–Landau equation. *Phys.D*, 56:303, 1992.

[12] M. van Hecke, C. Storm, and W. van Saarloos. Sources, sinks and wavenumber selection in coupled CGL equations. *Phys.D*, 134:1, 1999.

[13] R. Alvarez, M. van Hecke, and W. van Saarloos. Sources and sinks separating domains of left– and right–traveling waves: Experiment versus amplitude equations. *Phys.Rev.E*, 56:R1306, 1997.

[14] P. Holmes. Spatial structure of time periodic solutions of the GL equation. *Phys.D*, 23:84, 1986.

[15] A. Doelman. Traveling waves in the complex GL equation. *J. Nonlin. Sci*, 3:225, 1993.

[16] A. Doelman. Periodic and quasiperiodic solutions of degenerate modulation equations. *Phys.D*, 53:249, 1991.

[17] J. Duan and P. Holmes. Fronts, domain walls and pulses in a generalized GL equation. *Proc. Edin. Math. Soc.*, 38:77, 1995.

[18] A. Doelman. Slow time–periodic solutions of the GL equation. *Phys.D*, 40:156, 1989.

[19] J. M. Soto-Crespo, N. Akhmediev, and G. Town. Interrelation between various branches of stable solitons in dissipative systems. *Optics Comm.*, 199:283, 2001.

[20] N. Akhmediev, J. Soto-Crespo, and G. Town. Pulsating solitons, chaotic solitons, period doubling, and pulse coexistence in mode–locked laser: CGLE approach. *Phys. Rev.E*, 63:56602, 2001.

[21] D. Artigas, L. Torner, and N. Akhmediev. Robust heteroclinic cycles in the one-dimension CGLE. *Opt. Comm.*, 143:322, 1997.

[22] J. Satsuma and N. Yajima. Initial–value problems of one–dimensional self–modulation of nonlinear–waves in dispersive media. *Progr. Theoret. Phys. Suppl.*, 55:284, 1974.

[23] P. G. Drazin and R. S. Johnson. *Solitons: an Introduction*. Cambridge U. Press, Cambridge, 1989.

[24] J. D. Murray. *Mathematical Biology*. Springer–Verlag, Berlin, 1989.

[25] N.J. Balmforth. Solitary waves and homoclinic orbits. *Ann. Rev. Fluid Mechanics*, 27:335, 1995.

[26] N. Akhmediev. Pulsating solitons in dissipative systems. $4^{\text{th}}$ IMACS Conf. on Nonlinear Waves, Athens, Georgia, April 2005, 2005.

[27] M. Golubitski and D.G. Schaffer. *Singularities and groups in Bifurcation Theory*, volume 51. Springer, New York, 1985.

[28] J. Planeaux. *Bifurcation Phenomena in CSTR Dynamics*. PhD thesis, University of Minnesota, 1993.

[29] S. Roy Choudhury. Pulsating and snake solitons: Amplitude modulation via dissipation. In preparation.

[30] D.J. Kaup and B.A. Malomed. The variational principle for nonlinear waves in dissipative systems. *Physica D*, 87:155, 1995.

[31] E. Doedel and J. Kern'evez. AUTO: Software for continuation problems in ordinary differential equations. California Institute of Technology, Pasadena, CA.,1986.

[32] V.I. Arnold. Lectures on bifurcations in versal families. *Russian Math. Surveys*, 27:54, 1972.

[33] J. Guckenhemer and P. Holmes. *Nonlinear Oscillations, Dynamical Systems, and Bifurcations of Vector Fields*, volume 42. Springer–Verlag, New York, 1983.

[34] W.F. Langford. Periodic and steady–state mode interactions lead to tori. *SIAM J. Appl. Math.*, 37:22, 1979.

[35] L.M. Pismen. Dynamics of lumped chemically reacting systems near singular bifurcations points. *Chem. Eng. Sci.*, 39:1063, 1984.

[36] L.M. Pismen. Dynamics of lumped chemically reacting systems near singular bifurcations points–II. Almost Hamiltonian dynamics. *Chem. Eng. Sci.*, 40:905, 1985.

[37] V. Skarka and N. Aleksic. Generation and dynamics of dissipative spatial solitons. $4^{\text{th}}$ IMACS Conf. on Nonlinear Waves, Athens, Georgia, April 2005, 2005.

[38] A. H. Nayfeh and B. Balachandran. *Applied Nonlinear Dynamics*. John Wiley, 1995.

[39] M. Holodniok and M. Kubicek. *Computation of period doubling points in ODEs*. Institut für Mathematik Report TUM-8406, Technic Univ. of München, Germany, 1984.

[40] N. Akhmediev and A. Ankiewicz. *Dissipative Solitons in the CGLE and Swift–Hohenberg Equations*. Dissipative Solitons, Springer, Berlin, 2005.

[41] L. D. Fadeev and L. A. Takhtajan. Springer, Berlin, 1986.